Université de Lille

Ecole doctorale des Sciences de l'ingénierie et des systèmes

**Thèse**

Pour obtenir le grade de

Docteur de l'Université de Lille

Spécialité : Génie Electrique

Présentée et soutenue publiquement par

**Ryan Carlos de Oliveira Berriel**

Soutenue le 22 décembre 2023

---

# Reduction of energy consumption of a subway carousel

---

# Réduction de la consommation d'énergie d'un carrousel de métro

---

**Membres du jury :**

| | | |
|---|---|---|
| **Dr. HDR Jean-Christophe OLIVIER** | Nantes Université | Rapporteur |
| **Pr. Marie-Cécile PERA** | Université de Franche-Comté | Rapporteur |
| **Pr. Ali SARI** | Université Claude Bernard Lyon 1 | Président du Jury |
| **Pr. Alain BOUSCAYROL** | Université Lille, France | Directeur de la thèse |
| **Dr. Philippe DELARUE** | Université Lille, France | Co-encadrant de la thèse |
| **Dr. Clément MAYET** | Université Lille, France | Co-encadrant de la thèse |
| **M. Charles BROCART** | Métropole européenne de Lille | Invité |

# Acknowledgements

Résumé

L'urbanisation a entraîné une demande croissante en matière de mobilité urbaine efficace. À mesure que les villes se développent, la nécessité de solutions de transport durable devient essentielle. Les métros, caractérisés par leur grande capacité et leurs émissions relativement faibles, se sont imposés comme une solution privilégiée pour répondre à ce besoin croissant. Cependant, bien qu'ils offrent de nombreux avantages, ils présentent également des défis, notamment en ce qui concerne l'efficacité énergétique et la gestion d'énergie. La MEL (Métropole Européenne de Lille) s'engage à explorer les économies d'énergie potentielles sur son réseau des transports, soulignant l'importance de l'évaluation de solutions adaptées aux contextes urbains spécifiques.

Cette thèse explore les défis des systèmes de métro, en particulier les solutions visant à réduire la consommation d'énergie. Un modèle dynamique et un outil de simulation flexible pour l'étude énergétique des carrousels de métro sont développés. Ils sont validés par des résultats expérimentaux sur une ligne réelle, ainsi que par une plateforme expérimentale réduite et flexible, utilisant le principe de simulation Hardware-In-the-Loop. Cette dernière permet de tester des scénarios que l'on ne peut pas tester sur le carrousel réel. Des modèles simplifiés sont alors proposés pour réduire les besoins en calcul sans sacrifier la précision. Différents scénarios de simulation ont été étudiés pour mettre en évidence les principaux facteurs de réduction de la consommation d'énergie globale. Sur la ligne 1 de la MEL, réduire la vitesse maximale de 10 % entraîne une réduction de la consommation d'énergie de 6,7 % tout en augmentant le temps de trajet de moins de 2 minutes. Une légère modification de l'intervalle entre deux véhicules peut aussi entraîner une réduction de la consommation d'énergie globale allant jusqu'à 12 %. Le potentiel de la récupération de l'énergie de freinage a été analysé, montrant la possibilité d'alimenter des voitures électriques ou des bus électriques.

Urbanization has led to a surge in demand for efficient urban mobility. As cities grow, the need for sustainable transport solutions becomes vital. Subways, characterized by their high capacity and relatively low emissions, have emerged as a favored solution to address this growing interest. However, while they offer numerous advantages, they also present challenges, especially in the scope of energy efficiency and management. The MEL (Métropole Européenne de Lille) is committed to exploring the potential energy savings on its transport network, underscoring the importance of evaluating adapted solutions in specific urban contexts.

This PhD thesis explores the energy efficiency challenges of subway systems, particularly, solutions for reduction of energy consumption. A dynamical model and a flexible simulation tool for subway carousel energy studies is developed. They are validated by experimental results on a real track, as well by a dedicated reduced-scale and flexible experimental platform using the Hardware-In-the-Loop principle. This platform enables the test of specific cases, which are difficult to measure on the real track. Simplified models are then proposed to reduce computational demands without sacrificing accuracy. Different simulation scenarios have been studied to highlight the main factors to reduce global energy consumption. For line 1 of MEL, reducing the maximal velocity by 10% leads to a reduction of energy consumption by 6.7% while increasing the travel time by less than 2 minutes. A slight change of headway (time between two cars) can also lead to a reduction of global energy up to 12%. The potential braking energy recovery has been analyzed showing the use case to supply electric cars or electric buses.

# Table of Contents

*General introduction*

The demand for urban mobility has grown significantly in recent decades, as more people move to cities in search of better opportunities, access to services, and other benefits of urban living [UITP 22]. As a result, transportation systems have become a critical component of modern urban areas, facilitating the movement of people, goods, and services [UN 18].

There has been a significant increase in the proportion of the global population residing in urban areas, with more than half of the population now concentrated in such areas since 2018. This trend is projected to continue in the coming decades, which in turn, will incite the expansion of transportation networks. In this scenario, it is crucial for authorities and agencies to prioritize urban planning to ensure the overall well-being and quality of life of urban inhabitants.

At a basic level, urban transport systems are responsible for moving people from one location to another, whether it is for work, school, shopping or leisure. However, their importance extends far beyond simply facilitating travel. The transport network is also a key driver of economic growth and development, as it enables businesses to access new markets and distribute their goods and services more efficiently. Furthermore, the urban transport network also has important social impacts on the city and its citizens.

With the increasing demand for urban mobility, the urban transport network and infrastructure are continuously expanding. The subway is an important part of the urban transportation system and has become a popular mode of public transportation in many cities. Urban planning policies often prioritize actions that increase the number of vehicles, retrofits in the traction power supply, and the construction of new lines. These actions consequently result in a significant increase in energy consumption and power demand.

To address these challenges, urban planners must adopt a more sustainable approach that prioritizes investments in technologies aimed at optimizing the use of transport networks while minimizing the impact of its expansion. In general, light rail transit systems offer numerous advantages when compared to other modes of transportation. They provide a comfortable and punctual journey, while producing low greenhouse gas (GHG) emissions and consuming less energy per passenger-kilometer [IEA 22a]. However, due to their extensive use, they present significant impact on energy consumption and power demand.

As one of the most popular transit systems, subways are presented in most metropolises and big cities. Subway vehicles are equipped with electric drive systems composed of an electric machine combined with a bidirectional power converter. Thus, regenerative braking capability is a

natural consequence that can be harnessed. Regenerative braking energy is fed back into the electric transmission system and can be utilized by nearby accelerating vehicles, auxiliary loads or stored for further utilization.

The subway network is supplied by the Traction Power Substations (TPS). The typical TPS topology includes a transformer combined with a diode bridge. This configuration offers robustness and reliability when compared to technologies based on controlled power electronics. However, it presents a non-reversible characteristic. The braking energy cannot be recovered to the supply grid.

Energy efficiency improvements have been extensively discussed and tested in transport systems worldwide [Khodaparastan 19a]. Such improvements can lead to a consistent reduction in power demand and energy consumption from the local utility, resulting in substantial operational cost savings for the service company. However, most of works are based on a backward approach where a velocity profile is imposed regardless of systems limitation [Mayet 16a]. Also, electric dynamics, such as DC bus voltage fluctuation, and the supply line impact are often neglected.

In the city of Lille, France, to guarantee the quality of life of the inhabitants, the MEL (Métropole Européenne de Lille) has been planning to expand the subway transport capability. A modification in the subway system is expected to increase the transport capability of the urban network. A new subway vehicle (NMR Alstom) with capacity up to 498 users is in process of implementation on Line 1 of the transport network. The new vehicle is about double the length (52 m), when compared to the current vehicle (Siemen VAL), with 26 m.

Previously analyzes carried out showed a potential use of braking energy for this network. These studies were performed considering the actual subway vehicle (Siemens VAL) [Mayet 16a]. For the new subway, studies related to the model and use of braking energy are still necessary. In the framework of the CUMIN interdisciplinary program of University of Lille, a partnership with MEL has been established for the implementation of the REMUS (Recovery of Energy from Metros in University based on Sustainability of an eco-campus) project, where this thesis is one of the expected outputs.

This thesis aims to propose solutions for the energy consumption reduction of light rail transport systems, with a focus on the NMR. In the initial stage, an accurate model is developed, taking into account the specifications of the new vehicle. A forward approach is used to ensure the correct calculation of energy consumption. To face the complexity of the completed model of the

subway line, including non-linear parts and time-varying number of subsystems, the Energetic Macroscopic Representation (EMR Formalism) [Bouscayrol 12] is used to organize the model. Hence, a flexible simulation tool is established. To ensure the validity of the model, experimental results obtained from the real-world operation of the vehicle are compared with simulation results.

Chapter 1 focuses on the impact and development of urban rail transit systems, particularly focusing on their energy efficiency. It addresses the challenges and advancements in managing energy consumption within these systems, considering the rapid urbanization and increasing public transportation demands. This chapter also includes the local case motivations on MEL, emphasizing the role of local governance and innovative approaches in modernizing and improving energy usage in rail transit systems. The positioning and objective of the PhD thesis are thus defined.

Chapter 2 deals with the simulation tool development for the subway systems for energetic study. This chapter presents a comprehensive analysis of the system energy dynamics, emphasizing the importance of accurate modeling in order to perform energetic analysis. The chapter also explores experimental tests conducted to validate the model developed. Additionally, the development of the HIL simulation tool is presented to validate other cases that are difficult to measure on the real track.

Chapter 3 focuses on analyzing the energy consumption and efficiency in subway systems. This chapter provides a detailed examination of energy flows within subway carousels, emphasizing the impact of different operational parameters on energy usage. The chapter also discusses the impact of regenerative braking and the importance of managing this energy for system efficiency. The findings underscore the potential for reducing energy consumption through careful analysis, balancing the need for efficient transportation with operational requirements.

# Chapter 1:  Energy efficiency in light rail transit systems

# I. Context and impact of light rail transit systems

## I.1. Interaction of society, transport, and environment

The public transportation system has been an essential component of urban mobility for decades. It plays an important social and economic role connecting people to their workplaces, educational institutions, and other destinations. A subset of public transportation is urban rail transit systems. It involves the use of electrically powered rail cars that operate on a fixed track, often both within and between urban areas. Some examples of this transportation mode include tramways, monorails, subways.

Among the various modes of urban rail transit systems, the subway specifically has gained widespread popularity due to its speed, capacity, and reliability. In fact, according to the 2021 statistics brief published by the International Association of Public Transport [UITP 22], subway systems observed a significant increase in ridership, carrying 58.2 billion passengers worldwide in 2019 as compared to 43 billion passengers in 2012.

The first subway system was established in 1890 in London and by the end of 2020, subway networks were presented in 193 cities, with a total of 731 lines over a length of 17,000 km and 13,000 stations [UITP 22]. Asia has emerged as the dominant region in terms of length and ridership. The region accounts for 71% of the world total subway network length, with China alone operating nearly 40% of the global subway network [Mao 21]. Similarly, Asian cities account for 64% of the world total subway ridership, with cities like Beijing, Shanghai, and Tokyo carrying more than 10 million passengers daily [Shixiong 22] [Killada 18].

Apart from Asia, Europe and America also have a significant share in the global subway market. In Europe, subway systems are widespread and well-integrated, with many cities having multiple subway lines and stations. Europe has one of the highest densities of subway networks, with the city of Paris presenting 304 stations with a total of 225 km of length [OMNIL 22]. The Americas have witnessed an increasing interest in expanding subway networks [APTA 23], with many cities investing in expanding their transport systems to meet the growing demand for public transportation [Zelaya 21].

Hence, it is notable a significant growth in public transportation ridership across various regions of the world. The reasons for this growth may vary from region to region, but some of the contributing factors may include urbanization, population growth, and rising incomes. The growth

in ridership has led to an increase in demand for more extensive and efficient public transportation systems to accommodate the increasing number of passengers [UITP 22].

Further elaborating on the role of urbanization, the world urban population has been increasing rapidly in recent years (Figure 1-1). According to the United Nations [UN 2018], more than 55% of the world population resides in urban areas, and this figure is expected to rise to 68% by 2050. With an increasing number of people relying on public transportation for their daily commutes and other travel needs, cities face the challenge of providing accessible, reliable and environmentally sustainable transit options.

**Urban and Rural World Populations**
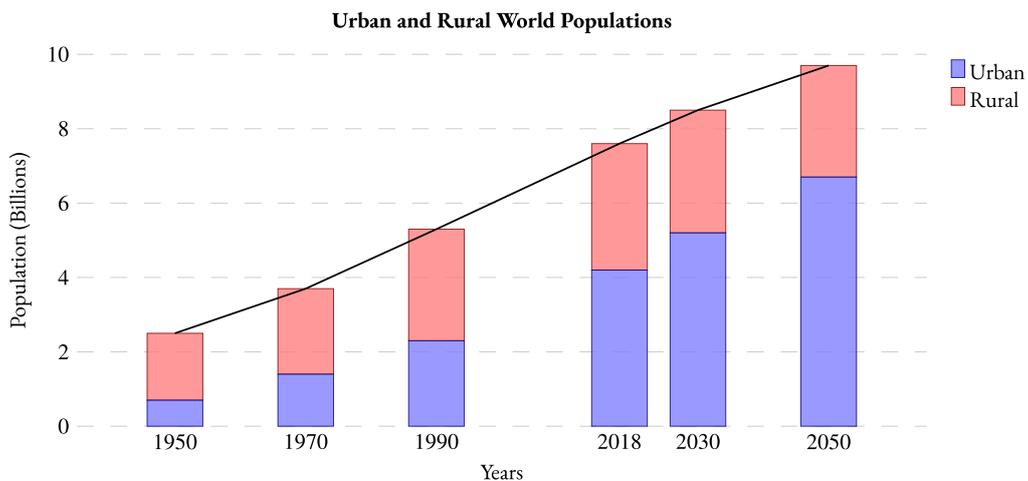


**Figure 1-1: Growth of urban and rural Population [UN 2018].**

The accelerated pace of urban life creates a higher demand among city dwellers for time efficiency, cost-effectiveness and convenience [Ceder 21]. Consequently, the appeal and success of future urban transportation is based on its ability to meet these user preferences. Given its inherent characteristics, subway systems emerge as a potential favorite mode of transportation providing reliable and economical travel.

Looking into transportation in general, to meet actual demands, its expansion has contributed to a significant environmental concern: the increase of energy-related carbon dioxide ($CO_2$) emissions. Energy-related emissions refer to the release of $CO_2$ into the atmosphere as a consequence of human activities related to the production and consumption of energy. These emissions constitute a substantial proportion of the overall global greenhouse gas emissions, accounting for approximately two-thirds of the total emissions [IEA 21]. Thus, it is vital to mitigate the adverse consequences of climate change and facilitate the transition towards a more sustainable energy system.

In 2022, global energy-related $CO_2$ emissions reached a new high of over 36.8 Gt, and transportation accounted for 23% of these emissions. The transportation sector is a significant contributor to climate change, and within this sector, the on-road traffic is responsible for most of emissions, about 75% [IEA 22a] (Figure 1-2). The use of internal combustion engines that rely on fossil fuel sources is a primary reason for the high emissions in the transportation sector [Figueroa 14]

Looking in more general form, rail-based is the least emissions-intensive mode of transport (Figure 1-2). Urban rail networks such as subway and light rail can have significantly lower emissions than other motorized urban transport modes, especially cars. In average, the global average of $CO_2$ equivalent emission per passenger kilometer of car is 148 gCO₂/pkm, while for light rail it is 19 gCO₂/pkm [IEA 22b].
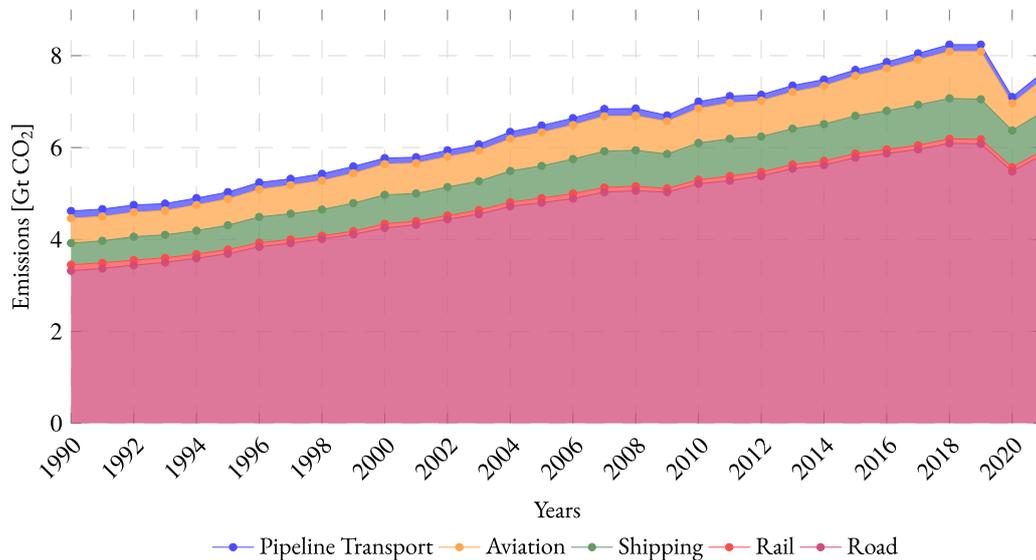


**Figure 1-2: Global CO₂ emissions from transport by sub-sector [IEA 22a].**

The data on Figure 1-2 demonstrates a significant decline in emissions between the years 2019 and 2020. This trend can largely be attributed to the COVID-19 crisis.

As a substantially electrified transport mode, urban rail transit systems have an advantage in terms of emissions and is inclined to continue to improve as the share of renewable energy in the global electricity grid continues to grow [IEA 22c] [UITP 23]. Moreover, they can help to decrease traffic congestion and associated air pollution in densely populated urban areas.

The energy intensity data for various transportation modes (Figure 1-3) reveals that rail-based transport systems exhibit low energy consumption per passenger-kilometer [IEA 18], making them one of the most environmentally friendly options. With an average of just 0.2 MJ/pkm, rail-based

transportation modes outperform not only individual vehicles like cars and motorcycles but also other public transportation methods, such as buses and minibuses. Encouraging the use of subways in urban areas can significantly reduce the overall energy consumption and GHG emissions associated with transportation.



**Energy Intensity of Passenger Transport Modes**
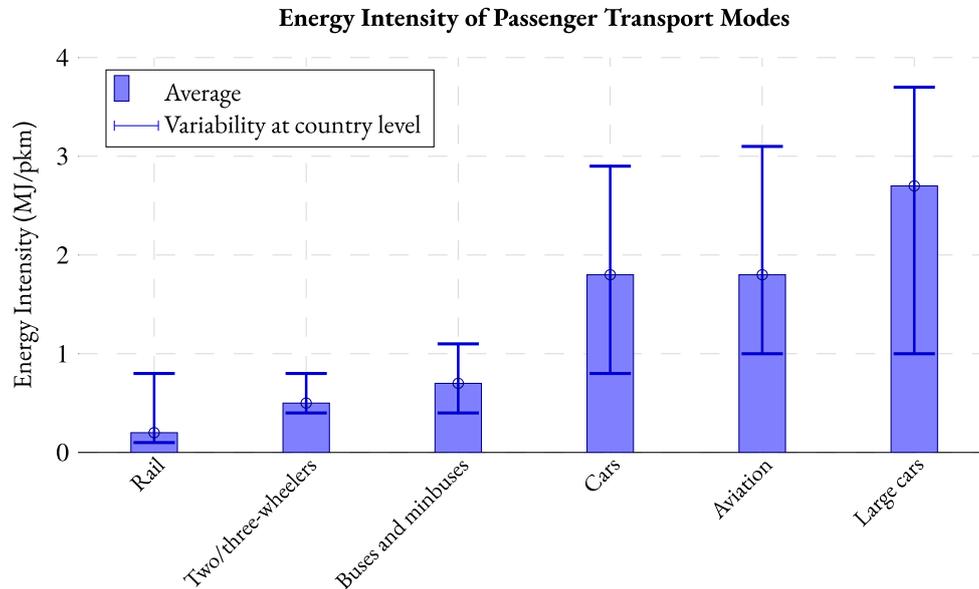
**Figure 1-3: Energy consumption per passenger-kilometer for different transportation modes [IEA 18].**

The expansion of a subway network not only consists in adding more vehicles and the construction of tracks. One of the main challenges consists in being able to provide the demanded electric power for its operation. Their location, traditionally in city centers, requires a specialized and effective power supply infrastructure. Hence, energy is a crucial factor for the operations of public transportation systems as it impacts both their operational costs and environmental impact. Despite being relatively more energy-efficient than individual car traffic, in terms of energy consumed per passenger transported, rail transport mode still represents a significant net consumer of energy. Thus, reducing energy consumption and mitigating carbon emissions in this sector is crucial to creating a sustainable city and society.

## I.2. Interest of urban rail transit systems

Efforts to reduce energy consumption and carbon emissions in the rail transport sector can take various forms. One approach focused on emissions consists of further integrating renewable energy sources into the electricity grid that powers rail systems. The increasing share of renewables in the global electricity mix can lead to a corresponding decrease in the carbon intensity of electrified rail systems. Another strategy is to improve the energy efficiency of urban rail systems themselves. This can be achieved through a combination of technological advancements,

infrastructure improvements and operational optimizations. This thesis focuses on the increase of the energy efficiency of a subway carrousel.

Modern transport systems, such as subways, trams and light rail systems, are equipped with electrical drives that ensure efficient and reliable means of transportation. These systems typically employ an electrical machine, such as synchronous machine or induction machine, coupled with a bidirectional power converter. This enables robust and reliable traction and propulsion of vehicles.

Regenerative braking capability is a natural and highly beneficial consequence of electrical drives in these urban transport networks. Regenerative braking refers to the process of converting the kinetic energy during the deceleration or braking of a vehicle into electrical energy. Braking energy, which would otherwise be lost as heat through conventional friction-based mechanical brakes, can instead be recovered.

The proper management of regenerative braking in urban transport systems provides significant benefits, including reduced energy consumption, lower operational costs, minimized wear on mechanical components. It also includes decreased environmental impact with reduction of fine particle emissions. As a result, these operations contribute to the development of sustainable and efficient public transportation solutions in urban environments.

The subway network relies on traction power substations (TPSs) to provide the necessary power for its operations. The TPSs are strategically located along the subway lines, ensuring efficient power distribution and minimization of transmission losses. The typical TPS topology consists of a transformer and a diode bridge, which provides a robust and reliable power supply when compared to other configurations that utilize controlled power electronics. However, this design also comes with a non-reversible characteristic (Figure 1-4).

One of the challenges faced by the subway network is the management of regenerative braking energy. In terms of technical operation, when a subway train decelerates, the regenerative braking energy can cause an increase in the rail DC voltage. This is observed in the absence of other accelerating vehicles or sufficient auxiliary loads to consume the surplus energy. This situation can become even more critical if multiple vehicles are braking simultaneously.
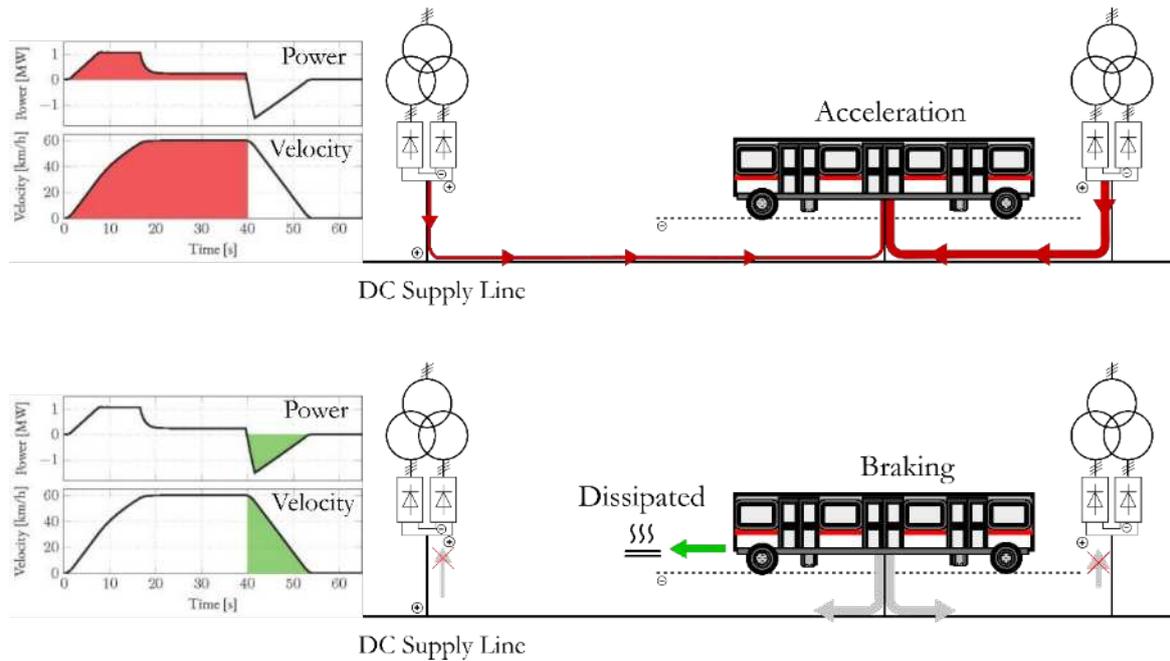
**Figure 1-4: Subway line regenerative braking energy limitation.**

To prevent potential damage to sensitive equipment, the subway system employs braking resistors or mechanical brakes to dissipate the excess energy in the form of heat. This event functions as a safety mechanism, ensuring that DC voltage is limited to a predetermined maximal value. While this solution effectively manages the surplus energy, it also results in a reduction of the overall system efficiency. This is because the energy that could have been harnessed, redistributed, or stored for future use is instead dissipated in the form of heat.

The increased interest in energy efficiency improvement for subway systems has led to a rise in demand for research in this field. Both academia and companies are exploring various strategies, such as optimizing train operations, adopting energy-efficient technologies, and implementing energy storage systems, to reduce energy consumption and associated emissions [Khodaparastan 19a]. In addition to technological advancements, policy measures and incentives are also being developed to promote energy efficiency in public transportation systems [Givoni 13].

In conclusion, the improvement of energy efficiency in subway systems has become an essential aspect to consider when planning for sustainable urban transportation. By enhancing energy efficiency, it is possible to mitigate the environmental impacts of subway system expansion. A more efficient system can support a larger network while maintaining the same level of energy consumption. This not only helps to reduce the carbon footprint of urban transportation but also contributes to an improvement of economical sustainability and operational affordability.

## II. Energy savings solutions for light rail transit system

As previously mentioned, urban rail transit systems have the potential to recover significant energy during braking phases. This energy, instead of being wasted as heat, can be utilized immediately by other trains, stored for later use, or fed back into the power grid. In general, solutions concentrate their efforts to improve line receptivity. This concept refers to the ability of a supply line to absorb the energy from a braking vehicle.

Overall, implementing energy-saving solutions has the potential to reduce urban rail energy consumption [González-Gil 14]. Many solutions are well established and have shown up to 40% of energy could be saved [Barrero 08]. These solutions include optimizing train timetables, implementing energy storage systems and installing reversible substations. Each method has its own advantages and challenges and their effectiveness varies depending on the specific characteristics of the rail transit system.

Recovering braking energy in electric rail transit systems is complex but crucial. It involves considering various parameters, including electric network characteristics, types of vehicles used, and timetables. Selecting the right energy recuperation technique requires a complete understanding of these parameters. This section aims to explore to provide a comprehensive overview of energy-saving solutions for urban rail transit systems.

### II.1. Driving and timetable optimization

Timetable optimization is the strategic planning of vehicles schedules. It can improve passenger service by reducing waiting times and ensuring better synchronization of multimodal transportation network [Hassannayebi 16] [Wei 17]. Additionally, it can contribute to the energy efficiency of the system by prioritizing energy transfer between vehicles (Figure 1-5).

The direct transfer of energy between a braking and acceleration vehicle results in the reduction of energy demand from TPSs for traction purposes. However, synchronizing this energy transfer is challenging due to the complexity of subway line operations. This solution does not require the implementation of additional devices such as electronic converters. Hence, if the goal is to maximize the recovery of regenerative energy, priority should be given to facilitating energy exchange between trains on the DC side of the power network [Khodaparastan 19a].
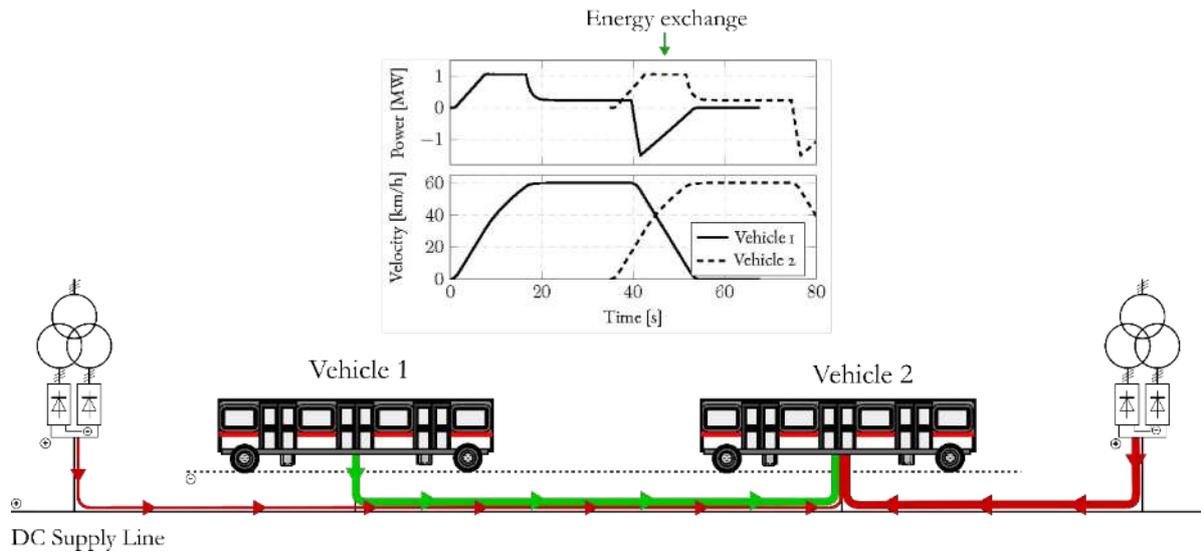
**Figure 1-5: Energy exchange in acceleration and braking phases.**

The advent of advanced technologies and methodologies, such as deep reinforcement learning, linear programming, and dynamic programming, has significantly contributed to the development of energy-saving solutions. For instance, the cooperative train control strategy proposed in [Liu 17] aims to reduce energy consumption by considering the interactions between trains. This cooperative control strategy leads to a more energy-efficient operation, demonstrating the potential of cooperative systems in energy-saving solutions. About 19% reduction of energy consumption is observed in the paper.

The work developed in [Mo 20] presents an integrated model for optimal train scheduling and rolling stock circulation planning. The objective is to maximize regenerative energy use and turn-around operations, reducing overall costs. The model also considers the passenger dynamics demand. Its results show its capability of providing a better balance between brake-traction time synchronization and operating cost. Regenerative energy utilization is based on overlapping time of acceleration and braking phases. However, it does not consider the dynamics of the input filter DC bus voltage.

In [Shang 23] an energy-saving train operation approach based on multi-agent deep reinforcement learning is presented. Each agent in the system represents a train, and through interaction with the environment and feedback, the agents learn to operate the trains in an energy-efficient manner. The findings indicate that the suggested method can successfully enhance energy efficiency.

Timetabling scheduling is a critical aspect of energy-saving solutions. The study realized in [Barrena 14] revolves around the non-periodic timetabling of single-line rail rapid transit under

16

dynamic passenger demand. The model takes into account the dynamic nature of passenger demand, leading to more efficient and energy-saving operations.

The work in [Caimi 17] concentrates on timetable design. It discusses various models for railway timetable optimization and its application in practice. The authors provide a detailed analysis of different models and discuss their strengths and weaknesses, providing valuable insights for practitioners. Its results indicate that the various models presented in existing literature satisfy the diverse objectives of different line operators.

The study by [Liu 19] presents a timetable optimization model that maximizes the utilization of regenerative energy using as decision variables the headway time and dwell time. Numerical experiments are conducted based on real line data showing the potential of significant energy savings. In [Yin 21] and [Yuan 22], a mathematical model aiming to reduce station congestion during peak-hours by simultaneously creating the best coordinated train schedules is presented. The dynamic passenger demand and integrated rolling stock assignment and short-turning strategy are considered.

The integration of multiple aspects of train operation into a single optimization model is a trend in the field. For example, the study in [Huang 16] presents a bicriteria train scheduling approach that optimizes both energy consumption and service quality. This approach leads to a more balanced and efficient operation, demonstrating the effectiveness of multi-objective optimization in energy-saving solutions.

Similarly, a dual-objective optimization approach for maximizing rail potential and minimizing total energy consumption in multi-train subway systems is the focus of the study in [Zhu 21]. The model optimizes both objectives simultaneously, leading to improved operational efficiency and energy savings. Its results indicate a reduction of 22% in total energy consumption.

In terms of velocity profile adaptation, the work in [Dominguez 12] discusses energy savings in metropolitan railway substations through braking energy recovery and optimal design of Automatic Train Operation (ATO) velocity profiles. A velocity reference is generated with the goal of improving regenerative energy. Up to 11% of energy savings is observed conserving passenger service quality.

A robust and energy-efficient train timetable for the subway system is presented in the work of [Liu 20]. Their model optimizes the train timetable considering both robustness and energy

efficiency, leading to a more reliable and energy-saving operation. Peak-hours and the propagation delay are considered.

The use of approximate dynamic programming to maximize regenerative energy utilization for subway is explored in [Xun 20]. The proposed approach adjusts the speed curve of the accelerating train in order to prioritize the energy transfer between accelerating and braking trains. Numerical results indicate an increase in regenerative energy utilization of more than 30%.

Deep reinforcement learning is applied in the optimization of ATO control, as demonstrated in [Chen 23a]. A real-time driving strategy is implemented according to the train operating state and environment. Simulation results show that the proposed control method reduces energy consumption by 12%. A comparison with traditional PID methods [Chen 19] is realized. No experimental validation is realized.

Many approaches are observed in literature. Different algorithms and strategies are employed to tackle the timetable optimization problem. Each technique is adapted to an application case. It can be noted that multiple variables such as velocity profile, departure time and headways can be modified to achieve the desired goal. The application of multi-objective optimization is commonly observed; however, the reduction of energy consumption remains a crucial goal.

There is still room for further research and development in this field, especially in terms of developing a framework with more efficient and robust models. The existing literature on timetable optimization for subway systems has several limitations that this thesis aims to address. Firstly, many studies simplify or neglect the rail supply line, treating it as a single ideal conductor. This simplification can lead to inaccurate estimations of energy consumption and utilization of regenerative braking energy.

Additionally, a significant limitation in the existing literature consists in neglecting the dynamics of the filter capacitor. Many studies, such as those employing dynamic programming, ignore this crucial component. The filter capacitor plays an important role in the system operation, as its voltage is a key variable in determining the system functionality [Mayet 16a].

Furthermore, most models employ a backward approach, considering all velocity profiles as possible, despite the presence of mechanical and electrical limitations. This can result in inaccuracies in energy consumption estimation and prevent the system from reaching the desired final position [Mayet 18].

The implementation of a carousel subway timetable presents significant challenges due to the unpredictable nature of incidents and delays, such as door blockages by users. These incidents can significantly alter the expected results. These unforeseen circumstances can lead to substantial deviations from the planned timetable, causing a ripple effect of delays throughout the entire subway system. Therefore, a realistic solution must be capable of considering these potential delays and adapting the timetable accordingly. This adaptive approach requires the integration of robust and flexible scheduling algorithms that can dynamically adjust to real-time conditions.

## II.2. Role of energy storage systems

Energy Storage Systems (ESSs) have emerged as a pivotal component in the efficient operation of light rail transit systems. They play a crucial role in harnessing braking energy, thereby enhancing the overall energy efficiency and sustainability of these transit systems. This section focuses on the role of ESSs, centering on onboard and wayside storage systems. Additionally, it offers insights into the advancements in this domain as evidenced by recent research studies. When exploring the utility of ESSs, different applications become apparent, including power peak reduction, catenary-free operation, and line voltage support.

II.2.a. Onboard Energy Storage Systems

Onboard energy storage systems are installed directly in the transit vehicles (Figure 1-6). They are designed to capture and store the energy recovered during braking phases directly in the vehicle. This energy can then be reused during traction phases, reducing the overall energy consumption from the supply network [Allègre 10a]. In [Drabek 11], the practical application of electrical energy storage systems in industry, including transport vehicles and power engineering systems, is discussed. The work highlights the importance of ESSs in balancing the supply and demand of energy, thereby improving fuel economy and reducing carbon emissions. A potential to reduce carbon emissions by up to 30% is indicated.

The study in [Cheng 18a] proposes an energy management strategy for an onboard hybrid energy storage system for light rail vehicles, which optimizes energy usage and enhances the efficiency of the system, resulting in 10% improvements in energy savings.
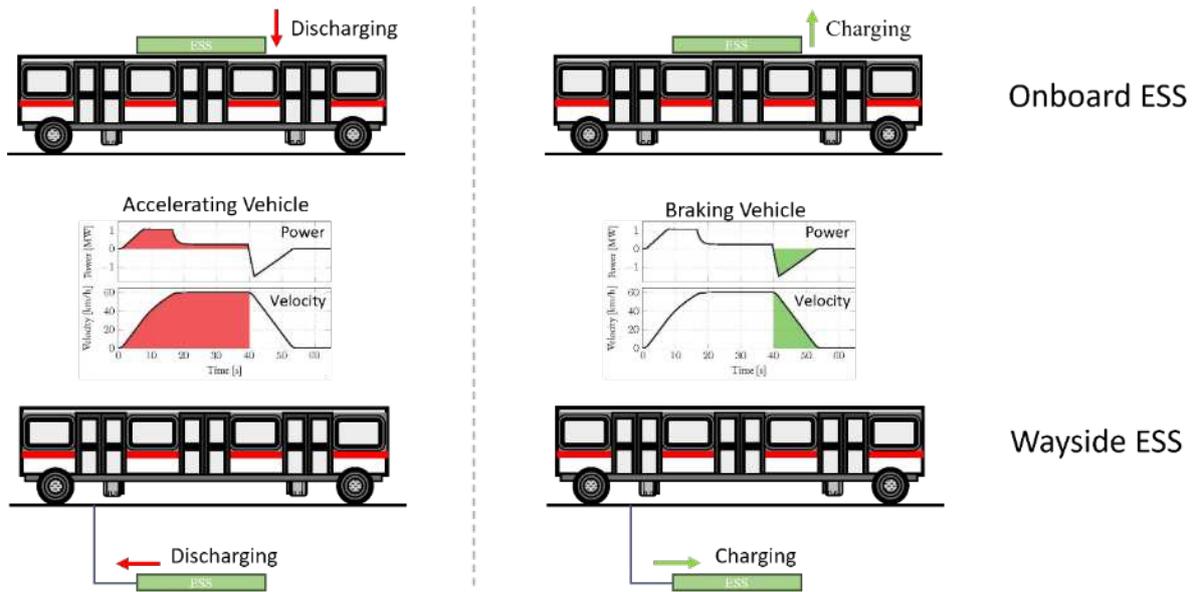
**Figure 1-6: Onboard and wayside ESS devices.**

Further, the research in [Cheng 18b] introduces the concept of fast-swap charging with the aim of reducing operational costs in light rail networks. This method involves a catenary-free operation where onboard ESSs are charged at optimal moments. The proposed Fast-Swap Charging approach presents an improvement of 18% on energy-associated costs, compared to traditional Catenary-Free Fast Charging methods.

The approach presented in [Meng 22] has the objective to minimize the net hydrogen consumption by co-optimizing both train speed trajectory and onboard energy management using a time-based mixed linear programming model. The study highlights the importance of ESSs in reducing net hydrogen consumption and improving the energy efficiency of fuel cell hybrid trains, achieving a 20% reduction in net hydrogen consumption.

II.2.b. <u>Wayside energy storage systems</u>

Wayside storage systems are also designed to capture and store the excess energy generated during vehicle regenerative braking. However, it is stationary and placed on supply line level. The integration of ESS in light rail transit systems offers a promising pathway towards enhancing energy efficiency and sustainability. Both onboard and wayside storage systems play complementary roles in harnessing regenerative braking energy and optimizing energy usage [Ramsey 21] [Yang 17] [Allen 21]. As research in this field continues to evolve, it is anticipated that further advancements in ESS technology will drive significant improvements in the operation and performance of light rail transit systems.

The study in [Khodaparastan 19b] explores the application of energy storage technologies, specifically flywheels and supercapacitors, in electric rail transit systems. These technologies are employed for various applications including peak demand reduction, voltage regulation, and energy saving through the recuperation of regenerative braking energy. Both technologies were found capable of reducing the peak demand by 10%. The study also includes a cost analysis to provide initial guidelines on the selection of the appropriate technology for a given transit system.

In [Dutta 20] a dual-stage modeling and optimization framework is presented to obtain an optimal combination and size of wayside energy storage systems for application in DC rail transportation. The research provides valuable insights into the optimal utilization of wayside ESSs, contributing to energy saving, voltage regulation, peak demand reduction, and system resiliency, with potential energy savings of up to 25%.

The impact of wayside and onboard ESSs supporting the DC railway infrastructure, on the bus voltages and branch currents of the AC grid, is investigated in [Graber 22]. The research provides a comprehensive understanding of the interaction between ESSs and the AC power grid, highlighting the importance of ESSs in maintaining the stability and efficiency of the power grid. A potential to reduce voltage fluctuations by up to 20% is observed.

Similarly, most of the works are based on a backward approach where the dynamics of the DC bus voltage and rail supply line are neglected. In fact, the DC bus voltage variable is crucial to determine the control strategy for charging and discharging phases of the ESSs [Grbovic 11]. The causal approach applied to this thesis highlights the system model development in such a way that the DC bus voltage is considered. Hence, ESSs charging and discharging rules can be correctly implemented and analyzed.

## II.3. Reversible substations

Reversible substations, also known as regenerative substations, represent a transformative technology in the field of urban rail transit systems. These substations harness the regenerative braking energy produced by trains, sending it back to the AC grid. This process enhances energy efficiency and reduces the overall carbon footprint of the rail transit system. The topology of reversible substations often involves a parallel configuration with traditional diode rectifier, offering robustness and facilitating the integration in existing infrastructure (Figure 1-7).
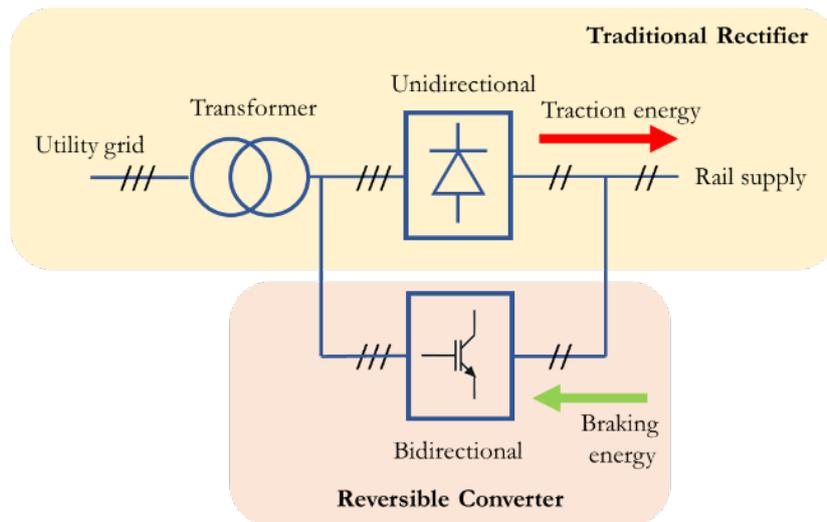
**Figure 1-7: Reversible substation traditional topology.**

The incorporation of reversible substations has been analyzed [Mohamed 17]. This work highlights the importance of advanced control strategies and power electronic devices in the operation of these substations. The authors propose an algorithm based on the Current Injection Method for the solution of DC rail networks composed of both reversible and non-reversible substations.

[Kleftakis 19] investigated the technical challenges associated with the integration of reversible substations into existing rail transit systems. key issues such as power quality, system stability, and safety require appropriate design and control strategies.

Another work, [Arboleya 18] presents a comprehensive set of steady-state models for power flow simulation studies of DC railway networks. Their work provided a detailed discussion on different types of substations connecting the AC distribution system with the DC traction system. This research underscored the potential of DC traction systems in various railway transportation systems and highlighted the reluctance of railway power system operators to include new technologies based on controlled power electronic devices and storage systems.

The potential of reversible substations to improve the power quality of the grid has been demonstrated in [Hao 20]. The research shows that these substations can significantly reduce voltage fluctuations and harmonic distortions, contributing to the stability and reliability of the power grid. This work further emphasized the broader benefits of reversible substations beyond energy efficiency.

The energy-saving potential of reversible substations has been explored in [Hao 21]. The work proposes an innovative control strategy for these substations, which optimizes the energy

recovery process. The work validates the proposed strategy through simulation studies, showing promising results in terms of energy efficiency and cost.

The study in [Cascetta 21] provides an in-depth understanding of the practical application of reversible substations in urban rail transit systems. The study presents the results of a measurement campaign conducted on a train operating on the metro line serving the city of Madrid, where a reversible substation has been installed. The installed measurement system allowed for accurate measurements of the energy flows and losses. The monitoring has been performed both when the substation acted as reversible and when it operated in a traditional way. The comparison provided valuable insights into the impact of these technologies in a real application. A new index is introduced to quantify the line unavailability to receive energy. The average value of this index can be reduced from 22% to 16% with the application of reversible substations.

In [Chen 23], it is presented a comprehensive study on the application of reversible substations in urban rail transit systems. The work highlights the significant energy-saving potential of these substations, demonstrating how they can effectively utilize the regenerative braking energy of trains. The work concludes that the implementation of reversible substations can lead to substantial reductions in energy consumption and $CO_2$ emissions.

Again, the dynamic of the DC bus is presented as a critical variable. The fluctuation of the voltage along the supply systems direct impacts on the control law for activation of the reversible substations. Most references neglect this variable, which implicates misestimation of the energy flow.

## III. Reference case: the subway of European Metropole of Lille

### III.1. Lille Metropolis transport network

The Lille Metropolis is a key economic hub renowned for its strategic location, robust transport infrastructure and dynamic economy. Its proximity to European decision-making centers such as London, Paris, Amsterdam, Brussels and Luxembourg make it a favored destination for foreign investors. Hence, mobility is a key factor for not only the quality of life of citizens but also it implicates direct economic impacts.

The transport network in the region of Lille is supervised and managed by an administrative entity known as the Métropole Européenne de Lille (MEL). The MEL serves a conglomerate of 95 municipalities. With a collective responsibility towards the welfare of approximately 1.2 million

inhabitants, as per the 2018 census [INSEE 18], the MEL performs its role of local governance and self-administration.

The area under MEL jurisdiction covers over 672 km² within the North department. It presents a mixture of urban and rural landscapes. This fusion of geographical and socio-cultural diversity features large active cities along with smaller villages. Six of the MEL communes, namely Lille, Tourcoing, Roubaix, Villeneuve d'Ascq, Wattrelos and Marcq-en-Barœul, concentrate approximately 50% of the MEL population. Lille is the most populous of these, housing more than 230,000 inhabitants, thus serving as the heart of MEL.

MEL exercises jurisdiction over several crucial spheres, including territorial and social development, spatial planning, sustainable development and quality-of-life enhancement. As the 4th agglomeration in France, behind only Paris, Lyon, and Marseille, the metropolis is a major player in the French urban landscape. Furthermore, it holds the second rank in terms of population density, highlighting the significant human activities and interactions within its jurisdiction.

Every day, MEL witnesses a high level of mobility, with approximately 5 million ridership across all modes of transport. One of its key duties is to ensure that all inhabitants of the metropolitan area can navigate the area under favorable conditions. This includes the responsibility of contributing to the reduction of atmospheric pollutants and energy consumption related to transport. To fulfill this ambition, MEL adopted its Territorial Climate Air Energy Plan (PCAET) in 2021. The PCAET is a plan for achieving carbon neutrality in the metropolitan area by 2050, outlining a comprehensive strategy for a sustainable future.

The PCAET encapsulates several key objectives aimed at transforming the metropolis into an example of sustainable living. These include accelerating the energy transition to favorize the use of renewable sources, creating a city resilient to climate change while enhancing air quality. MEL understands that the research capabilities, innovative solutions and educative influence of academic institutions can significantly contribute to these initiatives. Through such actions, MEL aims to create an inclusive future for all its inhabitants.

The MEL public transport network, known as "ilévia" since 2019, is a multimodal system consisting of:

- 6 TER lines and 1 TER Bus line (34 stations and stops),
- 2 fully automated subway lines (2 lines, 45 km, 60 stations),
- 2 tramway lines (2 lines, 22 km, 36 stations),

- over 100 bus lines (400 buses).

Traffic distribution heavily favors the subway, with it handling about 64% of the total of trips, followed by buses with 30%, and the tramway with 6%. Since the inauguration of the first subway line in 1983, the metropolitan network has experienced consistent growth in ridership. It took less than a decade for the subway to assume a dominant role in transport, securing over 50% of the total ridership by 1992.

In 2019, the ilévia network surpassed 200 million journeys. The transport demand overview is presented in Figure 1-8. Like the global scenario, local restrictions imposed due to the COVID-19 crisis are reflected in this evolution. Governmental restrictions led to a significant decrease in the number of trips between 2019 and 2020. It is also observed a fast-recovering trend back to normal levels after the year 2020.
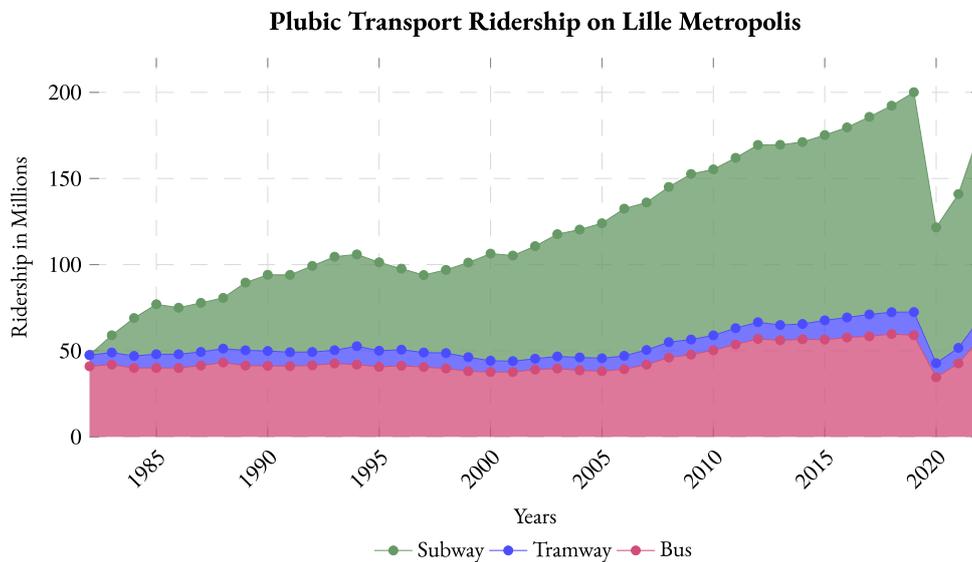


**Figure 1-8: Evolution of the use of public transport in MEL (source: MEL – Réseau ilévia).**

## III.2. Lille subway lines

In terms of subway line, the ilévia network possesses a fully automated system distinguished by its train dimensions (2m wide, 26m long). It presents one of the world highest vehicle frequencies (66 seconds during peak-hours). It operates a rubber-tired subway system, offering superior traction and noise reduction. The line presents closely spaced stops that require good acceleration and braking. The vehicles are powered by a 750V standard supply line, collected through brushes located on the two lateral guide rails, commonly named as third rail.

25

The current fleet comprises VAL[1]-type trains built by Matra (now Siemens Transportation Systems), as presented in Table 1. By 2025, ALSTOM-designed double-length trains (52 meters) are planned to be introduced in Line 1 and called NMR[2]. The goal is to increase passenger transport capacity while also increasing the interval between vehicles. In this sense, MEL presents a solid transportation network that is constant expansion to anticipate the increasing ridership demand.

**Table 1. Subway fleet in Lille, France (source: MEL).**

|  | **VAL206** | **VAL206Bis** | **VAL208** |
|---|---|---|---|
| Year of commissioning | 1983 | 1987-1989 | 1999 |
| "Comfort" capacity | 154 | 154 | 156 |
| Maximum Capacity [# of passengers] | 208 | 208 | 210 |
| Total fleet | 38 | 45 | 60 |
| Assignment Line 1 (yellow) | 0 | 0 | 53 |
| Assignment Line 2 (red) | 38 | 45 | 7 |

This PhD thesis is inserted the context of the integration of this new subway vehicle into the existing transit system. A MEL project entitled "52 m" (length of the new vehicle), has been conducted. Besides vehicle modification, the project also involves infrastructure development. The modernization of subway passenger stations and the resizing of the TPSs are also performed. The implementation of the new subway system presents an opportunity to conduct research studies that focus on the evaluation of energy-saving potential of this new vehicle. Figure 1-9 illustrates the actual and new vehicle.
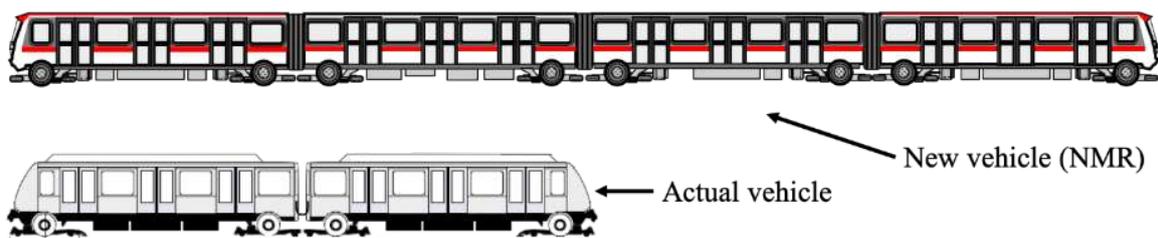


**Figure 1-9: Subway Vehicle Comparison.**

---

[1] Initially "Villeneuve d'Ascq Lille", then "Véhicule Automatique Léger" – (Light Automated Vehicle)

[2] « Nouveau Matériel Roulant » as transient name before exploitation

A correlated outcome of a scenario with increasing ridership demand involves a corresponding rise in energy consumption. In this sense, it is well observed that electricity is a vital resource for providing public transport services throughout the metropolis. Since 2019, MEL has been engaged with initiatives to optimize its electricity consumption for its rail transit systems and its future electric buses (battery and hydrogen powered). MEL sees innovation as a crucial area of focus and aims to make scientific research a strategic guidance for the metropolis.

A key aspect of MEL energy-saving strategy lies in the implementation of innovative solutions to improve the energy efficiency of its public transport systems. These could include the study of energy storage subsystems, reversible power supply stations and the optimization of energy consumption, particularly through the recovery of braking energy. The MEL initiative to reduce the energy consumption of its transport systems, despite their already low energy usage, underscores the commitment to finding innovative solutions to further diminish the environmental impact.

The future of public transportation in MEL is promising, with the potential for significant energy savings and improvements in energy efficiency. The MEL commitment to advancing these goals, coupled with the implementation of new technologies, plays a crucial role in transforming the subway system footprint. By prioritizing energy efficiency and flexibility on subway transportation mode, MEL is setting a powerful example for other metropolitan areas worldwide.

## III.3. CUMIN-REMUS project

The CUMIN (Campus of University with Mobility based on Innovation and carbon Neutrality) program is an innovative and ambitious initiative launched in 2016 by the University of Lille, in France. The primary objective of this program is to transform the university campus "Cité Scientifique" into a carbon-neutral environment [CUMIN 23]. This transformation is particularly significant considering that the mobility of users is the most substantial contributor to the campus Green House Gas (GHG) emissions. It accounts for 56% of the total emissions. Figure 1-10 presents the GHG emission in the campus "Cité Scientifique" of University of Lille for 2014.

CUMIN is an interdisciplinary program composed of various research groups from different disciplines to focus on projects tied to electro-mobility. It brings together electrical engineering skills from L2EP, mechanical engineering skills from LaMcube, emission analysis skills from LOA, socio-economics skills from CLERSE, scientific communication shills from GERIICA, and urban planning skills from TVES, fostering an interdisciplinary approach.
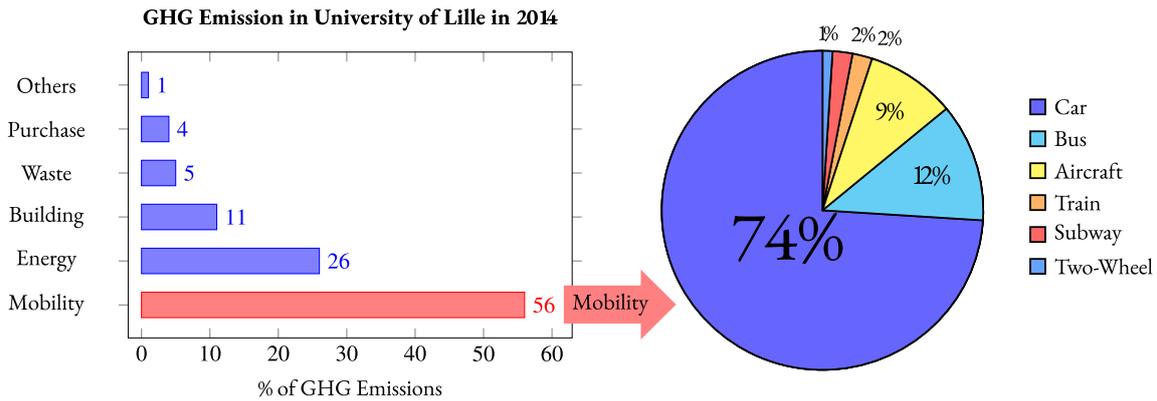
**Figure 1-10: GHG Emissions in the university of Lille and Mobility Emissions.**

Even though only 23% of home-university commuting trips are made by car, these are responsible for 74% of mobility-related GHG emissions. Hence, the CUMIN program aims to address this issue by progressively replacing thermal cars used on campus with electric vehicles [Bouscayrol 17]. Electric vehicles can be powered by renewable energy sources energy, thus significantly reducing the campus carbon footprint. This approach aligns with the global shift towards renewable energy sources and the reduction of GHG emissions.

The University of Lille campus "Cité Scientifique", with its 110 hectares and 78 buildings serving 22,000 users (about 20,000 students and 2,000 staff and faculty members), can be considered as a small city. This campus, with its unique characteristics and complexities, serves as an ideal demonstrator for the development of future eco-cities.

The "Cité Scientifique campus" has the unique benefit of having a portion of Line 1 subway that cross its area (Figure 1-11). On campus there are two stations, the *Cité Scientifique*, and the *4 Cantons*, with the latter also functioning as the terminal station for this line and hub for buses. This particular configuration presents the possibility of merging the efficient utilization of the subway braking energy with the growing demand for electric vehicle charging stations.

To this end, MEL and the L2EP have continued their partnership, with a concrete first application within the CUMIN program demonstrator: the REMUS project for "Recovery of Metro Braking Energy for a Sustainable University" [MEL 19]. Hence, launching the MEL plans to rely more on research to enhance the energy efficiency of its rail transit system. This PhD thesis is developed within the framework of the REMUS project.

This project focuses on enhancing the energy efficiency of MEL subway system. Hence, the project is contributing to the development of an e-mobility-based campus with the combination of

the utilization of regenerative braking energy on campus. The REMUS project comprises two interconnected parts:
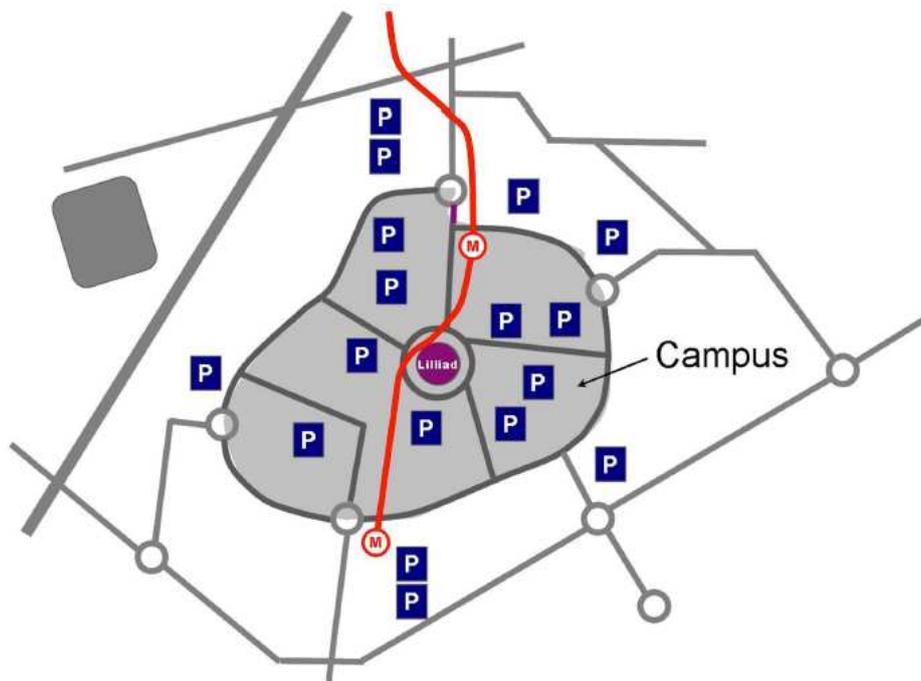


**Figure 1-11: Campus *Cité Scientifique* of University of Lille [CUMIN 23].**

1) The REMUS-Research element encapsulates a research project focused on exploiting traction energy for subway systems. The project essence is the development of an energy model for a subway carousel, incorporating the new rolling stock.

2) The REMUS-Demo part covers the improvements of a reduced-scale Hardware-in-the-Loop platform, located within the eV platform of the L2EP laboratory [Mayet 17]. It serves as a research tool for optimizing electrical consumption in a subway line. This device will 1) enable validations of simulation models that cannot be achieved on the real track, and 2) test new innovative concepts before integration on the real system.

The REMUS project aims to:

- develop a methodology for scrutinizing energy flows within guided transport systems,
- evaluate the potential for utilizing energy recovery from light rail transit systems,
- contribute to the development of the CUMIN demonstrator campus, leveraging the subway line that passes through it,
- test, consolidate, and capitalize on knowledge related to optimizing and recapturing energy from guided transport systems,
- enhance existing partnerships and forge new ones within the domain of e-mobility.

The subway system is responsible for a relatively small number of emissions when compared to other modes of transportation. This means that if more people use the subway and if its operations become even more energy-efficient, it can help in significantly reducing global emissions. The REMUS project specifically aims to focus on this aspect, working towards improving the energy efficiency of the subway system.

As the subway is one of the main modes of transport to the campus, the REMUS project targets a significant area of energy consumption and GHG emissions. Consequently, the strategies and technologies developed and implemented through the REMUS project could serve as a sustainable mobility model for other campuses and cities aspiring to reduce their carbon footprint.

In conclusion, the CUMIN program and the REMUS project represent a significant step towards sustainable mobility and carbon neutrality on the University of Lille campus 'Cité Scientifique'. Through innovative strategies and technologies, these initiatives aim to transform the campus mobility system and reduce GHG emissions. The success of these projects could serve as a model for other universities and cities worldwide, contributing to global efforts to mitigate climate change and promote sustainability.

## IV. Objective and thesis approach

### IV.1. Objective and positioning of the thesis

The objective of this PhD thesis is to propose innovative strategies for the reduction of energy consumption of subway lines and enhancing the utilization of its regenerative braking energy. This objective is aligned with the context of sustainable urban development in the Lille metropolis.

An additional contribution of the thesis is to establish the development of a Hardware-in-the-Loop (HIL) platform for multi-vehicle simulation. This platform aims to serve as a critical tool for validation of the proposed simulation tools and to study new concepts before integration in the real system.

The PhD thesis is positioned at the combination of energy efficiency research and practical application, leveraging the partnership of MEL and L2EP. This partnership has resulted in the REMUS project within the CUMIN program.

The PhD thesis is also aligned with the MEL ongoing efforts to modernize its subway system, including the introduction of new 52-meter vehicle on Line 1. This modernization presents an opportunity to conduct research studies focusing on the evaluation of the energy-saving potential of this new vehicle.

The objective is not only to contribute to the academic understanding of energy efficiency in light rail transit systems but also to provide practical recommendations for MEL and similar urban rail systems. Hence, this work aims to contribute to the creation of more sustainable and energy-efficient urban transportation systems.

Previous studies developed at L2EP servers as a base for this thesis. In [Verhille 07] the work, in collaboration with Siemens Mobility; is focused on the energetic macroscopic representation (EMR) of the subway vehicle VAL 206. This organization formalism enables a systematic controls scheme by its inversion. This work laid the foundation for further research in this field. Additional contribution consists in the development of a causal-based generation of velocity reference [Verhille 10]. The velocity profile is generated by taking into account passengers comfort constraints such as maximum jerk and acceleration values.

In the work in [Allègre 10b] special attention has been given to the modelling and energy management methodologies for mixed storage systems for electric and hybrid vehicles, in collaboration with Siemens Mobility. The importance of the use of ESSs has been presented in [Allègre 10a]. The work highlights the benefits of integration of supercapacitor in a subway system. Furthermore, it has validated the real-time control of the subway onboard storage system using supercapacitors with a reduced-scale experimental HIL arrangement using EMR [Allègre 10c].

The work in [Mayet 16a] provides the initial foundation for a flexible simulation tool for subway carousel operations in collaboration with Siemens Mobility. EMR has been employed in the model and control organizations of this system. This previous work established a solid basis for the vehicle model with interaction of several elements that constitute the subway line. This has been accomplished with the VAL 208 vehicle serving as the reference. The analysis of vehicle model simplification shows the importance of selecting an optimal model, balancing precision and computational efforts [Mayet 14]. The simplification strategy concerning the non-linearities of the TPS has been identified as crucial, forming a directive for this thesis, again emphasizing the need to consider a balance between precision and computational demands [Mayet 16b]. Furthermore, the simulation results highlighted the potential for the use of regenerative braking energy to

enhance the subway system overall efficiency. Hence, this work serves as a motivation for this thesis.

## IV.2. Thesis methodology

As in previous works, the methodology of this thesis is rooted in the EMR formalism, a graphical approach that provides a systematic way to organize functional models and develop the control structure of complex multi-domain systems. Developed in 2000 to analyze and control electromechanical systems [Bouscayrol 13], EMR has been extended over the years to cover different domains and applications [Bouscayrol 23].

### EMR principles

In the EMR, each element of the system is represented by a pictogram according to its energetic function. These pictograms can represent mono-domain or multi-domain elements, providing a clear and intuitive representation of the system energy flow.

EMR is based on the action-reaction principle. It is organized in such a way that the multiplication of exchanged variables on each pictogram quantifies the power exchanged [Bouscayrol 00]. This principle is systematically taken into account in the system organization, allowing for the systematic development of control laws. As a result, any power exchanged between two components of the system can be easily quantified.

EMR is also based on the causality principle [Iwasaki 94]. EMR element is exclusively described in integral causality. This property enables systematic deduction of control schemes. [Hautier 96]. It can be noted that the first application of EMR for a real system was the model and control of subway VAL 206 [Bouscayrol 02].

### Application of EMR on this thesis

In this thesis, the EMR formalism is applied to the model organization process, control development and energy management strategy of the carrousel system of the new MEL subway. The first step involves creating a unified organization of the vehicle model using EMR. This unified organization highlights the decomposition of the vehicle traction chain into various subsystems to be tested. Regardless of the models used for the same subsystem, this unified organization must be maintained.

The control structure is created based on the inversion principle of EMR. Finally, the mechanical braking strategy and energy management laws are defined and applied to the system according to measured variables. Model simplifications are also evaluated with the guide of EMR, in order to investigate the trade-off between accuracy and computational efforts.

## V. Conclusion

In conclusion, this chapter highlights the critical role of transportation, particularly light rail transit systems like subways, in the context of energy consumption and $CO_2$ emissions. As urbanization continues to accelerate, the demand for efficient and sustainable public transportation solutions is emphasized. Subways, with their potential for high capacity and low emissions, are uniquely positioned to meet this demand.

The chapter also highlights the challenges that subway systems face, particularly in terms of energy efficiency. The management of regenerative braking energy, for instance, is a complex issue that requires innovative solutions. When not properly managed, the surplus energy generated during the braking phase can lead to inefficiencies.

The European Metropolis of Lille is committed to addressing these challenges and is actively exploring innovative solutions. The partnership with L2EP and its expertise in energy conversion system and management are a significant asset in this work, promoting the development of research and innovation in this field. The EMR provides a clear and intuitive representation of the system energy flow, allowing for the systematic development of control laws and the quantification of power exchange between system components.

The next chapter thus aims to develop a complete model of the new subway carrousel of MEL for 1) the analysis of power flow for different operation modes, 2) the proposition of innovative concepts and solutions for saving energy.

*Chapter 2:    Modelling the subway carousel*

# I. Studied carousel

The studied carousel system consists of line 1 of the city of Lille, France. Since its inauguration in 1983 the subway vehicle type has changed a few times but all of them consist of VAL type vehicle. The new subway vehicle presents not only differences in terms of the vehicle length but also on the traction system.

The objective of this chapter is to develop a flexible simulation model for the new subway carousel of MEL. A description of the actual system based on VAL 208 vehicles is first presented. In sequence, the new vehicle characteristics are given and the modelling and control are developed using EMR for their organization. A model validation is proposed. Finally, the carousel topology is explored presenting the tradeoff between vehicle model simplifications and the methodology for a complete line simulation.

## I.1. Actual system

Line 1 of Lille is composed of VAL 208 type vehicles. It consists of a vehicle with a high level of automation. Its starting, halting, and door functions are entirely automated, eliminating the need for onboard personnel. This vehicle has been implemented to replace the VAL 206, a previous version. VAL 206 has been developed by Matra Transport, which was included later by Siemens Mobility. This company has developed VAL 208 as an extension.

In this system, each car comes with a pair of bogies. Each bogie has an LC input filter to supply both auxiliary loads and the traction subsystem. In this configuration each machine is connected to a wheel through a gearbox (Figure 2-1). The motor-wheel configuration is composed of a three-phase inverter and a permanent magnet synchronous machine. Disc brakes are employed for mechanical braking purposes. Hence, all the wheels present traction and braking capability.

Line 1 of the Lille is 12.5 kilometers long and serves 18 stations, ensuring efficient connectivity across the city and facilitating daily commutes for thousands of passengers across the metropolis. The position of each station as well as the time stop is given on Appendix B. The time to travel the line is around 23 minutes.

The VAL 208 vehicle presents a capacity of about 210 passengers. In order to meet the passengers demands, the interval between vehicles has been defined by statistical data. Different timetable models are employed to consider working days, weekends and cultural events in the metropolis. For instance, on a regular basis working day, an interval of 66 seconds is observed

during peak-hours in the mornings and afternoons. This ensures timely and frequent service for the population. This interval is close to the minimum allowed.
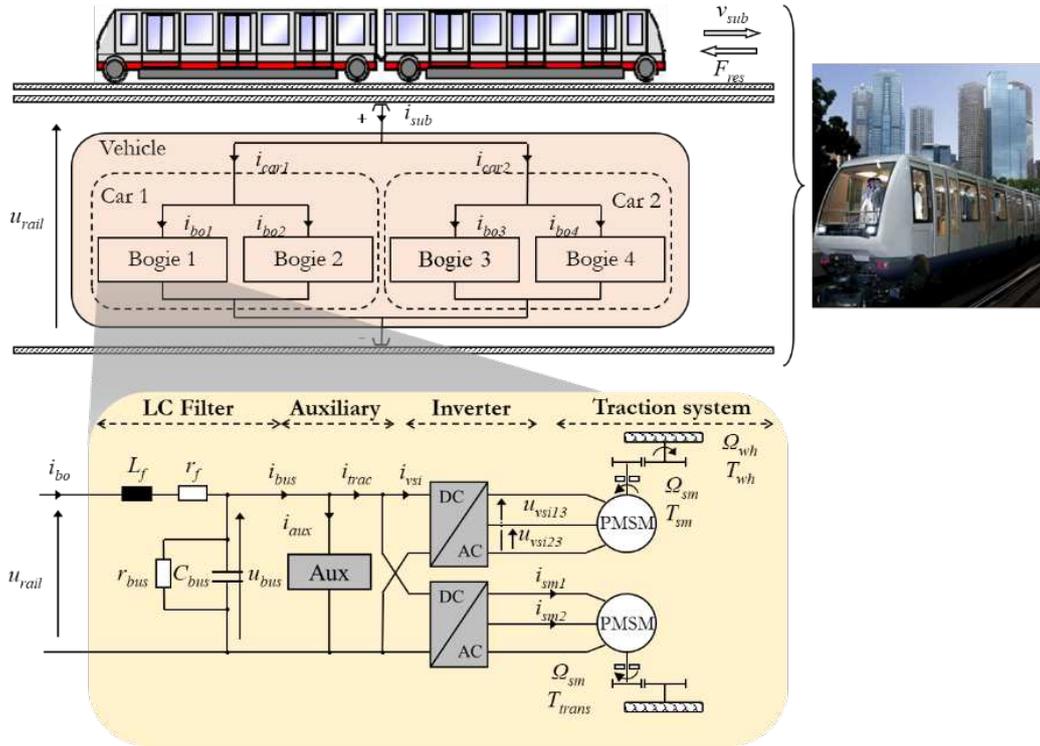


**Figure 2-1: VAL 208 traction system [Mayet 16a].**

The power supply is composed of TPSs (Taction Power Stations) that provide the required DC voltage to the system. It serves as an interface between the high voltage AC grid and the subway system. The power supply is performed by 7 TPSs that are geographically located along the line to distribute the supply power. The rectified voltage is captured by means of a third rail.

One of the characteristics of the VAL system is that the reference velocity is determined in function of the position. Located on the track level, two cables are placed crossing each other at regular intervals. This induces an electric field which is collected by the train. The distance between crossings is interpreted as the reference velocity. Finally, torque, acceleration and jerk limits are implemented in an on-board algorithm that drives the traction system [Verhille 10a].

The VAL 208 carousel system has been explored in [Mayet 16a]. A flexible simulation tool capable of estimating the energy consumption of a carousel system has been developed. An approach based on the EMR formalism has been conducted. The developed EMR of the VAL 208 is shown in Figure 2-2. The different pictograms represent each part of the system for the conversion between electrical energy and kinetic energy. A control structure is developed to impose

the assigned reference velocity. Additionally, a braking management strategy is implemented to keep the input capacitor voltage value on safety levels and enable energy recovery.
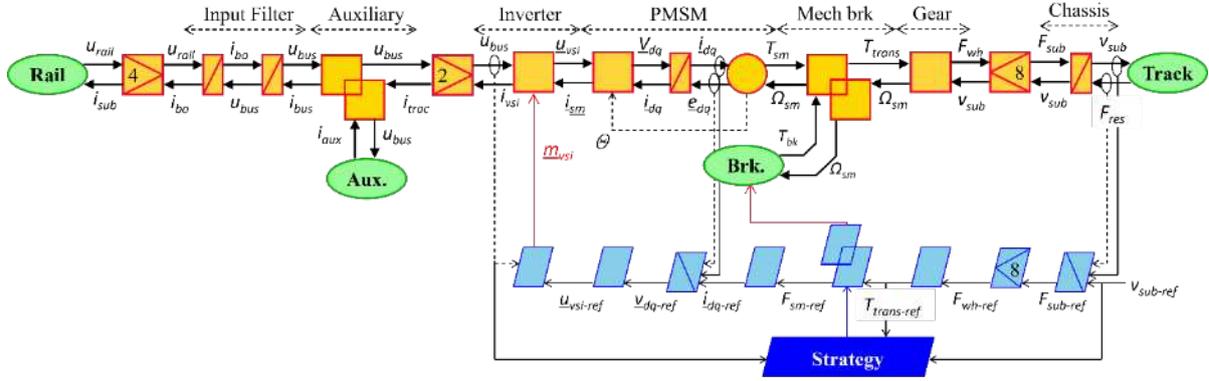


**Figure 2-2: EMR of dynamical model of the VAL 208 [Mayet 16a].**

## I.2. New system

The studied system is a new subway vehicle developed by Alstom. In this thesis, it is referred to as NMR (*Nouveau Matériel Roulant*). This subway vehicle has been developed according to the needs of the European Metropole of Lille subway network. The vehicle has a length of approximately 52 meters. It is formed by 4 cars that can be classified according to their function. It is composed of 3 driven-cars (traction cars) and 1 non-driven car (non-traction car). All 4 cars are equipped with mechanical braking.

In its design, the NMR has some dimensions similar to the VAL system. Thus, it can be fully compatible with existing line 1 infrastructures (Table 2.1). In this way, the transition between vehicles is easier and less costly due to no need to retrofit the track structure.

**Table 2. NMR Vehicle Dimensions.**

| Parameter | Value |
|-----------|-------|
| Height | 3.25 [m] |
| Width | 2.07 [m] |
| Length | 52.28 [m] |

Each car is composed of two bogies (Figure 2-3). Each bogie is responsible for supporting a pair of wheels. For traction cars, the bogie is responsible for electric traction and both electric and mechanical braking. Each traction bogie is equipped with an electric machine. The torque is divided for the wheels by means of mechanical transmission. Consequently, the vehicle has a total of 6 traction machines.

Traction machine        Mechanical brake
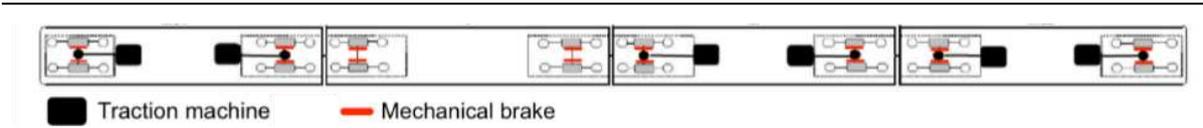
**Figure 2-3: Configuration of the NMR subway vehicle.**

In terms of electric power delivery, each traction car is connected to the supply rail through an LC filter. Every traction car is equipped with an induction machine (IM) supplied by a voltage sourced inverter (VSI). A differential gear is employed on each bogie to split the torque for a pair of wheels (Figure 2-4).
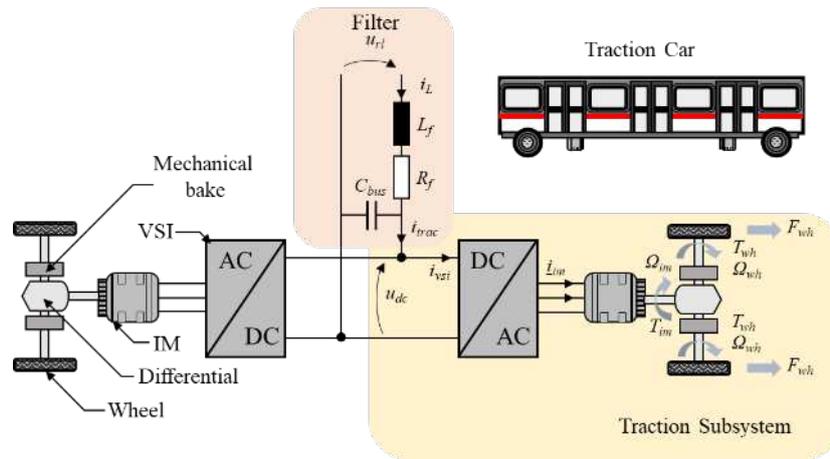


**Figure 2-4: Structure of the Traction Car.**

With the implementation of the NMR, some modifications are expected regarding the line operation. This new system is capable of transporting more passengers in a single vehicle. Hence, an increase in the interval between vehicles is possible while also increasing the passenger flow. Additionally, a margin to future reduce of interval is made possible, ensuring the meet the increasing passenger demand.

Followed by an increase in capacity, an increase in power demand is presumed. The NMR has a traction power of 1200 kW, versus 520 kW from the VAL. To ensure the correct voltage supply levels new TPSs have been constructed and connected to the existing system. A total of 10 TPSs are now present on the line. Additionally, some of the existing infrastructures have been retrofitted to increase the power capacity. The resume of the nominal power of TPSs can be seen on Appendix B.

## I.3. Model development

A subway line can be divided into three main subsystems: the vehicle, the TPS, and the supply rail. The model of the new vehicle is organized with the EMR formalism. First, the focus is on the

vehicle. Hence, it is assumed that the vehicle has a constant and stable voltage supply. The elements of the traction subsystem are presented with their respective temporal relations. The implementation of the TPS and supply rail in the model are analyzed in further sections.

For the vehicle model organization, a non-traction car imposes a path not connected to the supply rail, however, capable of imposing mechanical braking forces. Regarding the traction cars, the system is supplied by the rail which imposes a rail voltage $u_{rl}$. It is represented by a voltage source element (oval green), as in Figure 2-5.
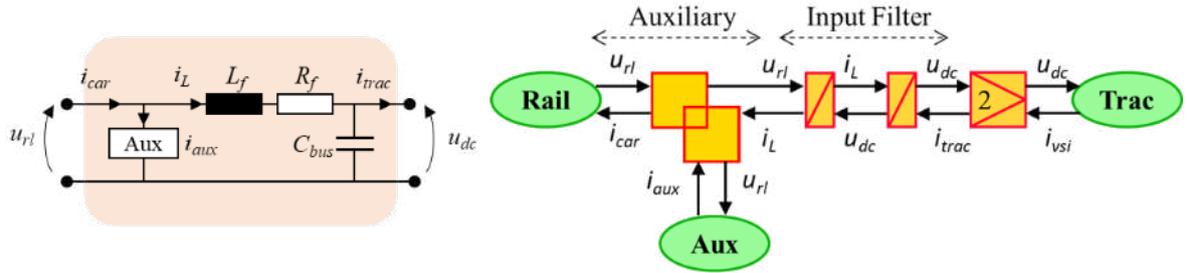


**Figure 2-5: Structural scheme and EMR of input filter and auxiliaries.**

The total car current is composed of the traction current $i_L$ and the auxiliary current $i_{aux}$. This energy distribution is depicted by a coupling element (double orange square),

$$i_{car} = i_L + i_{aux}.$$

(1)

The auxiliary current is calculated based on the auxiliary power $P_{aux}$ and rail voltage. The auxiliary power is considered as constant based on average power registered on operation,

$$i_{aux} = P_{aux} \frac{1}{u_{rl}}.$$

(2)

The input filter is composed of an inductor and a capacitor. They are depicted by 2 accumulation elements (crossed orange rectangle). The inductor current $i_L$ and capacitor voltage $u_{dc}$ are the output of theses elements as defined by the following equation, where $C_{bus}$ is the filter capacitance, $L_F$ the inductance and $R_f$ the inductor resistance,

$$u_{rl} - u_{dc} = L_f \frac{di_L}{dt} + R_f i_L$$

(3)

$$i_L - i_{trac} = C_{bus} \frac{du_{dc}}{dt}.$$

(4)

The combination of two traction subsystems per traction car is simplified by the use of adaptation element (orange square with nested triangle). In this sense, it is assumed that both traction subsystems impose the same VSI currents, hence, traction current $i_{trac}$ can be defined as,

$$i_{trac} = 2\,i_{vsi}. \tag{5}$$

The traction subsystem is responsible for the conversion between electrical energy and mechanical energy (Figure 2-6).
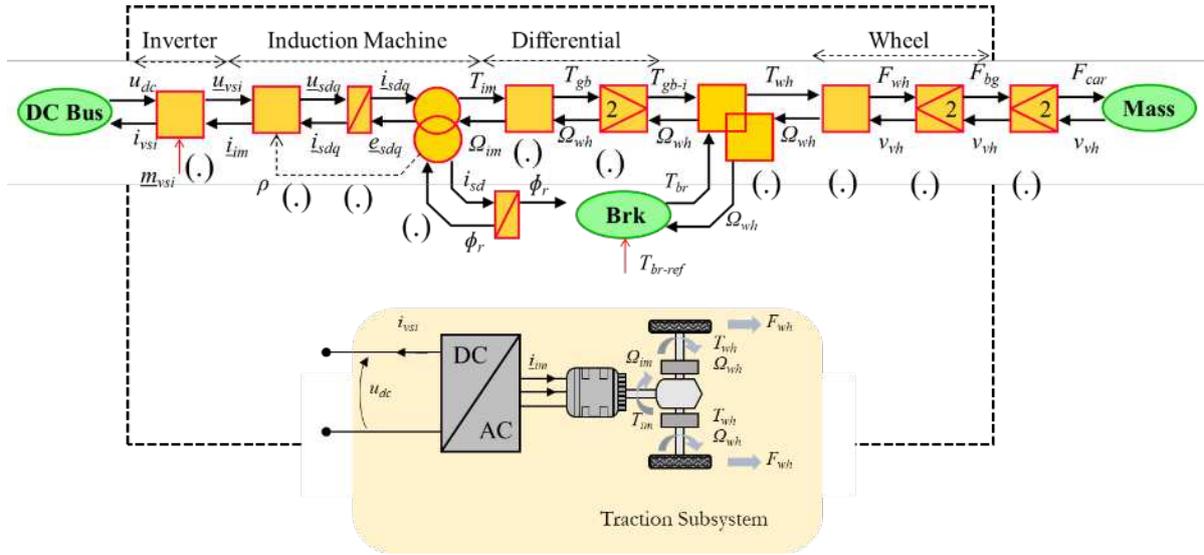


**Figure 2-6: The EMR and structure of traction subsystem.**

The VSI imposes a voltage vector $\underline{u}_{vsi} = [u_{13}\ u_{23}]^T$, which is a function of the DC link voltage and the modulation vector $\underline{m}_{vsi} = [m_{13}\ m_{23}]^T$. The VSI current $i_{vsi}$, is obtained based on the modulation vector, the machine current $i_{im}$ and the converter efficiency $\eta_{vsi}$,

$$\begin{cases} \underline{u}_{vsi} = \underline{m}_{vsi} u_{dc} \\ i_{vsi} = \underline{m}_{vsi}\underline{i}_{im}\eta_{vsi}^{\delta} \end{cases} \text{ with } \quad \delta = \begin{cases} 1, \text{ when } u_{dc}i_{vsi}\ \le 0 \\ -1, \text{ when } u_{dc}i_{vsi}\ > 0 \end{cases} \tag{6}$$

The IM is represented by four elements [Bouscayrol 15]. The first is a controlled conversion element responsible for the reference frame transformation. The machine stator voltage and currents in stationary frame are related to the rotational (d,q) frame variable ($\underline{u}_{sdq}$ and $\underline{i}_{sdq}$) according to the transformation matrix $P(\rho)$, where $\rho$ is the rotor flux angular position,

$$
\begin{cases}
\underline{u}_{sdq} = P(\rho)\underline{u}_{vsi} \\
\underline{i}_{sdq} = P(\rho)\underline{i}_{im}
\end{cases}
\quad \text{with} \quad
P(\rho) =
\begin{bmatrix}
\sqrt{\dfrac{2}{3}} \sin(\rho) & -\dfrac{\cos(\rho)}{\sqrt{6}} + \dfrac{\sin(\rho)}{\sqrt{2}} \\[2ex]
-\sqrt{\dfrac{2}{3}} \cos(\rho) & \dfrac{\cos(\rho)}{\sqrt{2}} + \dfrac{\sin(\rho)}{\sqrt{6}}
\end{bmatrix}. \tag{7}
$$

The rotational frame angular velocity can be defined as,

$$
\frac{d\rho}{dt} = \omega_{mr}. \tag{8}
$$

The stator winding is represented by an accumulation element with the stator current vector $\underline{i}_{sdq}$ as the state variable. In the rotor flux reference frame, the IM stator can be described according to the stator resistance $R_s$ and inductance $L_s$, dispersion factor $\sigma$ and e.m.f. $\underline{e}_{sdq}$,

$$
\sigma L_s \frac{d\underline{i}_{sdq}}{dt} = \underline{u}_{sdq} - R_s \underline{i}_{sdq} - \underline{e}_{sdq}. \tag{9}
$$

The electromechanical conversion is represented by the overlapped orange circle. The IM electromechanical torque $T_{im}$ and e.m.f. can be expressed in function of the currents, rotor flux $\phi_r$ and rotational speed $\Omega_{im}$. Where $k_1$ is a constant that depends on the machine characteristics, such as number of poles $p$ and rotor leakage factors $\sigma_r$,

$$
\begin{cases}
T_{im} = k_1 \phi_r i_{sq} \\
\underline{e}_{sdq} = f(\underline{i}_{sdq}, \phi_r, \Omega_{im})
\end{cases}
\quad \text{with} \quad
\begin{aligned}
& k_1 = \frac{3}{2}\frac{p}{2}\left(\frac{1}{1+\sigma_r}\right) \\[1ex]
& \begin{cases}
e_{sd} = \dfrac{L_s}{\tau_r}(1-\sigma)(i_{sd} - i_{mr}) - \sigma L_s \omega_{mr} i_{sq} \\[1ex]
e_{sq} = L_s(1-\sigma)\,\omega_{mr} i_{mr} + \sigma L_s \omega_{mr} i_{sd}
\end{cases}
\end{aligned}, \tag{10}
$$

where de current $i_{mr}$ is defined based on the relation between rotor flux $\phi_r$ and magnetizing inductance $L_m$,

$$
i_{mr} = \phi_r / L_m. \tag{11}
$$

Finally, for the IM, an accumulation element is used to represent the machine rotor flux $\phi_r$. This variable is expressed as a function of the stator current d-component, rotor time constant $\tau_r$ and magnetizing inductance $L_m$,

$$
\tau_r \frac{d\phi_r}{dt} = -\phi_r + L_m i_{sd}. \tag{12}
$$

The machine is connected to the differential gear, which is represented by a conversion element. The differential gear torque $T_{gb}$ and rotational speed $\Omega_{wh}$ are expressed according to the ratio $K_d$ and its efficiency $\eta_d^\delta$,

$$\begin{cases} T_{gb} = K_d \eta_d^\delta T_{im} \\ \Omega_{im} = K_d \Omega_{wh} \end{cases} \text{ with } \delta = \begin{cases} 1, & \text{when } T_{im}\Omega_{im} > 0 \\ -1, & \text{when } T_{im}\Omega_{im} \leq 0. \end{cases} \tag{13}$$

Moreover, it is assumed that the torque is divided equally for both wheels. Thus, an adaptation element is used to represent the individual side torque $T_{gb-i}$. The mechanical brake is represented by a source element that imposes the torque brake $T_{br}$. They are considered ideal, hence, there is no delay between reference and the applied value,

$$T_{br} = T_{br-ref}. \tag{14}$$

Furthermore, a coupling element is used to represent the combination of traction and brake torque, which results in the wheel resultant torque $T_{wh}$,

$$\begin{cases} \Omega_{wh} \text{ common} \\ T_{wh} = T_{gb-i} + T_{br}. \end{cases} \tag{15}$$

The wheel is represented by a conversion element. It expresses the traction force $F_{wh}$ and subway velocity $v_{vh}$ according to the wheel radius $R_{wh}$. It can be noted that the slipping phenomena is neglected as it does not significantly impact the energy consumption results [Verhille 07],

$$\begin{cases} F_{wh} = \dfrac{1}{R_{wh}} T_{wh} \\ \Omega_{wh} = \dfrac{1}{R_{wh}} v_{vh} \end{cases}. \tag{16}$$

The number wheels (two per bogie) and the number of bogies (two per car) determines the traction car force $F_{car}$,

$$F_{bg} = 2\, F_{wh} \tag{17}$$

$$F_{car} = 2\, F_{bg}. \tag{18}$$

The non-traction car is described similarly to the traction car, considering the fact that no traction subsystem is presented (Figure 2-7).
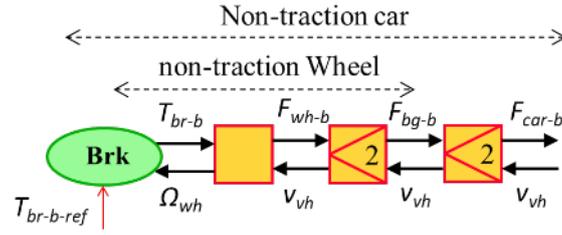
**Figure 2-7: The EMR of non-traction contribution.**

Thus, from a braking torque $T_{br-b}$, the non-traction car force $F_{car-b}$ is expressed according to (12) and adaptation elements to represent number of wheels and bogie,

$$\begin{cases} F_{wh-b} = \dfrac{1}{R_{wh}} T_{wh-b} \\ \Omega_{wh} = \dfrac{1}{R_{wh}} v_{vh} \end{cases} \tag{19}$$

$$F_{bg-b} = 2\, F_{wh-b} \tag{20}$$

$$F_{car-b} = 2\, F_{bg-b}. \tag{21}$$

The total force on the vehicle $F_{vh}$ can be defined as the sum of the forces of each traction car ($F_{car-1}$, $F_{car-2}$ and $F_{car-3}$) and the non-tractions car $F_{car-b}$. A coupling element is used to combine theses forces as

$$\begin{cases} v_{vh} \text{ common} \\ F_{vh} = F_{car-1} + F_{car-2} + F_{car-3} + F_{car-b} \end{cases} \tag{22}$$

The subway chassis (Figure 2-8) is described by an accumulation element. Its velocity is expressed as a function of the traction $F_{vh}$ and resistance $F_{res}$ forces, where $M_{vh}$ is the dynamical mass of the subway. The dynamical mass combines the static mass of the vehicle, including passengers, with the rotating inertia brought down to chassis level [Pam 21],

$$\frac{dv_{vh}}{dt} M_{vh} = F_{vh} - F_{res}. \tag{23}$$
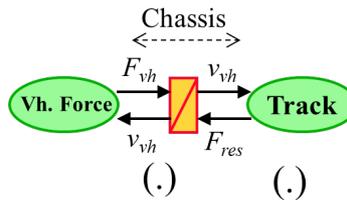


**Figure 2-8: The EMR of the chassis.**

45

The resistance force $F_{res}$ is imposed by the track topology, aerodynamics characteristics and friction. It is represented by a source element. It is defined as a function of the subway velocity, number of cars $N_{cars}$, static mass $M_{vh}^s$, gravitational acceleration $g$, slope θ, drag coefficient $C$, wind velocity $v_w$, rolling resistance $B$ and static force $F_0$,

$$F_{res} = N_{cars}F_0 + Bv_{vh} + C\,sign[v_{vh} - v_w](v_{vh} - C)^2 + \theta g M_{vh}. \qquad \textbf{(24)}$$

The global EMR of the new vehicle is constructed by associating the different EMRs. Coupling elements are used to combine the contribution of each car to determine the vehicle total force $F_{vh}$ and traction current $i_{trac}$. The formalism allows the development of a forward approach; hence, the control law must be defined. The global local control of the entire subway vehicle is thus systematically deduced from the EMR by mirror effect (Figure 2-9).
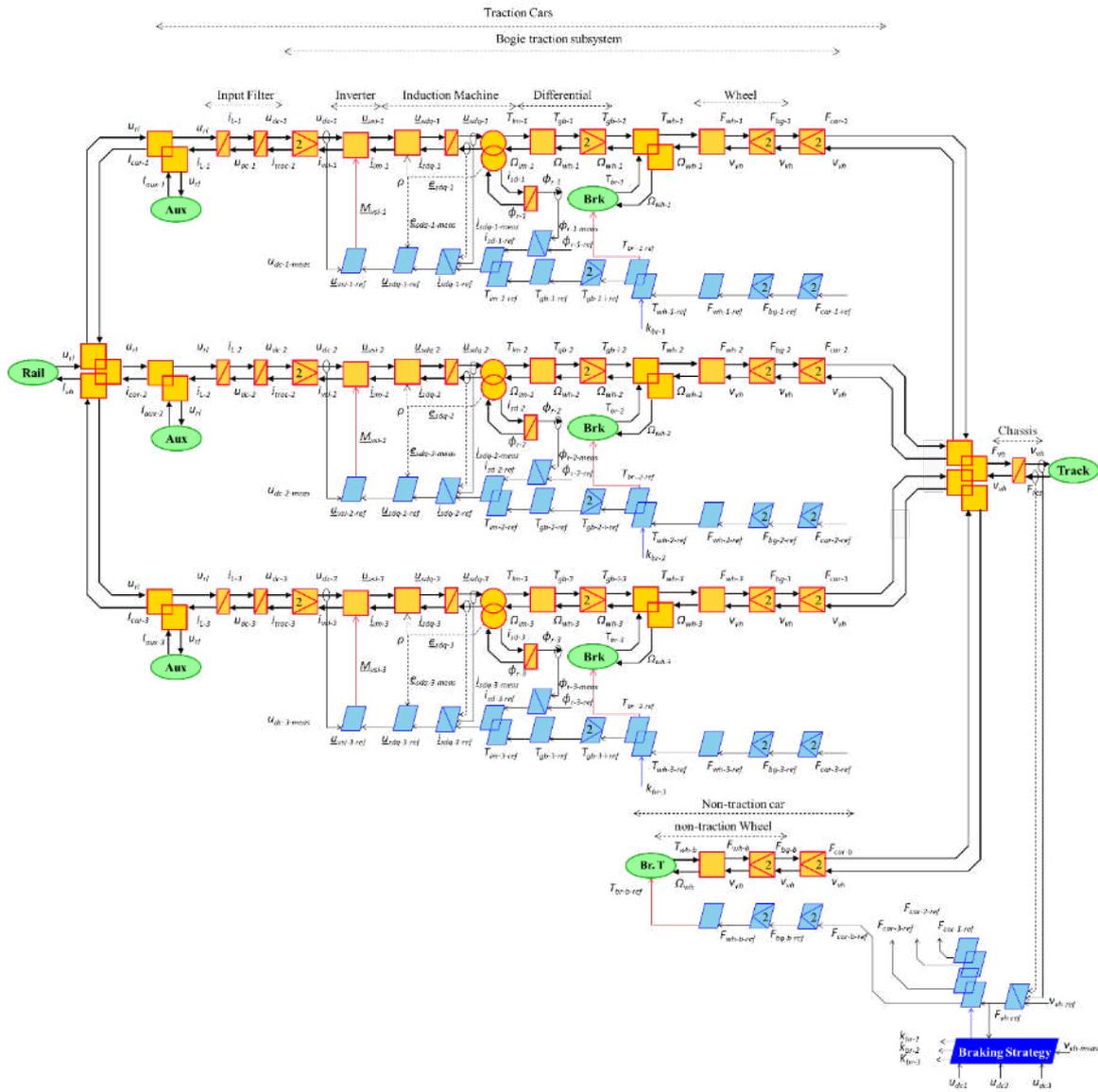


**Figure 2-9: Complete EMR of the new vehicle.**

## II. Vehicle simulation and experimental validation

### II.1. Dynamical simulation model of the vehicle

The complete EMR of the new vehicle, as depicted in Figure 2-9, exhibits a complex structure. The distribution of efforts necessitates an equally complex control law designed to effectively manage the power distribution across different car types. To realize the implementation of the control scheme and strategy, one might assume that traction cars exert identical efforts and possess consistent dynamics.
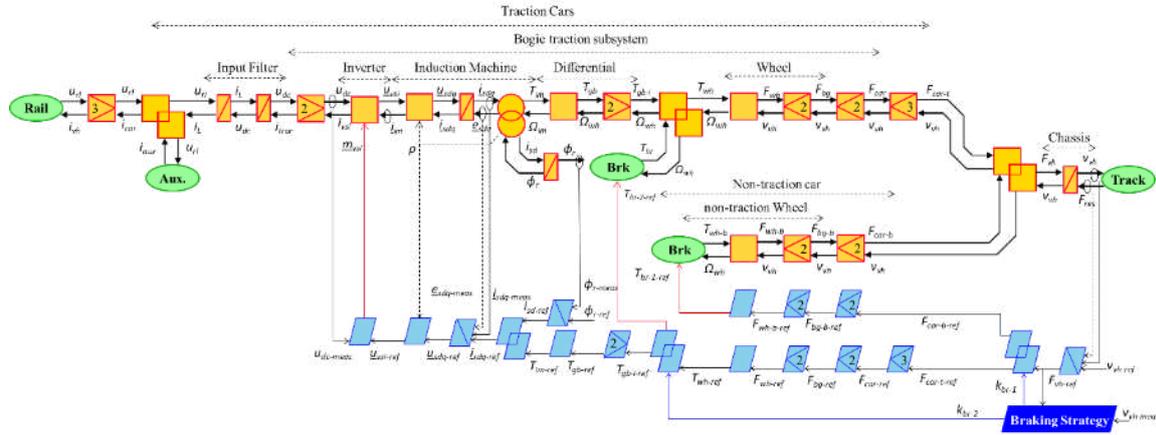


**Figure 2-10: EMR and control of the new vehicle.**

Incorporating adaptation elements proves beneficial in this context (Figure 2-10). Thus, a unique traction car is considered with the related adaptation element. Furthermore, this simplification significantly diminishes the computational demands for simulation. Hence, the total force from traction cars $F_{car-t}$ can be redefined from an individual traction force and the number of traction cars. It is assumed that the traction force is equally divided among the vehicles,

$$\begin{cases} v_{vh} \text{ common} \\ F_{car-t} = 3\, F_{car} \end{cases}. \tag{25}$$

The same consideration is taken on electrical side. The total vehicle demanded current is recalculated based on the number of traction vehicles and an individual car current,

$$\begin{cases} u_{rl} \text{ common} \\ i_{vh} = 3\, i_{car} \end{cases}. \tag{26}$$

II.1.a. <u>Maximal control scheme</u>

The control structure derived from the EMR ensures that the subway achieve a reference velocity of $v_{vh-ref}$. This is accomplished by inverting each pictogram using the mirror effect. The

accumulation elements at both the chassis and IM levels require the use of a closed-loop control system, as indicated by the light blue crossed parallelogram. The essence of this closed-loop control is to continuously measure the error between the actual and reference variables, subsequently, adjusting the control variable to minimize this error. The controllers, $C_v(t)$, $C_i(t)$ and $C_f(t)$, for the control of velocity, current and flux, respectively, play a pivotal role in this adjustment process. While they can be of the proportional-integral type, other controllers may also be considered based on the specific requirements of the system. First, the required force $F_{vh-ref}$ is determined by the velocity controller. A part of this force can be assigned to the non-traction car by the distribution coefficient $k_{br-1}$,

$$F_{vh-ref} = C_v(t)\big(v_{vh-ref} - v_{vh-meas}\big) + F_{res-meas} \qquad (27)$$

$$\begin{cases} F_{car-t-ref} = (1 - k_{br-1})F_{vh-ref} \\ \quad F_{car-b-ref} = k_{br-1}F_{vh-ref} \end{cases}. \qquad (28)$$

The wheel reference torque $T_{wh-ref}$, on traction car, can be obtained by the direct inversion of wheels and differential gearbox. The multiplication factor of each adaptation elements must be considered,

$$F_{car-ref} = \frac{1}{3}F_{car-t-ref} \qquad (29)$$

$$F_{bg-ref} = \frac{1}{2}F_{car-ref} \qquad (30)$$

$$F_{wh-ref} = \frac{1}{2}F_{bg-ref} \qquad (31)$$

$$T_{wh-ref} = R_{wh}F_{wh-ref}. \qquad (32)$$

A distribution coefficient $k_{br-2}$ is employed to determine the mechanical braking, $T_{br-2-ref}$. This variable assigns the contribution of mechanical brakes of the traction car. It may be noted that both $k_{br-1}$ and $k_{br-2}$ only influence subway braking phases. Both variables are assigned to zero during traction phases. Hence, the IM reference torque $T_{im-ref}$ can be found from the direct inversion of differential gearbox and the adaptation element,

$$\begin{cases} \quad T_{br-2-ref} = k_{br-2}T_{wh-ref} \\ T_{gb-i-ref} = (1 - k_{br-2})T_{wh-ref} \end{cases} \qquad (33)$$

$$T_{gb-ref} = 2T_{gb-i-ref} \qquad (34)$$

$$T_{im-ref} = \frac{1}{K_d} T_{gb-ref}. \tag{35}$$

The same method is used to determine the non-traction car braking torque $T_{br-1-ref}$. It can be determined from

$$F_{bg-b-ref} = \frac{1}{2} F_{car-b-ref}$$

$$F_{wh-b-ref} = \frac{1}{2} F_{bg-b-ref}$$

$$T_{br-1-ref} = R_{wh} F_{wh-b-ref}.$$

The IM machine torque, $T_{im-ref}$, is controlled using its maximal control scheme [Bouscayrol 15]. The field-oriented control is applied and will not be detailed in this thesis. The machines currents reference $i_{sd-ref}$ and $i_{sq-ref}$ are obtained, thus, the use of a closed loop control is used. The machine stator voltages reference $\underline{u}_{sdq}$ are obtained from the controller $C_i(t)$ and measured e.m.f., $\underline{e}_{sdq-meas}$. The stator reference dq voltages are transformed to a stationary frame $\underline{u}_{vsi-ref}$ from direct inversion of (7). Finally, the converter modulation variable is expressed in function of the measured DC bus voltage $u_{dc-meas}$,

$$\underline{u}_{sdq} = C_i(t)\left(\underline{i}_{sdq-ref} - \underline{i}_{sdq-meas}\right) + \underline{e}_{sdq-meas} \tag{36}$$

$$\underline{u}_{vsi-ref} = P^{-1}(\rho)\underline{u}_{sdq-ref} \tag{37}$$

$$\underline{m}_{vsi} = \frac{1}{u_{dc-meas}} \underline{u}_{vsi-ref}. \tag{38}$$

II.1.b. <u>Braking energy management</u>

The mechanical braking references torque are dependent on the variables $k_{br-1}$ and $k_{br-2}$. These variables are defined according to safety requirements and braking efforts distribution between the wheels. In braking phases, a part of the force demand can be applied using mechanical brakes instead of regenerative braking. For that, a variable $k_s$ is defined to determine the share of the reference force that is applied using mechanical brakes $F_{mech}$,

$$F_{mech} = k_s F_{vh-ref}. \tag{39}$$

The variable $k_s$ is determined by a combination of operational limitations and safety regulations. Initially, an accordance with the machine maximal torque during the braking phase is necessary. As such, the reference torque magnitude must remain below the maximal allowable limit. This constraint is quantified through the relationship between $T_{im-ref}$ and $T_{im-lim}$, leading to the definition of $k_{s1}$.

For safety considerations, when the subway velocity is below a predetermined threshold $v_{lim}$, set at 5 km/h for this subway system, both electrical and mechanical braking mechanisms are activated. This is regulated by $k_{s2}$.

Furthermore, the braking strategy is required to control the DC bus voltage. Pure mechanical braking is assured at 950V, with a smooth transition occurring between 900V and 950V. This regulation is managed by $k_{s3}$ (Figure 2-11). To ensure compliance with all the aforementioned conditions, the value of $k_s$ is obtained by selecting the maximum value among previously defined variables ($k_{s1}$, $k_{s2}$, and $k_{s3}$) [O. Berriel 20].

$$k_{s1} = \left(1 - \frac{\min\{|T_{im-ref}|, |T_{im-lim}|\}}{|T_{im-ref}|}\right), \qquad k_{s2} = \left(1 - \frac{\min\{v_{vh}, v_{lim}\}}{v_{lim}}\right) \qquad (40)$$

$$k_s = \begin{cases} \max\{k_{s1}, k_{s2}, k_{s3}\}, \text{ with } k_s \in [0,1] & \text{in braking phase } (P \geq 0) \\ 0 & \text{in traction phase } (P < 0) \end{cases} \qquad (41)$$
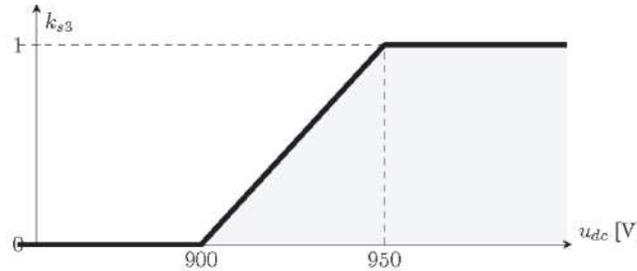


**Figure 2-11: Coefficient for mechanical braking activation vs. DC bus voltage.**

In subway operation, it is considered that the mechanical brakes in both traction and non-traction cars should exert equal braking torque. Specifically, $T_{br-1-ref}$ must be equivalent to $T_{br-2-ref}$. Under this framework, each car contributes to one-fourth of the total mechanical braking force. Consequently, $k_{br-1}$ and $k_{br-2}$ can be directly assigned in accordance with,

$$\begin{cases} k_{br-1} = \dfrac{k_s}{4} \\ k_{br-2} = \dfrac{3k_s}{4 - k_s} \end{cases}.$$  (42)

## II.2. Vehicle experimental validation

The vehicle model and control mechanisms have been developed using Matlab Simulink©. Subsequently, experimental data has been gathered by operating the vehicle on Line 1 in Lille. Detailed parameters of the vehicle can be found in Table 2. To realize a comparison between experimental and simulation results, the recorded velocity profile and dc bus voltage level are imposed into the model. Additionally, the real line topology conditions, including aspects like slope and the tunnel effect, are accurately replicated in the simulation.

A specific test has been conducted between two passenger stations, encompassing both an acceleration and a braking phase. To ensure the line remains receptive during braking phases, additional vehicles were introduced into circulation in proximity to the test site. This setup ensures that negative currents can be registered and confirms the energy transfer between vehicles. Given that voltage fluctuations are influenced by external factors unrelated to the vehicle, these fluctuations are also imposed to the model.

**Table 3. Subway parameters.**

| Dynamical mass | 64.9 [t] | Gear ration | 8.2 |
|---|---|---|---|
| Filter capacitance | 7800 [uF] | Gear efficiency | 0.955 |
| Filter inductance | 1.0 [mH] | Auxiliary power | 3.2 [kW] |
| Rail rated voltage | 850 [V] | IM Machine power | 200 [kW] |
| Wheel radius | 0.467 [m] | Inverter efficiency | 0.92 |
| Abs. max. acceleration | 1.3 [m/s²] | Abs. Max. jerk | 0.65 [m/s³] |

For the purpose of validating the model, two distinct scenarios are examined. The initial scenario involves a pronounced acceleration phase followed by an intense braking phase. The second scenario features a milder acceleration and similar braking process. Both scenarios are evaluated based on their demand current and energy consumption. Results are put together for comparison. During this test a special configuration on the vehicle is imposed where mechanical activation in function of dc bus voltage is deactivated. This is considered to better visualize regenerative braking phase.

II.2.a. <u>Test 1</u>

In the initial interstation journey, the vehicle movement is imposed at a specified velocity (Figure 2-12a). The current displays a negative value, which can be attributed to the energy being transferred to another vehicle that is in the process of accelerating, (Figure 2-12c). The discrepancy in energy consumption is relatively minimal, with an error of 2.4%, (Figure 2-12e). Remarkably, energy recuperation during this journey is recorded at approximately 51%. This significant energy recovery rate can be explained by the nature of the test site, which featured a descending gradient. Consequently, the model effectively demonstrates its capacity in representing energy exchanges between distinct vehicles and accurate energy consumption calculations.



a)



b)



c)

e)
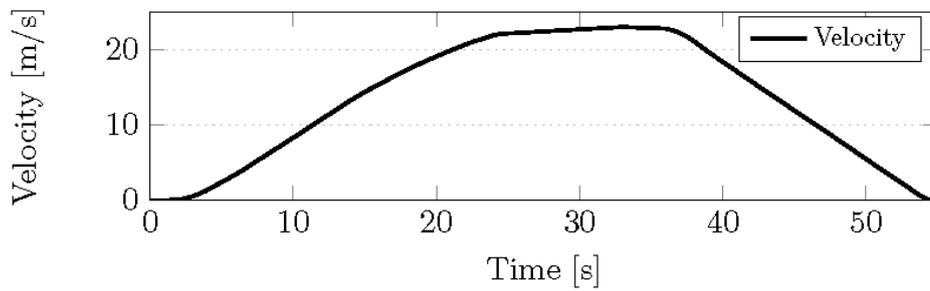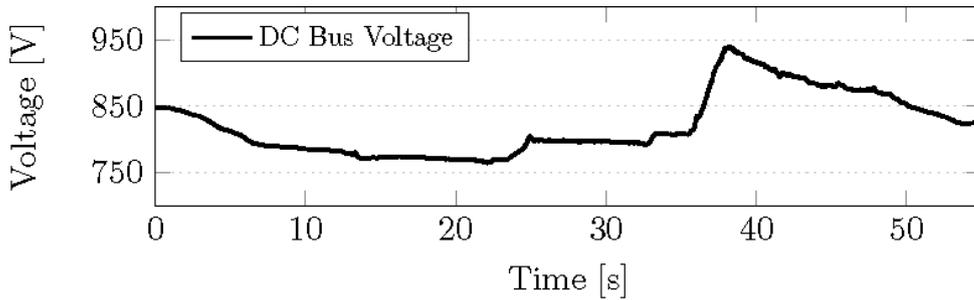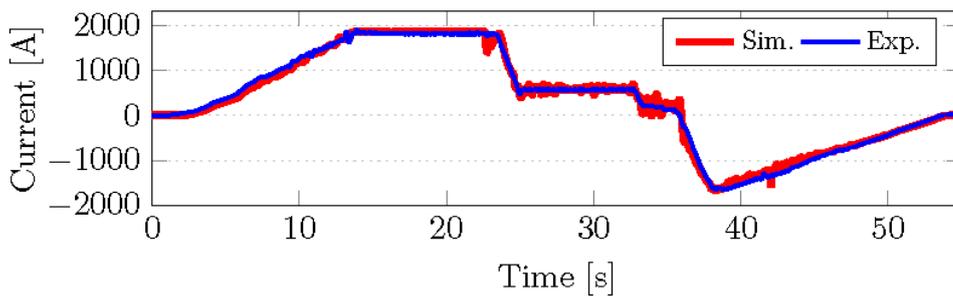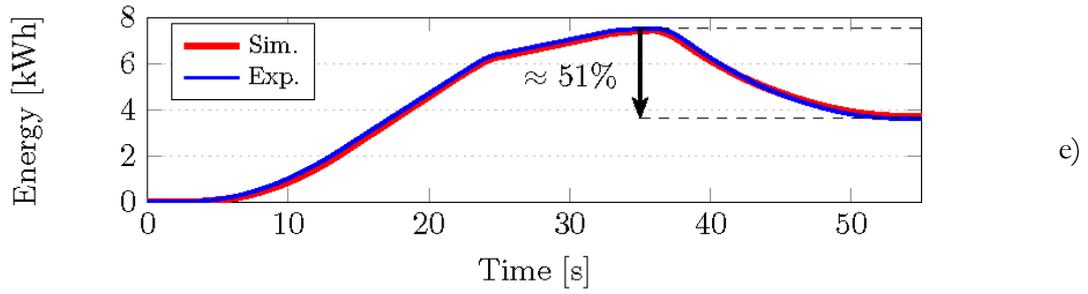
**Figure 2-12: Simulation vs. experiment results with strong acceleration and braking.**

The outcome of the simulated current shows noticeable fluctuations. These fluctuations in relation to the experimental findings arise due to the voltage and current data being sourced from a sample taken every 20ms. In contrast, the simulation processes data in integration steps of 0.1ms. The current observed root mean square deviation (RMSD) stands at 82.2A. For the consumed energy, a maximum error of 2.6% is noted throughout the simulation.

II.2.b. <u>Test 2</u>

In the second test, a soft acceleration phase is noted, succeeded by a brief cruise phase (Figure 2-13a). The maximal velocity and braking intensity are comparable to those in the first test. The current similarly shows a negative value, aligning with the patterns observed in the experimental measurements (Figure 2-13c). The error is energy consumption is also small, with a value of 2.1% (Figure 2-13e). The energy recovery rate is marginally higher at 53%. Both experimental tests underscore the model high accuracy.



a)



b)

c)



e)
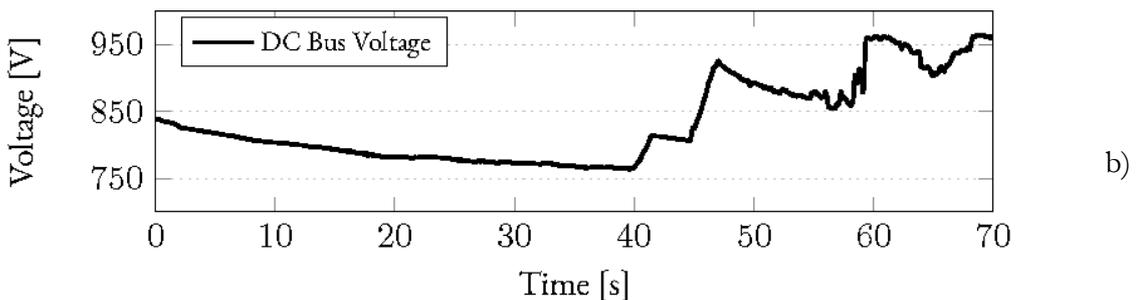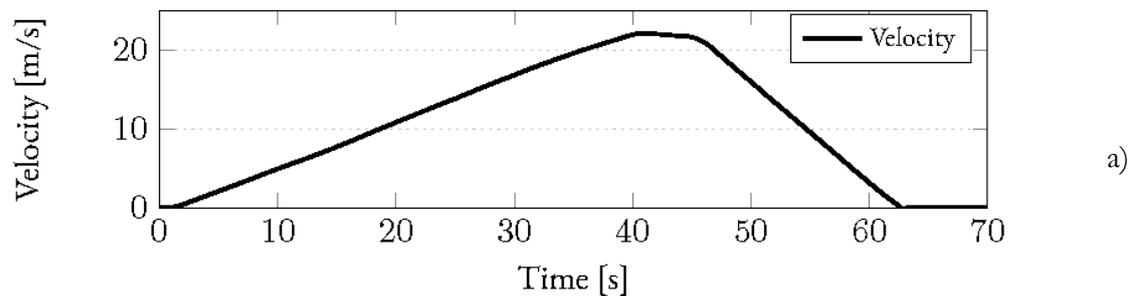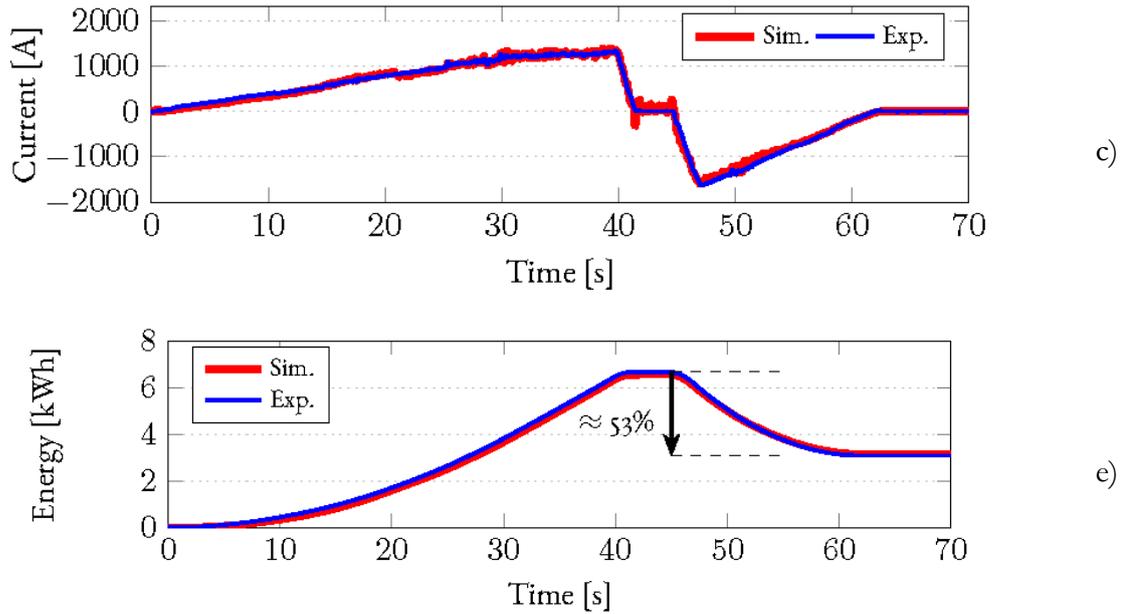
**Figure 2-13: Simulation vs. experiment results with soft acceleration and strong braking.**

For this case, the RMSD stands at 55.7A. For the consumed energy, a maximum error of 2.8% is noted throughout the simulation.

## II.3. Simplified models

The accurate calculation of currents and energy consumed by a vehicle is made possible through the dynamical model. Yet, achieving such detailed results demands a significant discretization of simulation time. This results in a longer duration due to the necessity of a smaller time step. When considering the simultaneous simulation of multiple vehicles and subsystems, it becomes crucial to reduce this time while ensuring accuracy [Mayet 16b].

Simplifications in the model aim to reduce computational complexity in simulation environments. To analyze the effect of simplifications in the model, simulation results obtained from the dynamical model are used as a reference. The instantaneous power as well as the final energy consumption are compared. To compare the power error, the RMSD is applied. The vehicle is imposed to a generic outbound trip with a total of 20 stations.

II.3.a. <u>Quasi-static model</u>

In the quasi-static model, the primary dynamics of a system are retained while faster dynamics are omitted. This thesis simplifies the system by substituting the dynamic model of the IM with a static electric drive [Mayet 16b]. The input filter dynamics are preserved. In this reorganized model, the torque reference is directly integrated into the system, eliminating any delay between the

reference and the actual torque value. Moreover, a constant efficiency rate of 86.0% is imposed. Figure 2-14 illustrates the model simplification, presenting the incorporation of the static electric drive.
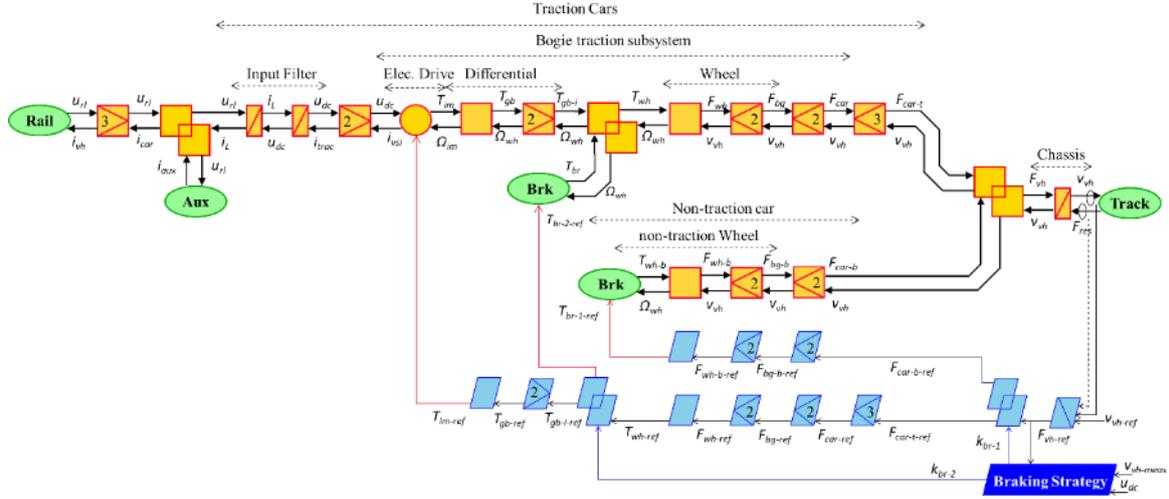


**Figure 2-14: EMR and control of quasi-static model of new subway vehicle.**

The IM and VSI are combined and depicted as a multi-domain conversion element, (an orange circle). It is referred to as electrical drive. The applied torque, $T_{im}$, follows immediately the torque reference, $T_{im-ref}$. The VSI current, $i_{vsi}$, is derived from factors including the torque, rotational speed $\Omega_{im}$, DC bus voltage, and the efficiency of the machine $\eta_{im}$.

$$\begin{cases} i_{vsi} = \dfrac{T_{im}\Omega_{im}}{\eta_{im}^{\delta} u_{dc}} \\ T_{im} = T_{im-ref} \end{cases} \quad \text{with} \quad \delta = \begin{cases} 1, \text{when } T_{im}\Omega_{im} > 0 \\ -1, \text{when } T_{im}\Omega_{im} \leq 0 \end{cases} \tag{43}$$

The power demand comparison result can be seen in Figure 2-15. A RMSD of 16.6 kW is obtained. That represents about 1.4% of the vehicle nominal power. An error of 2.0% on final energy consumption is registered.
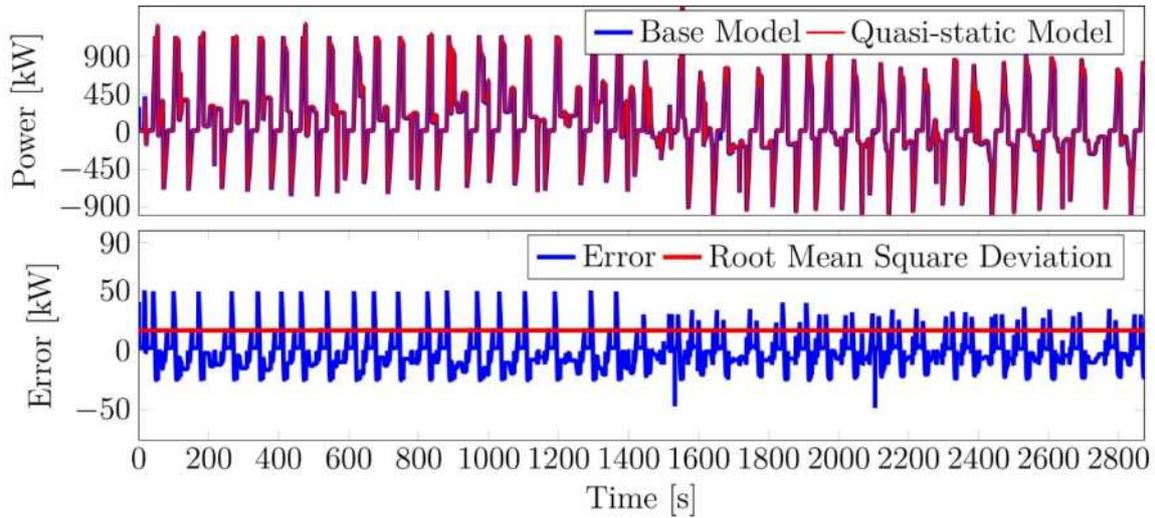
**Figure 2-15: Power Comparison for Quasi-static Simplification.**

II.3.b. Track Slope Removal

In the context of subway operation, the track slope depends on the trip topology. To account for this in simulation models, look-up tables are essential. However, precise knowledge of topology is often not available. In this simplified model, the assumption is made on the track level, neglecting any slope. In Figure 2-16, the error in instantaneous power calculations becomes more pronounced as the track slope increases, resulting in a RMSD of 89.1 kW. That represents about 7.4% of the nominal power of the vehicle. An error of 9.9% on energy consumption is obtained. Results suggest that this parameter is not neglectable.
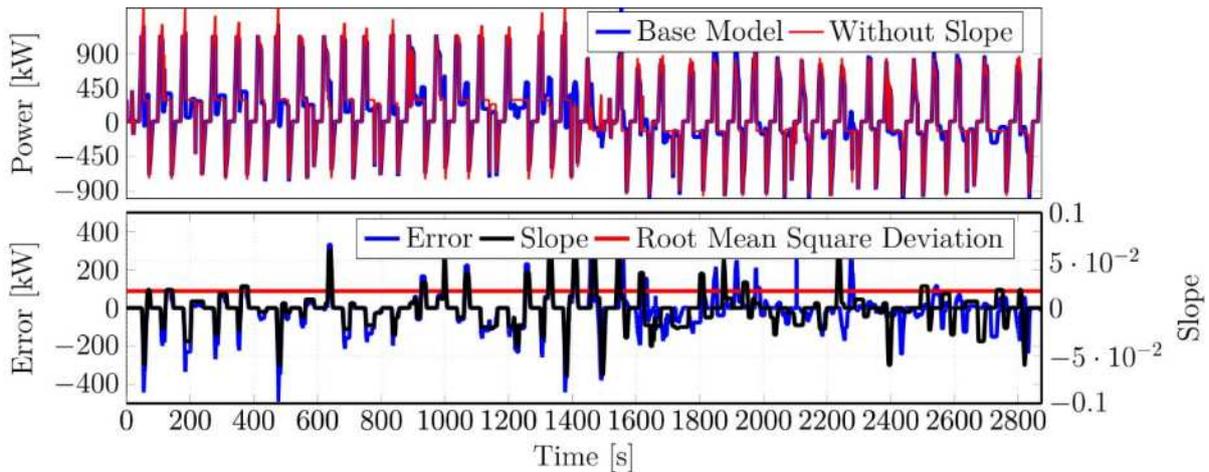


**Figure 2-16: Power Comparison for Slope Removal Simplification.**

56

II.3.c. Tunnel effect simplification

For each location of the subway along the track, the model determines whether the subway is operating in a tunnel or on an above-ground segment. Due to data storage constraints within the simulation environment, the impact of considering a constant value for the simulation is analyzed. The tunnel effect constant value is taken as a weighted average considering each underground and above-ground sections. Figure 2-17 illustrates a discrepancy in error between the phases when the subway is in a tunnel versus when it is on above-ground tracks. A RMSD of 7.9 kW is observed. For this simplification 0.1% of error on energy consumption is obtained. Results indicate that tunnel effect has no important impact on energy consumption.
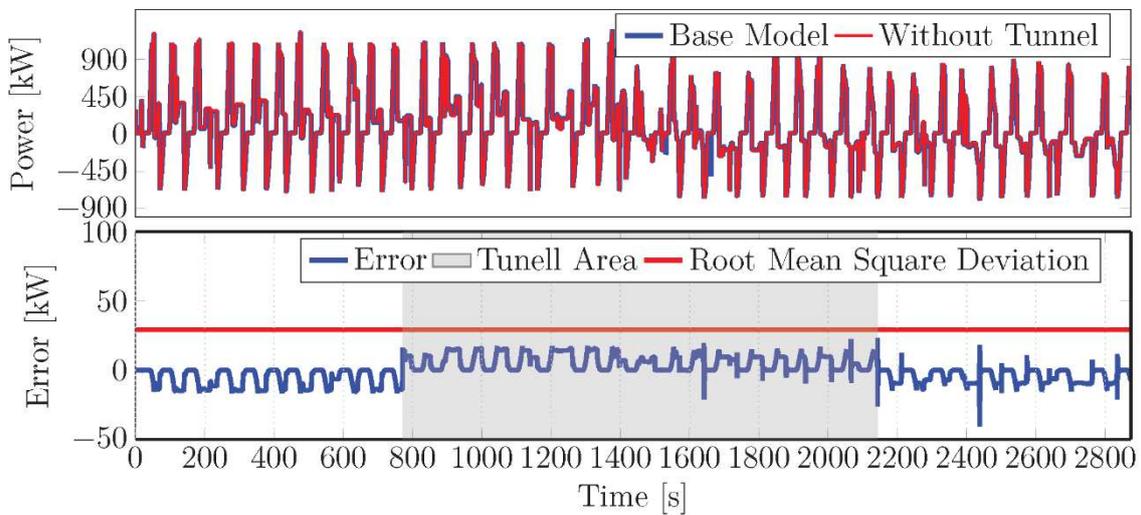


**Figure 2-17: Power Comparison for Tunnel Effect Simplification.**

II.3.d. Non-traction car simplification

The mechanical braking forces exerted by the non-traction car can be effectively integrated at the traction-car level. By doing so, it is possible to bypass the complex process of distributing these forces. From a control perspective, this approach simplifies the distribution of mechanical braking, representing it with a singular variable, $k_{br}$.

$$k_{br} = \frac{k_s}{3} \tag{44}$$

It is noteworthy that while the electrical forces remain consistent during both acceleration and braking phases, the mechanical braking torque at the car level tends to register a marginally elevated value. However, when calculating energy consumption, this slight increase in mechanical braking torque has no impact and can be overlooked. The efforts experienced on electric machine

level remain the same. No error is presented in terms of energy consumption and electric power demand.

II.3.e. <u>Model comparison</u>

For each simplification performed, the total value of the energy consumed at the end of the trip is recorded. The calculation is computed from the integral of instantaneous power in relation to time. The result is summarized in Table 3.

The elimination of the non-traction car shows no modifications in terms of energy consumption and power demand. The reduction in model complexity and control is significant. The Quasi-static simplification gives a small difference in terms of energy consumption with 2.0% difference. It also presents a relatively small RMSD. Slope elimination presents 9.9% of difference in terms of energy consumption. Additionally, it presents the highest RMSD value in terms of power.

**Table 4. Energy Consumption and Error Comparison.**

| Simulation type | Value | Difference in energy consumption | Power RMSD | Simulation time reduction |
|---|---|---|---|---|
| Dynamical model | 83.4 [kWh] | Base | Base | Base |
| Non-traction car simplification | 83.4 [kWh] | 0% | 0 [kW] | 7.4% |
| Quasi-static simplification | 85.1 [kWh] | 2.0% | 17.9 [kW] | 93.9% |
| Slope neglecting | 92.1 [kWh] | 9.9% | 89.1 [kW] | 6.8% |
| Tunnel effect neglecting | 71.5 [kWh] | 0.1% | 7.9 [kW] | 0.5% |

In terms of simulation time, a notable reduction is observed for quasi-static simplification (93.9%). This reduction is mainly due to the increase in simulation integration steps. The non-traction car simplification also presents notable reduction in simulation time (7.4%). This is quite important because no difference in the measured variables is observed. Slope neglecting presents a reduction on simulation time (6.8%); however, an important error is followed. Finally tunnel effect neglection presents no significant reduction on simulation time (0.5%).

For the simulation of a subway carousel multiple vehicles are simulated at the same time, hence, the dynamical model becomes impractical to be implemented due to the high computation time. For the carousel study it is chosen the quasi-static model combined with the non-traction car simplification (Figure 2-18). This solution allows the increase of the integration step time by eliminating fast dynamics and reducing the number of calculations performed.
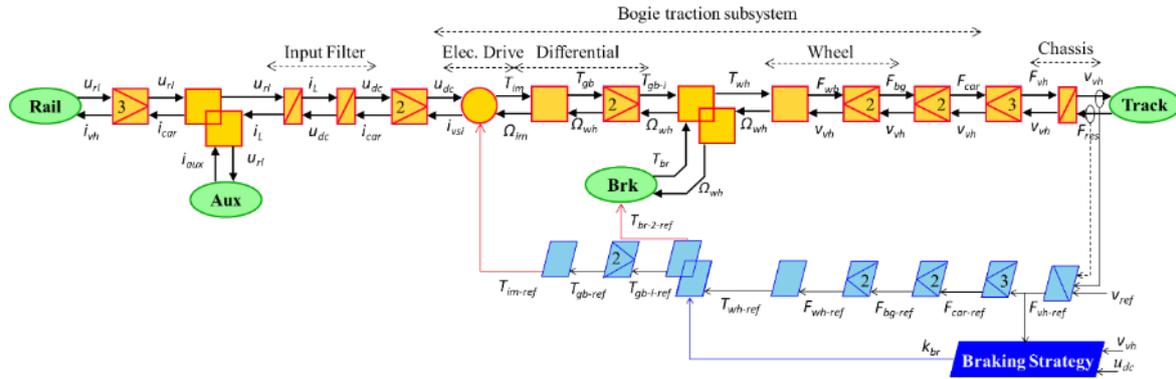
**Figure 2-18: EMR and control of quasi-static and non-traction car simplification.**

## III. Simulation model of the subway carousel

The subway carousel simulation is a comprehensive representation that brings together the various subsystems that make up the entire metro line. This process involves a systematic approach where each subsystem is integrated to form an organized structure. The foundation of this simulation is based on a previously established vehicle model. This model serves as the core, which is then associated with different subway line constraints, such as stop time at passenger station, interval between vehicles, and track profile.

Through the integration of these components, a complete and flexible model emerges. This simulation tool not only encapsulates the physical attributes and functionalities of the subway carousel but also offers flexibility for modifications or adjustments to individual elements. Such adaptability is crucial for understanding of the interactions between the various subsystems. Whether assessing the impact of a new energy savings solution or analyzing flow dynamics during peak hours, the simulation model stands as a robust framework for diverse studies and evaluations.

### III.1. Simulation model of TPS and rail supply line

III.1.a. The traction power substation

The TPS plays an important role in feeding the rail supply mechanism. The design consists of a power transformer paired with a diode rectifier, making it a nonlinear component. Simplified models are frequently proposed for numerical benefits. [Arboleya 22] [Chiniforoosh 16]. In this thesis, a static model is adopted. While a detailed model offers greater accuracy in assessing current peaks and transients, this study primarily centers on energy consumption. Therefore, a simplified model is considered adequate. Previous research into several TPS models showed that the chosen model only differs from the more complex model by 0.8% in terms of energy consumption [Mayet

16b]. Simplified models are attractive for their efficacy in assessing energy consumption while reducing computational costs.

The approach on this thesis is based on the work developed in [Mayet 16a]. The TPS can transition between two states, the conduction phase (ON) and the non-conduction phase (OFF). During conduction, the voltage noted at the TPS connection point is either equivalent to or less than the rectified rated voltage. Here, the model is considered as a perfect voltage source with a consistent value matching the rectified nominal voltage.

The switch between states is conditional on the current and voltage at the connection point. When in conduction mode, the TPS imposes a fixed voltage and has as reaction the current demanded. In this case, the change of state occurs by observing the current supplied. When this current goes to zero, the state change is made. On the other hand, if the TPS is initially in a blocked state, it imposes a null current and the voltage is taken as the system reaction. In this case, the TPS switches to conduction mode once the voltage reaches a value equal to or less than the rectified nominal value. The EMR of the TPS under consideration is illustrated as well as a transition table between states (Figure 2-19). The switching element is used to represent the different working states.



| Actual state | Event | Next state |
|--------------|-------|------------|
| ON | $i_{ss} \leq 0$ | OFF |
| OFF | $u_{ss} > u_{nom}$ | ON |
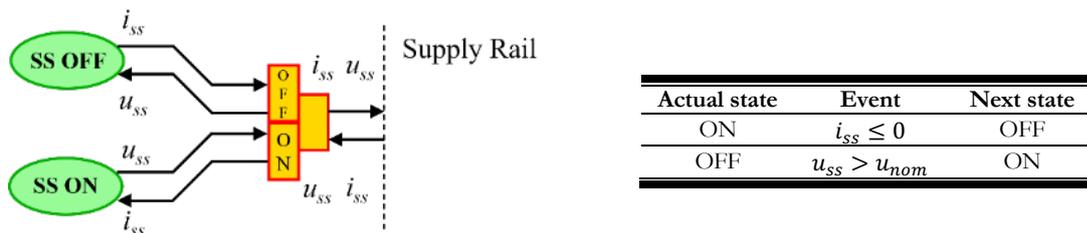
**Figure 2-19: The EMR of TPS and transition table.**

III.1.b. <u>The rail supply line</u>

The supply line is the element that connects the vehicles on the line to the power substations. This element can be thought of as a transmission line in which there are connections along the conductor. This conductor can be represented as a resistive element. The connection position is fixed for TPS, but this is not the case for vehicles. As a vehicle moves along the line, the resistance between the elements changes and directly impacts the energy flow in the network.

The approach adopted should effectively capture these resistance variations among the components. To illustrate, consider two arbitrary components A and B located on the track. The

equivalent resistance between them, denoted as $r_{AB}$, is determined based on their respective positions, $x_A$ and $x_B$, coupled with the linear resistance, $\Lambda_{rail}$, inherent to the conducting material. It is considered that positive and negative path have the same linear resistance, hence, a multiplying factor of 2 is considered,

$$r_{AB} = 2\Lambda_{rail}|x_A - x_B|. \tag{45}$$

Other factors such as linear inductance and parasitic capacitance can be incorporated into the model, but their implementation would result in the presence of fast dynamics, making it necessary to reduce the integration step. A purely resistive line is widely accepted for studying DC railway supply lines [Mohamed 17].

In the simulation of subway lines, the network demands a standard circuit resolution where the node count aligns with the total physical components, including both TPSs and vehicles. As these positions move over time, the system equations are not consistent.

The method of Modified Nodal Analysis (MNA) is employed for the circuit resolution [Ho 75]. Within this framework, different subsystems can be considered as a current or voltage source. As the position of vehicles changes with time, every integration step necessitates a recalculation of both the solution matrix topology and its admittance values, as suggested by (45). This method has been detailed in [Mayet 16a] and is applied to this thesis.

A common issue encountered when solving circuits involving railway systems using diode rectifiers is when all TPS are blocked. In this specific situation, the circuit voltage reference is lost because they switch to a zero current imposition mode. This problem can be addressed by adjusting the vehicle model. By removing the inductive nature of the vehicle input filter, the connection point to the distribution network acquires a capacitive characteristic, meaning it imposes a voltage on the network (Figure 2-20). This voltage gives reference to the network circuit.
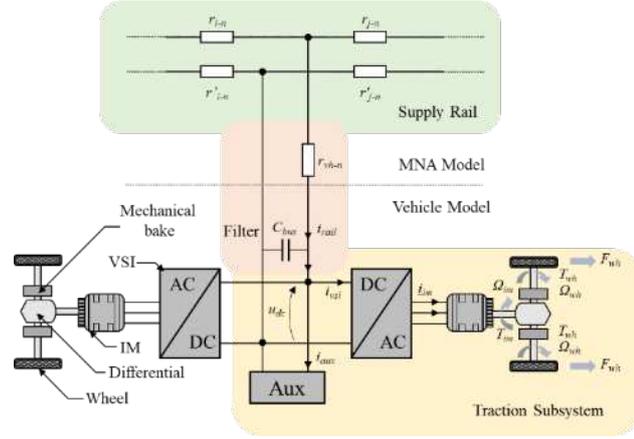
**Figure 2-20: Traction vehicle structure without filter inductance.**

Furthermore, the resistance of the inductive element is combined with the resistance of the vehicle connection point (contact shoe) and is represented at the distribution circuit level as $r_{vh}$. Moreover, the connection resistances of the TPS, represented as $r_{ss}$, is sequentially incorporated (Figure 2-21).
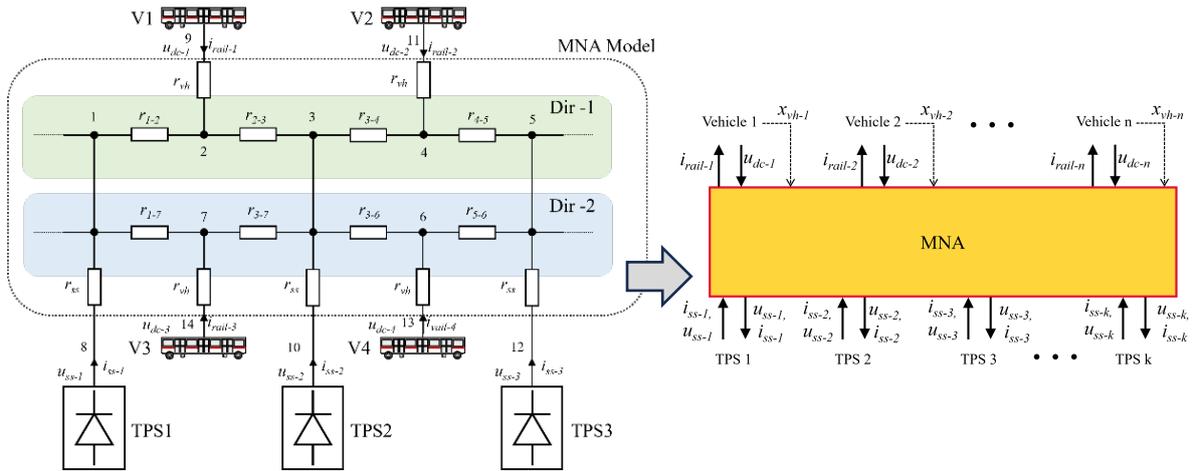


**Figure 2-21: Circuit representation on metro network and MNA solution block.**

In addition to the voltage and current quantities, the MNA block element also receives information on the positions of the vehicles. This information, together with knowledge of the state of the TPS, as a source of voltage or current, makes it possible to develop the circuit matrix solution,

$$\begin{bmatrix} \underline{G} & \underline{B} \\ \underline{B}^T & \underline{D} \end{bmatrix} \begin{bmatrix} \underline{U} \\ \underline{J} \end{bmatrix} = \begin{bmatrix} \underline{I} \\ \underline{V} \end{bmatrix}. \tag{46}$$

Given N nodes on the circuit (Figure 2-21). The matrix labeled as $\underline{G}$ is constructed as an N×N matrix through a two-phase process. Initially, every element within the diagonal matrix is

determined by the aggregate of the conductance linked to the respective node. In the subsequent phase, elements outside the diagonal represent the inverse value of the conductance linked to the associated nodes. Assuming $N_v$ elements with voltage source characteristics. The $\underline{B}$ matrix is an $N \times N_v$ matrix that, in this application case, can assume either 1 or 0. Value 1 marks the position of corresponding node. The D matrix is an $N_v \times N_v$ matrix that is composed entirely of zeros since no controlled current is present in this application.

The $\underline{I}$ and $\underline{V}$ matrixes hold the independent current and voltage sources. The $\underline{I}$ matrix has dimension of $N \times 1$ with each element corresponding to a particular circuit node. The value of each element is determined by the current sources in the corresponding node. In this particular case all elements are 0 since the only element that can assume a current source characteristic is a blocked TPS, and it imposes null current in this condition. The matrix $\underline{V}$ has dimensions $N_v \times 1$ where each element corresponds the value if its respective independent voltage source.

The $\underline{U}$ and $\underline{J}$ matrixes hold the unknown quantities. The $\underline{U}$ matrix has dimension $N \times 1$ where its element corresponds to the voltage value on the respective node. The $\underline{J}$ matrix has dimension $N_v \times 1$ and indicates the current on each independent voltage source. The solution of the system is given by the manipulation of (40) where the unknown variables are found,

$$\begin{bmatrix} \underline{U} \\ \underline{J} \end{bmatrix} = \begin{bmatrix} \underline{G} & \underline{B} \\ \underline{B^T} & \underline{D} \end{bmatrix}^{-1} \begin{bmatrix} \underline{I} \\ \underline{V} \end{bmatrix}. \qquad (47)$$

The use of the EMR formalism proves vital for the applied methodology. Variables for matrix solution can be readily identified. The input and output variables (action and reaction) of each subsystem correspond precisely to the variables required to construct the matrix. Evidently, obtaining the position information of each vehicle is essential for understanding the resistance between elements.

## III.2. Simulation of subway carousel

The framework for modelling and organization of different subsystems has been established. The methodology in [Mayet 16a] is used, but now for a new vehicle. The next step is the implementation of the computational simulation. Each component, along with the algorithm to solve the MNA, is implemented using Matlab Simulink©. The vehicle model has been updated, specifically by removing the inductor from its input filter.

As a result, vehicles are represented in the MNA solution as an independent voltage source, imposing the voltage $u_{dc}$ (Figure 2-22). Hence, circuit solution is ensured to have a reference voltage when TPS are blocked. A comprehensive line management system has been developed to supervise and control the introduction of vehicles onto line. This system provides flexibility, allowing adjustments to the intervals between vehicles and their stopping durations at stations, ensuring that the vehicles respect a set timetable.
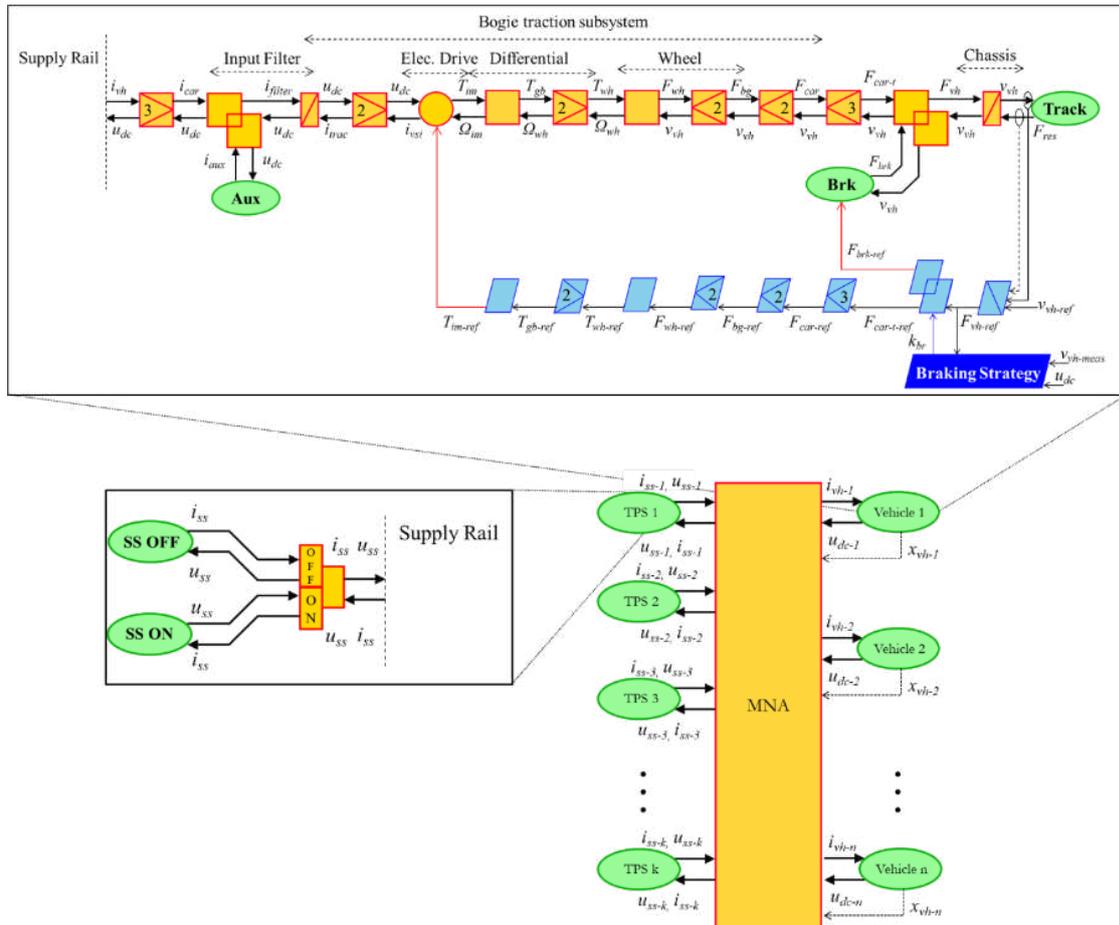


**Figure 2-22: Representation of MNA, TPS and subway vehicle for subway a line simulation.**

The work presented in this thesis draws its foundation from the Lille metro Line 1, and as such, its topology has been integrated into the model. Real-world data, as detailed in Appendix B, dictates the positioning of passenger stations and TPS.

A comprehensive line management system has been developed to supervise and control the introduction of vehicles onto line. This system provides flexibility, allowing adjustments to the intervals between vehicles and their stopping durations at stations, ensuring that the vehicles respect a set timetable.

The line operates with a position-dependent reference speed, constrained by specific segments of the track. To maintain safety and efficiency, the velocity management system is tasked with ensuring that both acceleration and jerk remain within the safe and comfort values [Verhille 10].

III.2.a. <u>Carrousel experimental validation in non-receptive mode</u>

An experimental validation process involves running a vehicle over a designated section of the transit line. This test is strategically scheduled outside the regular operating hours where only one vehicle is in circulation on the line. Such a setup results in a non-receptive line, eliminating the possibility for the vehicle to feed energy back into the network and thereby preventing the recording of any negative currents. However, this scenario inhibits other circulating vehicles from influence on the line voltage fluctuation.

Rather than setting a fixed voltage for the vehicle model, it is now treated as a simulated system variable for comparative analysis. The configuration depicted in Figure 2-22 is used. The TPS are placed respecting line configuration, and one vehicle is integrated to the simulation.

The system is provided with reference velocity and accurate initial positioning to mimic the real-world conditions faced by the test vehicle. Key metrics such as the demanded current, voltage variations, and total energy consumption are then compared for evaluation. The value of supply line linear resistance and connection point resistances are presented in Table 5.

**Table 5. Supply rail and connection point resistances (source: MEL).**

| | |
|---|---|
| Equivalent linear resistance | 22 [mW/m] |
| TPS connection resistance | 30 [mW] |
| Vehicle connection resistance | 20 [mW] |

In the experimental test, a velocity profile is established (Figure 2-23a). Various accelerations and decelerations are executed to emulate a standard operation of the line. A maximal velocity of 72.2 km/h is recorded, which closely approaches the operational limit of the line. During the acceleration phase, the filter voltage experiences a drop (Figure 2-23b). This behavior results from the resistances in the supply line and connection points. It can be seen that the model can accurately replicate this behavior.

Considering only one vehicle in operation, the current does not display negative values. This indicates that the regenerative braking recovery phase is not executed (Figure 2-23c). This experimentally highlights the importance of supply line receptivity in reducing energy

consumption. The current behavior is well-represented by the developed model, where the RMSD is less than 105 A. Considering that values in the order of 2000A are presented.

Despite the significant variations and modes experienced by the vehicle, the energy consumption error remains below 2.1% (Figure 2-23e). A maximal error of 2.5% in energy consumption is registered during the simulation. Consequently, the global model is validated for a full line incorporating diverse velocity patterns, slopes, and stop times, although for a non-receptive line.
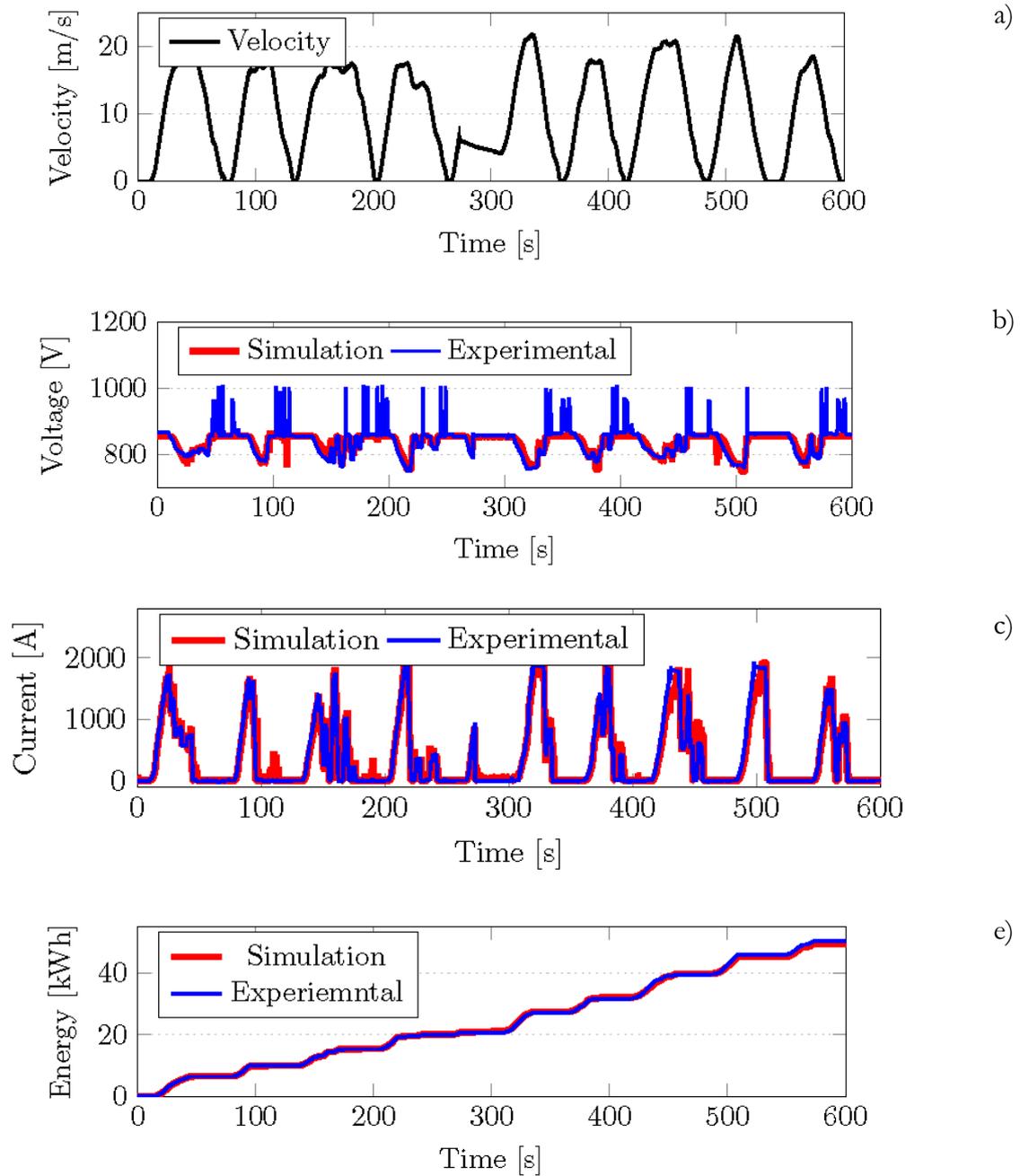


**Figure 2-23: Carousel validation experimental test.**

# IV. HIL simulation tool

## IV.1. HIL Setup

### IV.1.a. HIL setup objective

Simulation tools rely on mathematical models that come with certain simplifying assumptions. While simulations and models offer invaluable insights, there is an inherent challenge in their practical validation. Unfortunately, a full-scale validation of the carousel with multiple subways operating concurrently on an active line is not feasible. This presents a significant gap in the ability to establish the credibility of such models. To bridge this, a HIL setup has been designed, specifically planned for this purpose. Nonetheless, it is fundamental to understand that this HIL setup is of a reduced scale. Hence, the implications of this scale reduction need to be rigorously validated to ensure its authenticity and accuracy. Once validated, this HIL setup promises to serve as an instrumental platform to validate multi-TPS multi-vehicle carousels studies.

Past research has successfully implemented a HIL for subway systems, achieving a multi-train setup using a rheostat to mimic the variation of resistance between moving vehicle and a TPS [Mayet 17]. However, this method has its constraints, especially concerning the number of substations and train connections. It has enabled the validation of a carrousel model with 1 TPS and 2 subways running in the same direction. An extension is needed for the validation of a more complex carousel.

This thesis proposes an alternative: replacing the rheostat with an arrangement of resistors and regulated switches [O. Berriel 22]. This design discretizes the supply line, allowing for the connection of multiple vehicles or substations at different locations along the line.

The developed setup on this thesis makes it possible to perform HIL simulations with three TPS and six vehicles simultaneously. A modular topology allows straightforward extension of the simulation tool. The methodology of the developed HIL simulation consists in replacing part of the simulation system with real components. The challenges involve the representation of the complex dynamics of each subsystem and the proper connection of all the devices considering the time-varying position of the vehicles.

As the vehicle model has been validated with an imposed supply voltage, the components in the Loop will be the TPSs, the supply track and the on-board DC capacitor. Indeed, this capacitor

is key element that will activate the mechanical barking and block the diode rectifier. In the test for validation of the subway model, there was no regenerative braking, the capacitor was not validated.

Instead of using real-scale power elements, which involve voltages and current levels that are difficult to handle, the use of reduced scale electrical variables is preferred. Thus, reduced power components can be used to represent the TPSs, rail and vehicle. Scale coefficients are determined for voltage, $K_v$, and current, $K_i$, as a relation between the full-scale and reduced-scale quantities,

$$\begin{cases} u_{real\text{-}system} = K_v \, u_{reduced\text{-}scale} \\ i_{real\text{-}system} = K_i \, i_{reduced\text{-}scale} \end{cases}. \tag{48}$$

In addition, an impedance scale factor $K_r$ can be determined based on the previous definition according to Ohm's law, as

$$R_{real\text{-}system-} = K_r \, R_{reduced\text{-}scale} \quad \text{with} \quad K_r = \frac{K_v}{K_i}. \tag{49}$$

To simplify the notation, reduced scaled variables are written with the prime symbol '.

IV.1.b. <u>The subway vehicle</u>

For the subway representation, the input filter capacitor is physically implemented and the rest of the system is simulated in full-scale in real-time (Figure 2-24). In this approach the electromechanical system is preserved in full scale. From this simulation, the subway demanded power is obtained according to the necessary traction force and auxiliary loads. Based on the voltage measured at the capacitor $u_{dc}$, the demanded current $i_{vh}$ is determined. Through the power adaptation block, the feedback voltage measurement is inserted in the simulation of the traction power and auxiliaries. Then, the reduced-scale current reference is obtained based on its respective full-scale value and as in (42). The HIL simulation process is executed using a MicroLabBox provided by dSPACE. Thus in Figure 2-24, all models running in real-time are depicted in purple colors as they are now estimation models (and they do not represent the physical systems, depicted in orange).
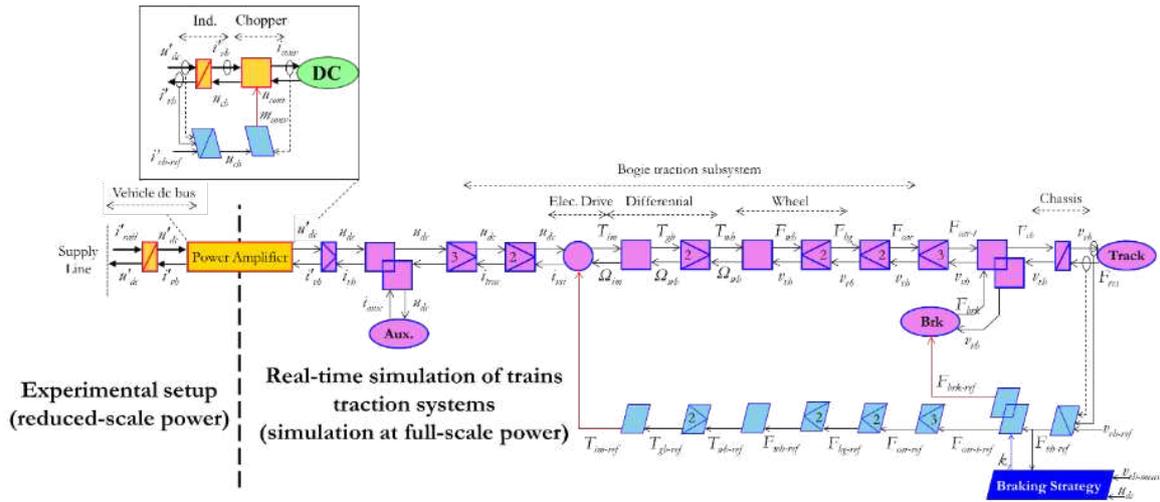
**Figure 2-24: EMR of a reduced-scale HIL simulation of a subway vehicle.**

A power amplifier block is a component capable of imposing a scaled-down reference current, denoted as $i'_{vh}$. This device should have a fast response to the reference signal. An electronic converter with a choke inductor is used for this purpose. An external bidirectional DC source is used to provide or absorb the energy required for the simulation.

IV.1.c. <u>Supply line variable resistance</u>

The variable resistance between the subsystems is complex a characteristic to represent in the HIL platform. The rail has an equivalent linear resistance $\Lambda_{rail}$ that depends on its conductor material and cross section area. This means that any resistive element used to represent the rail in the experimental setup, with $R$ Ohms, can be refereed as segment of rail, with length $D$ in meter given by

$$D = \frac{R}{K_r \Lambda_{rail}}. \tag{50}$$

From (44), it can be seen that the represented length is proportional to the resistance of the element. Thus, if a set of small resistive elements, in the order of milliohms, are placed in series, a discretization of the rail can be physically performed. Inspired by the rheostat concept and functionality, a customized structure is presented. This element is composed of several resistances is series and switching devices (Figure 2-25.).
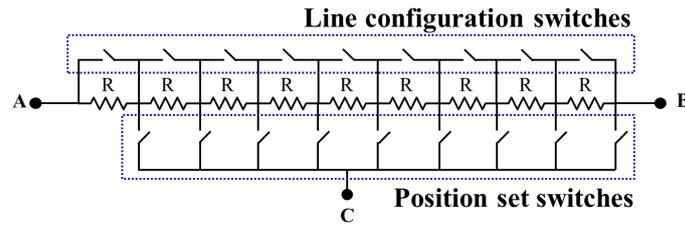
**Figure 2-25: Basic resistance array structure.**

In the presented structure, there exist switches placed in two distinct configurations, with different functionality. The line configuration switches, on the upper part, can be used to configure the total resistance (or length) of a determined segment. This switch adds flexibility to the element in terms of length representation. The equivalent length of segment $D_{eq}$ with $N$ resistor and $S_L$ closed line configuration switches is given by

$$D_{eq} = (N - S_L)\frac{R}{K_r \Lambda_{rail}}. \tag{51}$$

The position set switches, bottom part, are used to vary the resistance between terminal C the externals A and B points. If the emulated current is drained in terminal C the moving characteristic of the subway can be emulated by closing the resistance set switches one by one, according to the subway position. During the transition, in order to avoid system damage, one switch is only opened if the adjacent is closed. The response time of the device must be respected.

The structure presented in Figure 2-25 can represent only one direction and a small part of the supply rail. For bidirectional consideration, an identical structure is duplicated. In this study, the combination of both directions is termed a "block." To expand the supply line capacity, multiple blocks can be sequentially connected.

As a train moves on the supply line, it transitions between blocks. To account for this, additional equipment is utilized to maintain the correct block connections. A "matrix" of relays acts as the intermediary between the converters and the blocks, as illustrated in Figure 2-26. For the control of relay an external controller that receives simulation variables is realized.
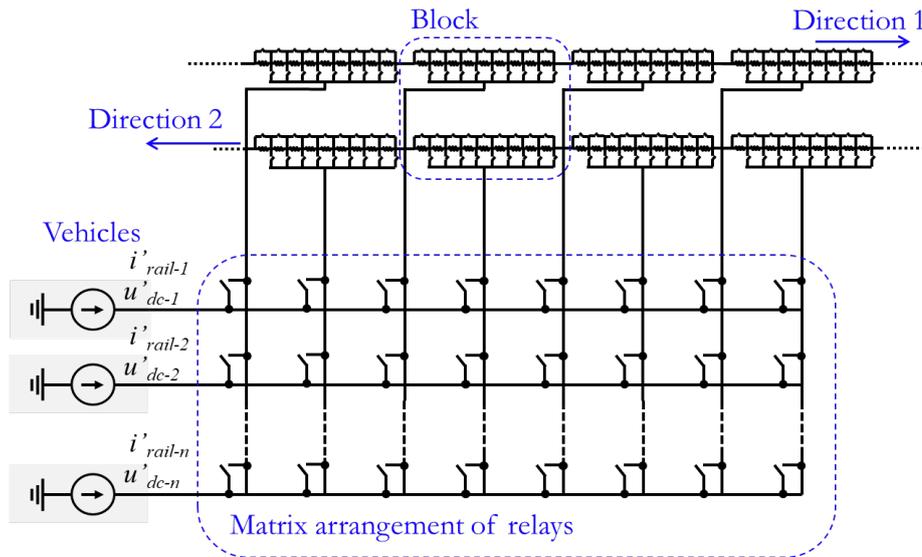
**Figure 2-26: Matrix representation of line resistances.**

The TPS is physically implemented respecting its traditional configuration. The power transformer is customized to respect the system scaling coefficient. The diode bridge consists in an off-the-shelf element with nominal voltage and current levels that tolerate the order of magnitude of the reduced-scale experiment. Finally, the concept of the complete setup can be seen in Figure 2-27.
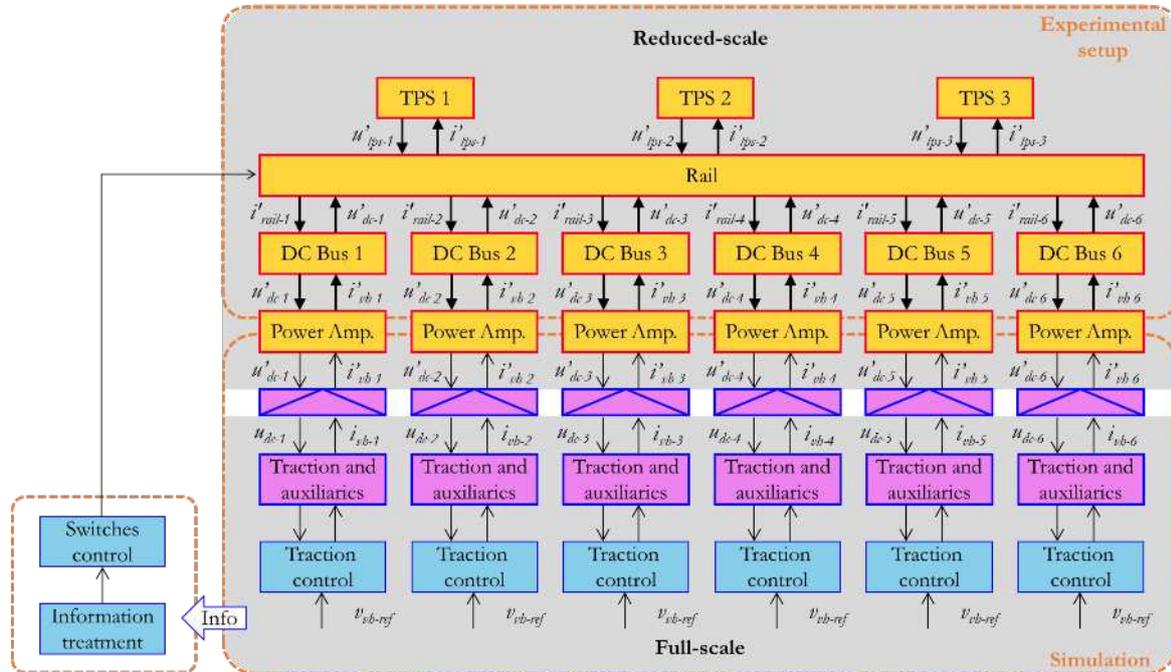


**Figure 2-27: Concept of the HIL platform.**

71

## IV.2. Validation of the HIL Setup

The validation of the experimental platform is conducted using the same experiment and principle as that of the purely simulation-based model validation. Unlike the actual line, the HIL setup comprises only three TPS. Therefore, it is essential to select a segment of the path in which primarily only three TPS are utilized.

Based on the understanding of the experimental conditions and combined with the analysis of the TPS demand and consumption, it is feasible to determine a route for system validation. Consequently, a numerical simulation is carried out, and the results are analyzed (Figure 2-28).
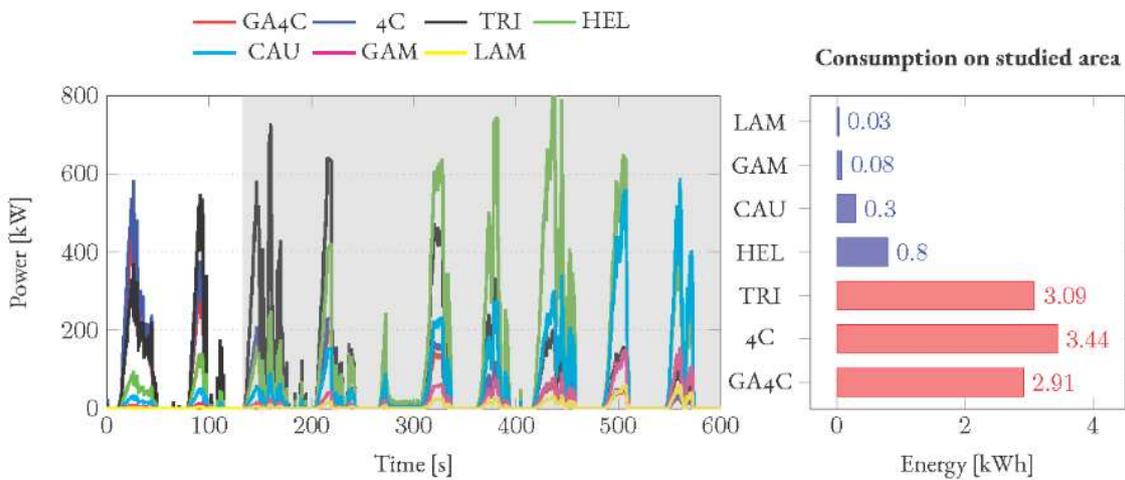


**Figure 2-28: Power demand and energy consumption of TPS.**

Between the start of the simulation and t=133s, it is observed that the substations GA4C, 4C, and TRI predominantly contribute to the energy supply of the system. For the chosen segment, the energy provided by all the TPS in the system is calculated (Figure 2-28). In this context, the contribution from the aforementioned three TPS accounts for 89% of the total. Therefore, this segment is selected for simulation and validation of the HIL platform. It is crucial to highlight that the substations farther from this segment exhibit negligible consumption, which is expected based on system topology.

IV.2.a. <u>HIL simulation</u>

The system is then implemented with a combination of hardware and software elements that enable real-time execution. The three TPS are coupled to the series of resistances that represent the power supply line. The capacitor that represents the input filter of the vehicle is connected to the matrix element for correct positioning on the power line. The vehicle traction system is

simulated in real time in the dSPCACE Microlabbox. Current and voltage probes are used to control and calculate the parameters of interest. A control and data acquisition environment is set up at the Control Desk (Figure 2-29).
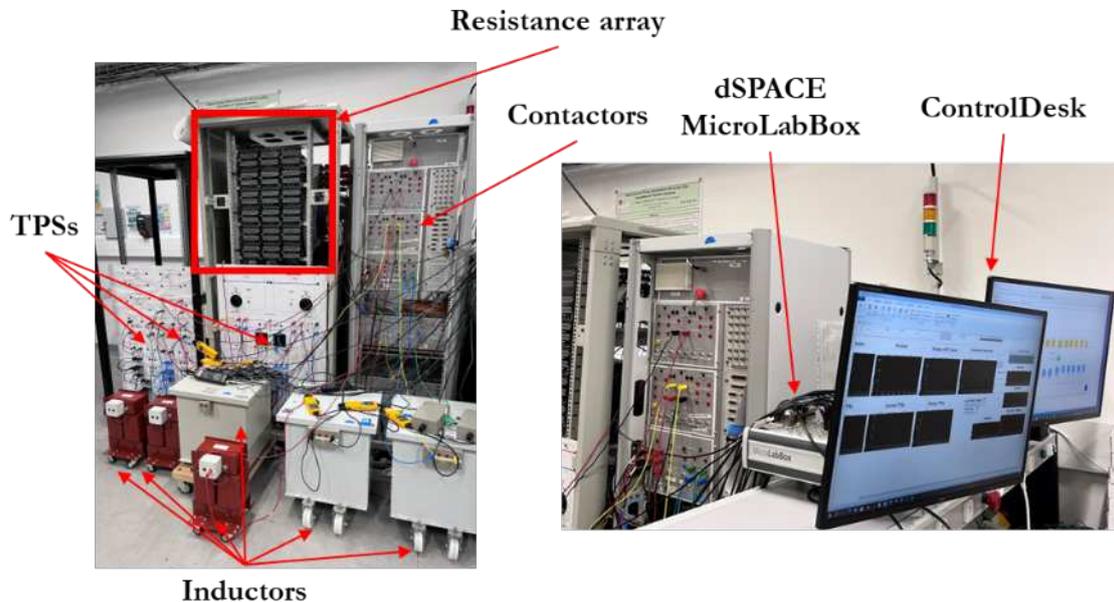


**Figure 2-29: HIL simulation setup.**

The selected segment is replicated in the simulation setup. The developed configuration allows access to multiple connection points for the accurate placement of the TPS, adhering to the distances and resistance between the elements. The HIL simulation variables and experimental results on the actual line are compared. The chosen segment consists of two phases of acceleration and braking, covering a distance of 1.3 km.

For the comparison of electrical magnitudes, these are converted to their equivalent values in real scale through the multiplication of scaling coefficients. The HIL simulation is capable of replicating the behavior of real magnitudes. The speed profile is imposed on the simulated model. The control system effectively enforces the demanded speed (Figure 2-30a). The input filter voltage is compared, and it is observed that the voltage is represented by the HIL simulation (Figure 2-30b). The voltage drop on acceleration phase follows real measurements. The spikes presented on real voltage measurements are due to an attempt of the subway vehicle to active regenerative braking mode after full mechanical braking activation. This functionality has not been considered on the model.

The comparison of the demanded current is also conducted (Figure 2-30c). Positive values can be observed during the vehicle's acceleration phase. The HIL simulation aligns with the expected values. Fluctuations and discrepancies might stem from errors and oscillations in the

voltage measurement of the filter, given that this is used as an input for the real-time simulated model. Overall, the consumption profile on vehicle level is well-represented (Figure 2-30d), with an error margin of 3.3%.
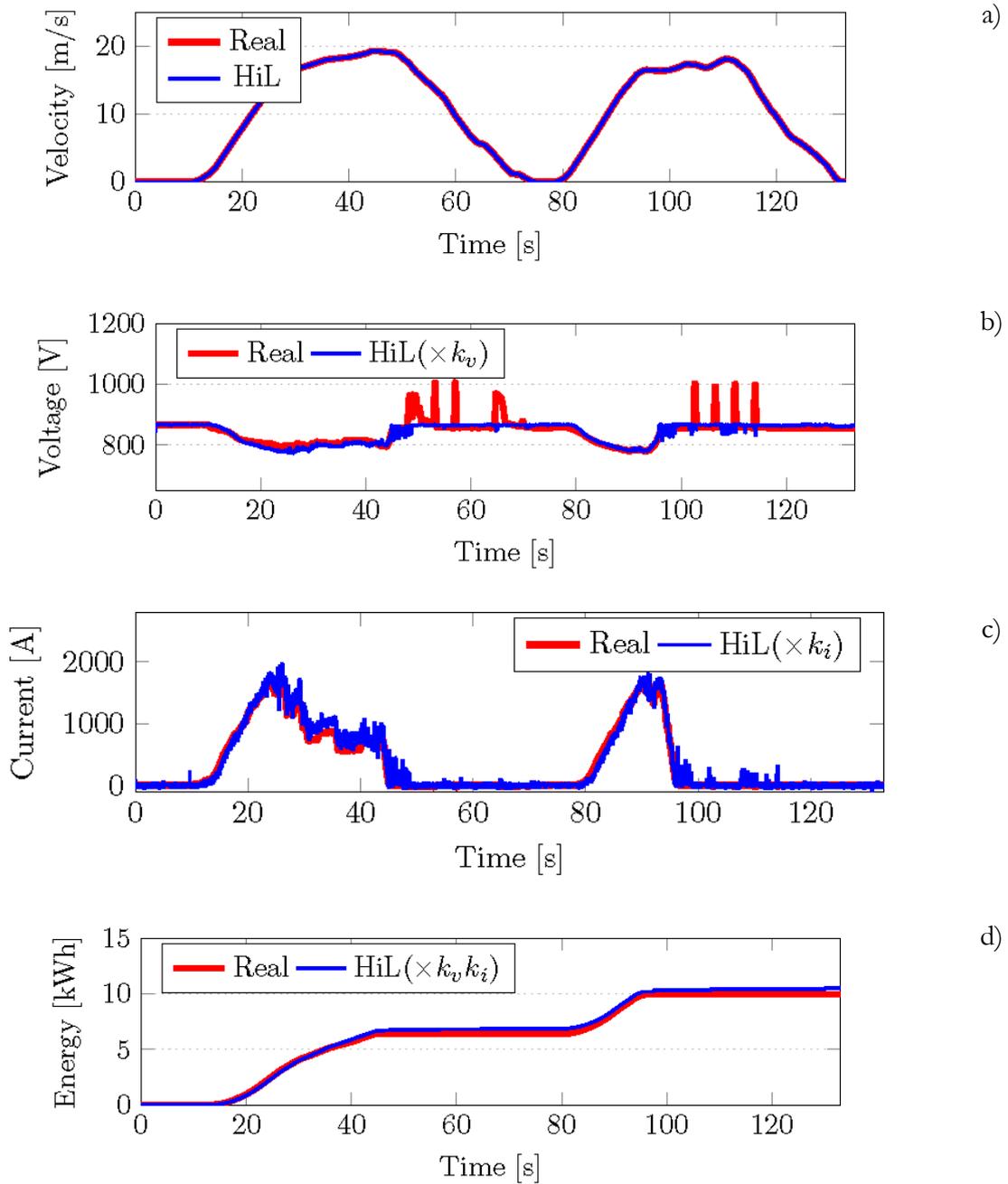


**Figure 2-30: HIL simulation compared to experimental measurements.**

IV.2.b. <u>HIL Multi-vehicle multi-TPS simulation</u>

A demonstration of the capability of the HIL simulation platform is realized. Now, up to 6 vehicles are circulating simultaneously in a carousel configuration. The simulated line has 2.5 km

length and an interval between vehicles (headway) of 110 seconds is considered. The evolution of the position of the vehicles is presented (Figure 2-31a). The current of each vehicle demonstrates the importance of favoring the energy exchange between vehicles (Figure 2-31b). At the beginning of simulation only two vehicles are circulating and they accelerate and brake at the same moment. Consequently, the voltage of the system raises (Figure 2-31c) and no regenerative braking energy is seen. By the time more vehicles are inserted into the line the acceleration and braking phases are combined and energy exchange is noted. This is proved by the presence of negative current. As on of the key advantages of the HIL simulation tool, the instrumentation of the system possible and the energy consumption can be measured on the TPS level (Figure 2-31d).

d)
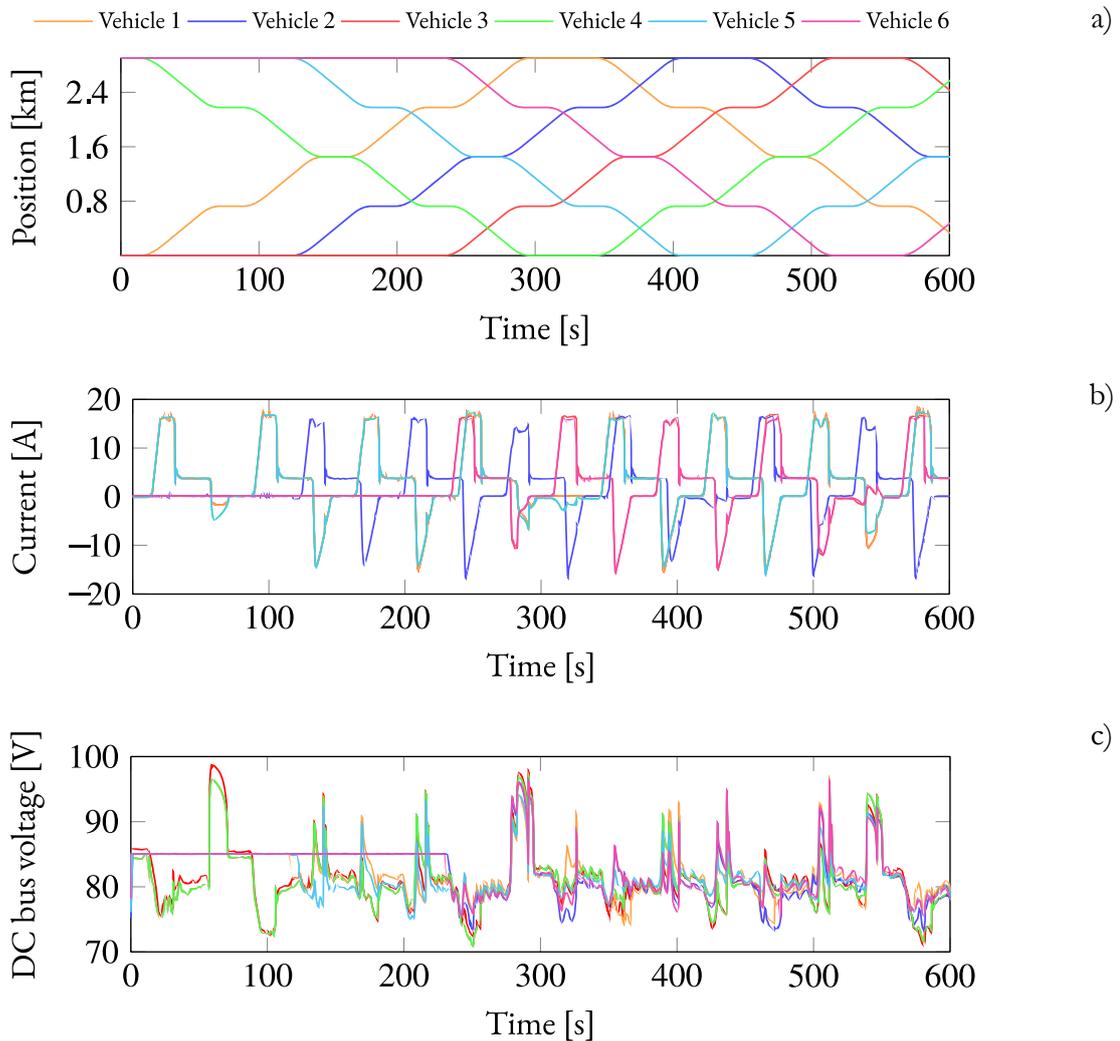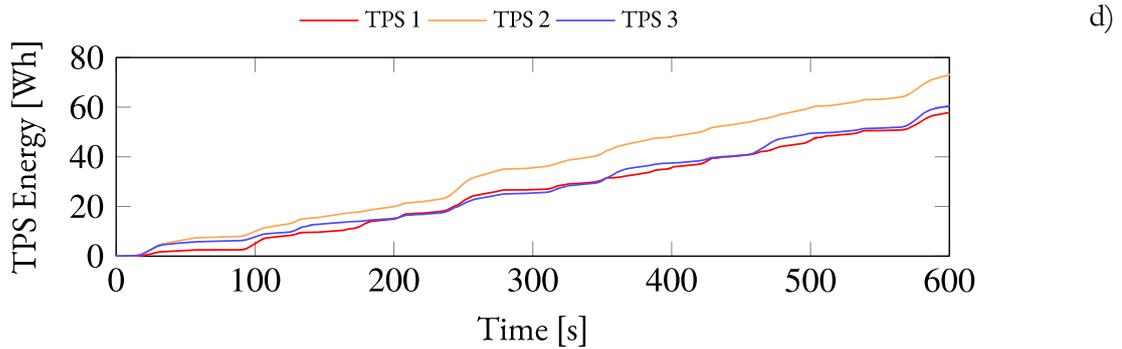


**Figure 2-31: HIL simulation with 6 vehicles and 3 TPSs.**

# V. Conclusion

The methodology used in this chapter presents a contribution to the field of subway carousel modeling, offering a comprehensive framework for understanding and simulating the dynamics involved. A robust dynamic model has been developed that accurately simulates the behavior of subway carousels, capturing essential parameters such as velocity, current, and energy consumption. The forward approach enables the consideration of the capacitor filter dynamics. This is crucial to correctly determine the braking strategy and consequently the energy flow of the system. Tests using real-world scenarios and experimental data validated the model with high degree of accuracy. Providing minimal error in energy consumption assessment.

To address the computational complexity inherent in such detailed simulations, simplified models have been introduced. These models successfully reduced computational time. A model is selected for carousel simulation without significantly compromising accuracy, making it essential for scenarios involving the simultaneous simulation of multiple vehicles and subsystems. A complete simulation of the HIL is realized with 6 vehicles and 3 TPS. The next chapter focuses on incorporating real scenarios to test the model robustness and exploring the capability to evaluate the energy consumption measures on a subway line. Hence, solutions are proposed to reduce the energy consumption of the system.

*Chapter 3:     Energy flow analysis on subway*

*carousel*

# I. Carrousel Simulation

The reliable simulation model is now a valuable foundation for investigating potential reduction of energy consumption on subway lines. To quantify savings potential, analyses are carried out at two levels. Firstly, focusing on the operation of a single vehicle on the line, secondly, extending to the entire subway line as a unified system. In the analysis, particular attention is paid to the complex interactions among multiple vehicles, the power supply line and TPSs.

This research is based on Line 1 of Lille subway system. Within the context of this specific line, the vehicle model under analysis is the previously defined NMR. The significance of these simulations is dual. They contribute to a clearer understanding of how energy is exchanged among the various subsystems. Additionally, simulation results serve to guide measures and technological initiatives aimed at achieving better energy efficiency for the subway system.

It is essential to note that while the results and conclusions obtained are directly applicable to this specific line, they possess the potential for general application. In other words, the findings can be extrapolated to suit other subway systems with similar operational and structural characteristics. To facilitate such broader applications, the study also incorporates examples of a generic fictitious subway line. This serves to uniform and highlight the impact that certain parameters can have on the performance and efficiency of the system. The research methodology used is flexible, enabling customization of system parameters. This adaptability is crucial for studying different subway line layouts, making it a valuable tool for transit systems globally.

## I.1. Simulation concepts

### I.1.a. Line receptivity

The concept of line receptivity concerns the power supply network capability to absorb energy when a vehicle is on braking phase. To understand the potential advantages in terms of energy savings, it is essential to compare simulation results with those from a system that presents a receptive line. This specific operating condition, where energy absorption is improved, is achieved by implementing a modification to the TPS model. A high supply line receptivity is achieved if the TPS operates uniquely in an ON (or conductive) mode.

In this context, when informed that it involves a receptive line simulation, this modification is imposed. This essentially means that the TPSs can manage energy in two directions: both

absorbing and providing it. Under such operating conditions TPS is represented by a source-type element that imposes a rectified nominal voltage, denoted as $u_{ss}$ (Figure 3-1).
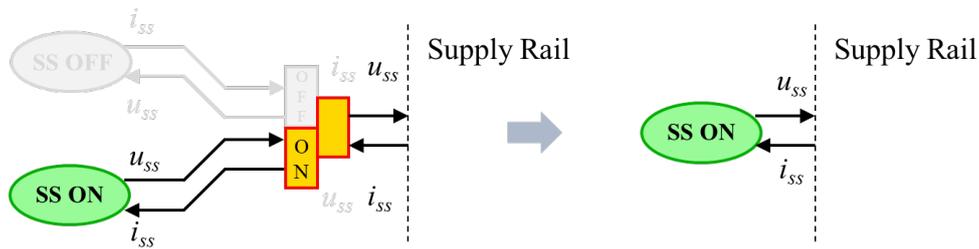


**Figure 3-1: TPSs representation on receptive supply line.**

I.1.b. <u>Fictitious line</u>

A fictitious line represents a theoretical framework where the subway line topology is simplified. This adaptation aims to more precisely evaluate a given study variable, such as impact of interval of vehicles and velocity profile. Essentially, the fictitious line is a condensed segment of the actual line. By adopting this approach, both the number of vehicles and the travel time are minimized. As a result, it is gained the advantage of a less computational costing simulation, enabling more complex studies to be conducted.

On this fictitious line, the distances between passenger stations are maintained at a constant value of 740 m, (Figure 3-2). Additionally, the distances between TPSs are standardized at 1480 m, aligning with the average distances found in the real line. The line topology has been simplified for this representation, excluding factors like slopes and tunnel effects. A stop time of 15 seconds at each station is considered.
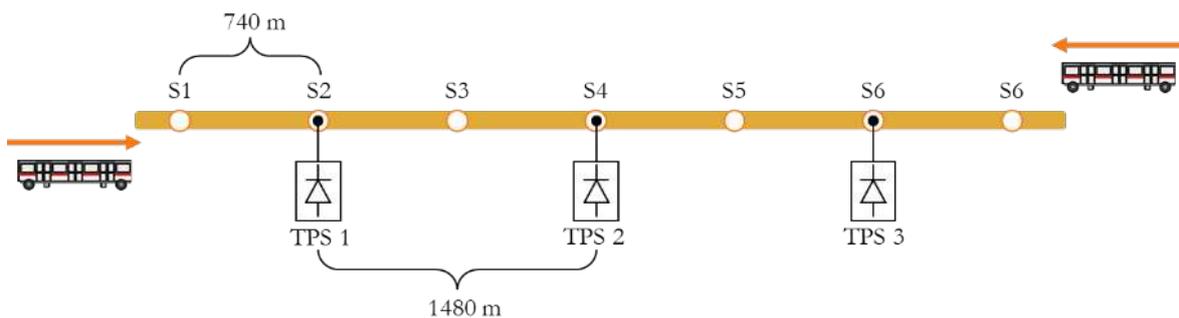


**Figure 3-2: Structure of a fictitious line.**

I.1.c. Injection time

Essentially, the injection time refers to the exact moment at which a vehicle is introduced into the system. For a given injection event $k$, the injection time for the vehicle $t_I^k$ is determined by adding the headway $H_k$ to the injection time of the previous vehicle $t_I^{k-1}$ (Figure 3-3). Unless mentioned otherwise, the injection time is uniform across the system. This means that the moments at which vehicles are introduced at both terminus of the subway carousel are identical, ensuring synchronized operations. Hence, an injection event happens when the simulation time $t_s$ is equal to $t_I^k$,

$$t_I^k = t_I^{k-1} + H_k. \tag{52}$$

Headway, in transportation terminology, refers to the time interval between successive vehicles on a specific route. In traditional transit operations, this interval is not static, it fluctuates over the day. The logic behind these adjustments in headway is based on passenger demand. During peak-hours, shorter headways might be employed to accommodate a higher influx of passengers, Conversely, during off-peak hours, longer headways might be more appropriate given the reduced passenger volume. In a real line operation, different values of $H_k$ are found across the day.
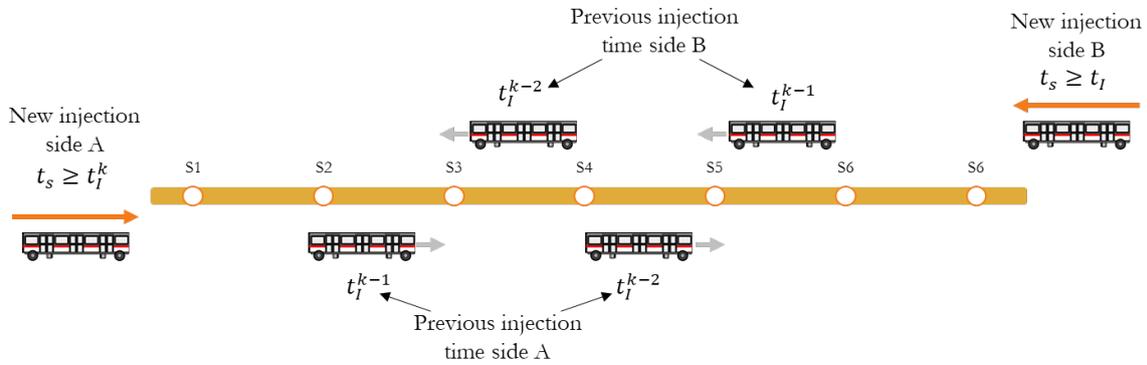


**Figure 3-3: Representation of the concept of injection time.**

I.1.d. Backward approach

In some case studies of this chapter, the simulation using the forward approach becomes infeasible due to the computational effort required. To aid in understanding the system behavior, a backward approach is undertaken. The individual power of each vehicle is summed to estimate the system total demand. In this method, accuracy diminishes as the dynamics of the dc bus are neglected. However, it makes possible simulations whose results can guide interventions in the system. Results are always subsequently validated with a forward approach.

A backward approach starts by taking the outcome (velocity) to identify its cause (necessary power). A differential equation is applied using the causality derivative. This method strength is that it does not demand any control. However, a limitation is that one must know in advance the velocity profile due to the need to derive from the velocity. Moreover, the system limitations cannot be taken into account: an ideal behavior is assumed [Barrero 12]. Using this backward approach, the mechanical power at the machine level is directly determined. To determine the electrical power $P_{elec}$, the traction drive efficiency is considered and the auxiliary power added (Figure 3-4). In order to preserve the physical organization of the system, the backward model is organized from EMR in an EMR-based backward organization of the model [Horrein 15]. EMR enables thus a fast and efficient way to derive the backward model from the forward model [Mayet 16a].
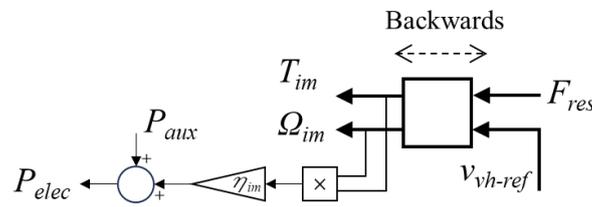


**Figure 3-4: EMR-based backward approach for calculation of demanded electrical power.**

I.1.e. <u>Carousel energy losses</u>

When a subway vehicle moves along its track, it inevitably results in energy consumption in the TPSs. Using the developed model and organization methodology, the calculation of the consumption is facilitated and observed on different levels. This not only provides a clearer understanding of the system, but also facilitates the implementation of measures aimed at reducing energy consumption. The EMR formalism permits easy identification of the variables that need to be measured to calculate the losses. These losses can be categorized as follows:

**Mechanical braking losses ($E_{m-brk}$):** these refer to losses associated with the mechanical brakes, calculated using the mechanical braking force $F_{brk}$ and the vehicle velocity $v_{vh}$,

$$E_{m-brk} = \int F_{brk} v_{vh} dt. \tag{53}$$

**Motion resistance losses ($E_{res}$):** these refer to losses associated with mechanical resistance when moving the vehicle along its path. This can be calculated using the environmental resistance force $F_{res}$ and the vehicle velocity $v_{vh}$,

$$E_{res} = \int F_{res}v_{vh}dt. \tag{54}$$

**Traction and auxiliaries losses ($E_{trac}$):** this refers to the energy consumption by auxiliary components and losses in the electromechanical conversion system. It comprises the electric drive and gearbox. These losses can be computed using the electrical quantities of the inverter, specifically the dc bus voltage, $u_{dc}$, and inverter current, $i_{vsi}$. Also, with variables on wheel level, the torque, $T_{gb}$, and wheel angular speed, $\Omega_{wh}$, for mechanical power calculation. Essentially, $E_{trac}$ is calculated based on the difference in power between the input and output of the subsystem comprising the electrical drive and gearbox. Additionally, the number of bogies ($N_{bg}$) should be taken into account to consider the entire vehicle. The absolute value is taken for calculating losses both in traction and regenerative braking modes. Finally, auxiliaries power $P_{aux}$ is considered for calculation,

$$E_{trac} = \int (N_{bg}|u_{dc}i_{vsi} - T_{gb}\Omega_{wh}| + P_{aux})dt. \tag{55}$$

**Power supply losses ($E_{sup}$):** this refers to the losses in the power supply system and connection resistances of the TPSs and vehicles. These losses can be calculated using the voltages and currents in the TPSs ($u_{ss}$ and $i_{ss}$) as well as the voltage and current in the vehicles ($u_{dc}$ and $i_{vh}$),

$$E_{sup} = \int \left| \sum_{i=1}^{N_{tps}} u_{ss-i}i_{ss-i} - \sum_{j=1}^{N_{vh}} u_{dc-j}i_{vh-j} \right| dt, \tag{56}$$

where $N_{tps}$ denotes the number of TPSs and $N_{vh}$ the number of vehicles.

## I.2. Receptive vs Non-receptive Line: Single Vehicle Simulation

An initial step in the study focuses on the isolated observation of a single vehicle as it operates on the line. This is an initial stage where the complexities introduced by the interactions of multiple vehicles are intentionally excluded. Particularly, the energy exchange capacity between vehicles. This approach has the intention to understand the energy flow on vehicle level. A forward approach is employed where the objective is to arrival at the destination. The input filter voltage fluctuation as well as traction limitations are considered.

For this study two distinct simulations are undertaken. The first simulation operates under normal conditions. The traditional unidirectional TPS provides a non-receptive characteristic. The

activation of mechanical braking is expected due to the lack of mechanisms to absorb the regenerative braking energy. In the second simulation, the line is adjusted to a receptive condition.

The analysis is conducted considering both the fictitious line condition and a round-trip journey on the real line. By quantifying the losses, a clearer understanding of the energy flow behavior among the various components of the vehicle is achieved. This approach ensures a broad evaluation, highlighting insights into potential areas for optimization and improvement.

I.2.a. <u>Simulation on fictitious line</u>

Two simulations have been conducted for the segment of the fictitious line. In both simulations, the vehicles follow the same trajectory and maintain an identical velocity profile. An occupancy rate of 4 passengers per square meter has been taken as the standards for this and further analysis. The velocity profile (Figure 3-5a) and the energy consumed (Figure 3-5b) are analyzed.
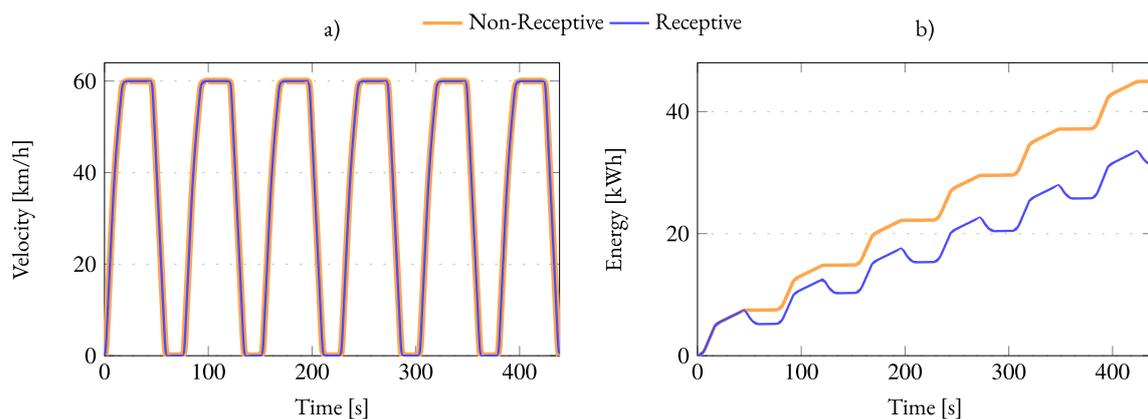


**Figure 3-5: Velocity profile and energy consumption for fictitious line.**

The observation indicates a reduced energy consumption under the condition of a receptive line, which aligns with what is expected. It is observed the presence of energy recovery phases on the consumption curve for the receptive case, which is aligned with the braking phases. For the receptive line, the final consumption stood at 31.4 kWh, in contrast to the non-receptive line with 44.9 kWh. This accounts for a 30.0% decrease in energy consumption for the chosen route. A more in-depth analysis of the energy losses is conducted (Figure 3-6). The most significant outcome is the substantial difference in energy dissipated in the mechanical brakes. For the non-receptive line, the total value is 16.9 kWh, whereas it significantly drops to <0.1 kWh for the receptive line.
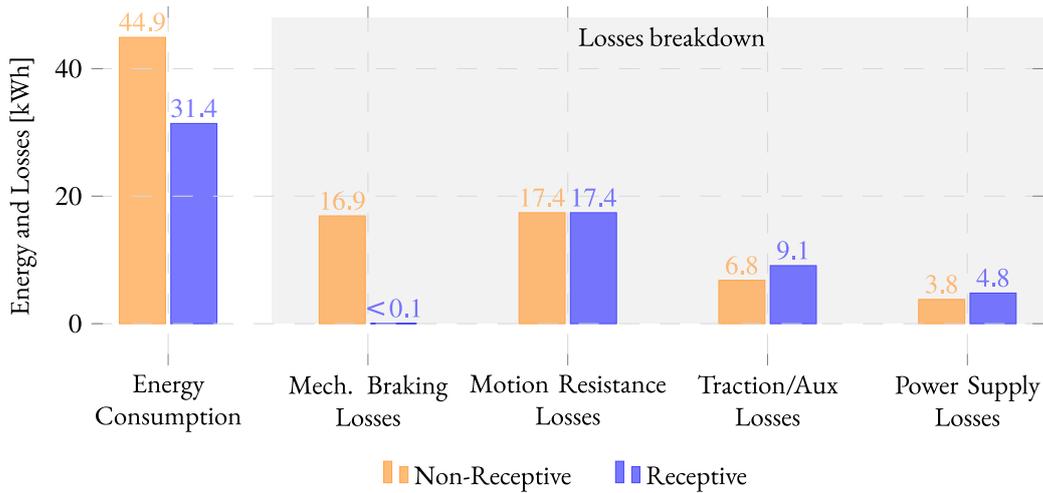
**Figure 3-6: Energy consumption and losses detail on a subway vehicle.**

The remaining presence of mechanical braking losses in a receptive line can be attributed to the activation of brakes at low speeds for a complete stop, according to previously established braking strategy. Motion resistance losses remain constant, for the same velocity profile. The losses in the traction and auxiliaries system and power supply line are marginally higher for the receptive line. This fact can be explained by the increase of energy flowing in the electric traction system on a receptive line.

I.2.b. <u>Simulation of real line</u>

The same scenario is repeated, but now considering the real track topology. A round-trip route is taken into account to ensure that the vehicle returns to its initial altitude. Once again, only a single vehicle is deployed on the track. The entire trajectory covers a distance of 12.5 km and includes 18 passenger stations. Detailed information regarding stop durations and the location of these passenger stations is provided on Appendix B. The velocity profile of the vehicle (Figure 3-7a) and the energy consumed (Figure 3-7b) are presented.
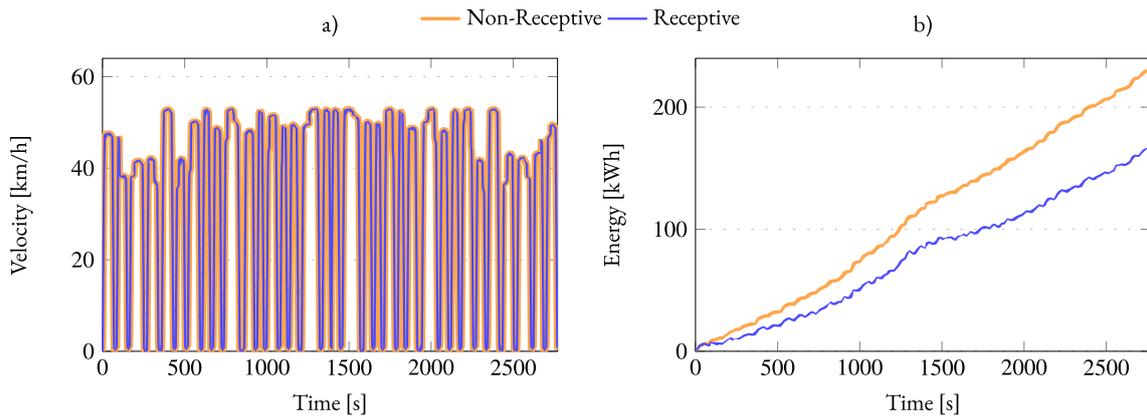
**Figure 3-7: Velocity profile and energy consumption for real line.**

The findings indicate a reduction of energy consumption for a receptive line, consistent with earlier observations on fictitious lines. The energy consumption for a receptive line stood at 164.3 kWh, while the non-receptive line consumed 229.9 kWh. This represents 28.5% on energy saving. With respect to detailed losses (Figure 3-8), the mechanical braking losses are significantly reduced, dropping from 78.9 kWh to 0.2 kWh. Motion resistance losses are consistent in both scenarios. Traction and auxiliary and power supply losses are also marginally higher for the receptive line.
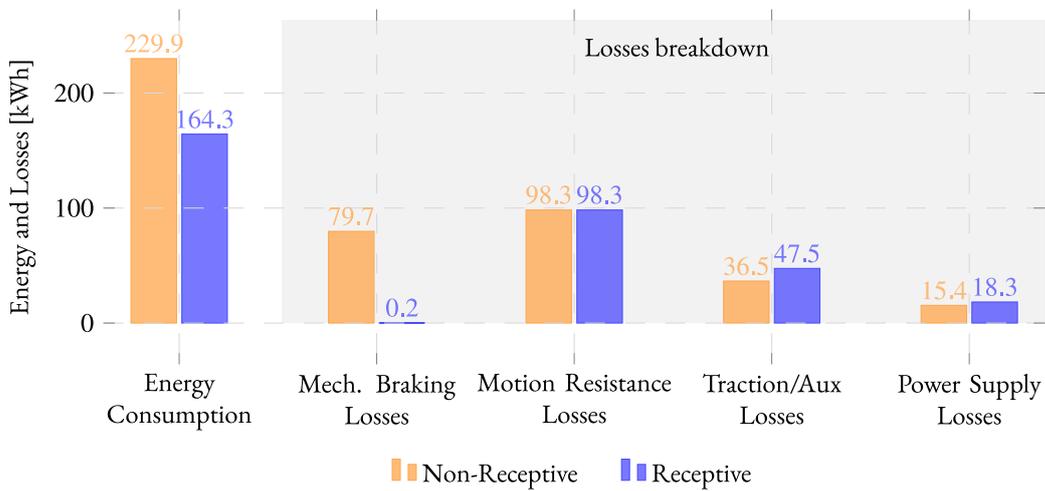


**Figure 3-8: Energy consumption and losses detail on a subway vehicle.**

The results for both the fictitious and real lines exhibit similar behavior. Clearly, the magnitude of consumption differs. On the real line greater distances are covered and variations in the track slope are taken into account. However, it can be concluded that, for single vehicle evaluation, the fictitious line and the real one exhibit the same behavior.

## I.3. Receptive vs Non-receptive Line: Carrousel Simulation

The individual analysis of a vehicle is pivotal in understanding energy losses and flow in each part of the vehicle. However, there are energy exchanges between circulating vehicles.

As previously indicated, the interval between vehicles is adjusted during line operation. As a result, this adjustment directly impacts the interaction between active vehicles. Line receptivity is impacted as a function of accelerating and braking vehicles phases. Therefore, the headway variable becomes essential in analyzing the carousel system. In this section, focus is placed on analyzing the influence of headway on energy consumption. Results are provided for both fictitious and real lines.

I.3.a. Carousel simulation on fictitious line

For the fictitious carousel line, multiple simulations have been conducted. On each simulation a constant headway is considered. Subsequently, results are compared to evaluate the impact of this specific parameter. Vehicles are presumed to be available at the terminals of the line and are introduced based on the chosen headway.

The carousel simulation can be categorized into three distinct phases (Figure 3-9). The transient-start phase encompasses the duration from the start of the simulation until the moment at which the first introduced vehicles reach the final destination. The steady-state phase is characterized by a constant frequency in the number of circulating vehicles. During this phase, recurring acceleration and braking sequences can be observed in a cyclical pattern. Lastly, the transient-stop phase is determined by the return of vehicles to the line terminals.

This simulation routine ensures that the kinetic energy at the vehicle level is zero at both the beginning and end of the simulation. The simulation is performed in a such manner that, beyond a specified point in time (e.g., $t_s$ >3600s), no new vehicles are introduced. The simulation terminates when the last vehicle arrives at the terminal.
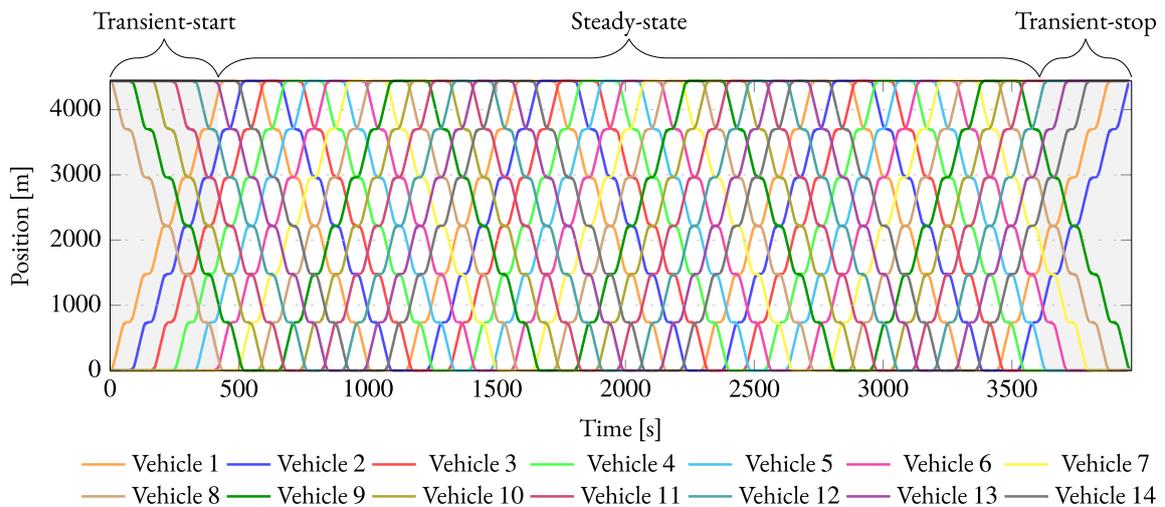
**Figure 3-9: Example of vehicle position on carousel simulation for fictitious line.**

An overview of the impact of the headway on energy consumption is provided initially. It should be emphasized that this result is displayed in relation to the headway. This implies that each data point represents the outcome of a simulation, for instance, the total energy consumption. For comparative purposes, for each headway introduced, an additional simulation is conducted for a scenario on a receptive line. This enables the analysis of potential energy savings at a specific operating point.

A trend can be observed, showing higher global energy consumption for shorter intervals (Figure 3-10a). This observation is anticipated, as a larger number of vehicles are operating on the line. However, this tendency is not true for all points. It can be seen that in certain instances, reducing the headway suggests a decrease in energy consumption. This means that even with an increase in the number of operating vehicles and the distance traveled, energy consumption can be reduced. Two points are highlighted in the provided figure to elucidate. When comparing the result with the case of a receptive line, it can be seen that global consumption is reduced for all operation points and the oscillatory profile is not observed. In fact, the oscillatory profile is a consequence of the existence of intervals that favor the use of regenerative braking energy.

One method to assess the system energy consumption is by calculating the consumption with the unit "energy per passenger-kilometer" (Wh/pkm). As the name suggests, the consumption is calculated related to the product of the distance traveled by all vehicles and the number of passengers transported (Figure 3-10b). In this context, local minima can be highlighted, indicating intervals at which better travel efficiency is achieved.
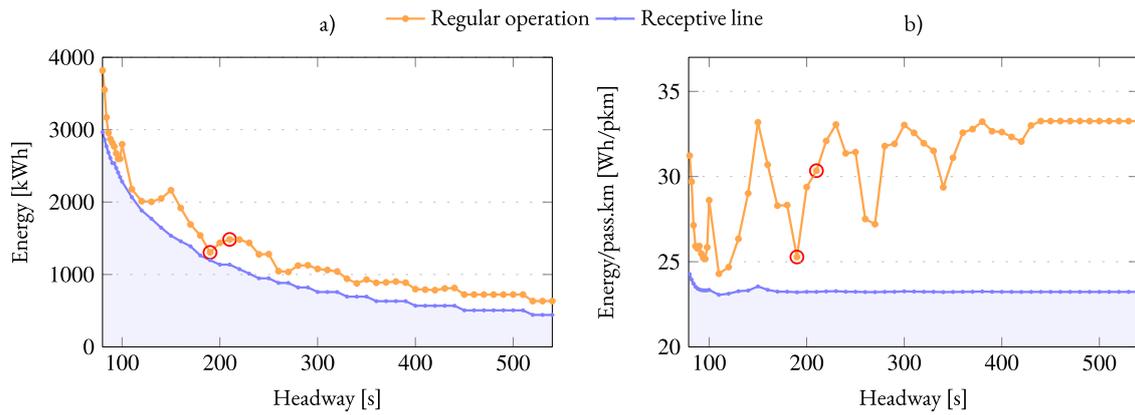
**Figure 3-10: Global Energy and energy per passenger-kilometer for the fictitious line.**

To better investigate the observed pattern, the losses at the highlighted points are analyzed in detail (Figure 3-11). These points correspond to the headways of 190 seconds and 210 seconds. It is observed that operating within the 190-second headway results in a globally lower consumption compared to the 210-second headway.

The losses due to motion resistance are higher for 190-second headway following the increase of number of circulation vehicles. However, it can be seen that the losses from mechanical braking are considerably lower for the 190-second interval. This suggests that this interval induces better synchronization of acceleration and braking phases of vehicles, facilitating energy exchange between them. Traction and auxiliaries losses are greater for the shorter interval, following the trend observed on a more receptive line.
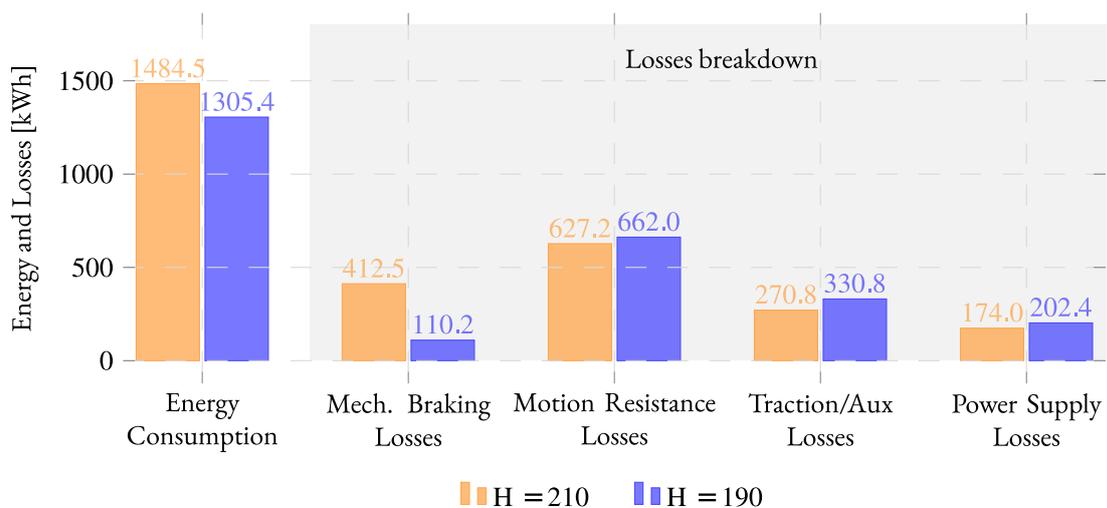


**Figure 3-11: Energy consumption and losses detail for H=210 and H=190 on fictitious line.**

The observed global consumption at the 190-second interval is relatively close to the consumption observed for results on a receptive line (Figure 3-10). It suggests that this operation point tends to favor the condition for a receptive line. In this case, a better utilization of regenerative braking energy.

In general, an oscillatory pattern with local maxima and minima is observed. This indicates the presence of specific points that either facilitate or make it more difficult the synchronization of vehicles to favor the use of regenerative braking. For long intervals (greater than 400 seconds), there is minimal fluctuation in consumption. This phenomenon can be explained by the absence of other vehicles on the line that can absorb the regenerative braking energy. Even if two vehicles move in opposite directions, their acceleration and braking phases are synchronized due to the symmetry of the fictitious line.

It is essential to highlight that the energy consumption profile, as well as the local maximum and minimum points presented are representative exclusively of this fictitious line. Altering variables such as distances between stations or stop time would produce different consumption profiles. However, it can be concluded that if the aim is to operate a more efficient subway line certain intervals should be prioritized. Based on the conclusions obtained from the fictitious line, it is possible to proceed to the simulation of the real line.

For better comprehension, the previous result from a forward approach simulation is compared to one with backward approach (Figure 3-12). It is noted that although the values differ in terms of magnitude, the points of local maximum and minimum remain consistent. Indeed, the backward simulation does not take into consideration the dynamic of the dc bus voltage and rail supply losses. Due to these simplifications the energy consumption on backward approach presents lower values compared to the forward simulation. However, the oscillatory profile is similarly reproduced. Hence, it can serve as a guideline for headway analysis.
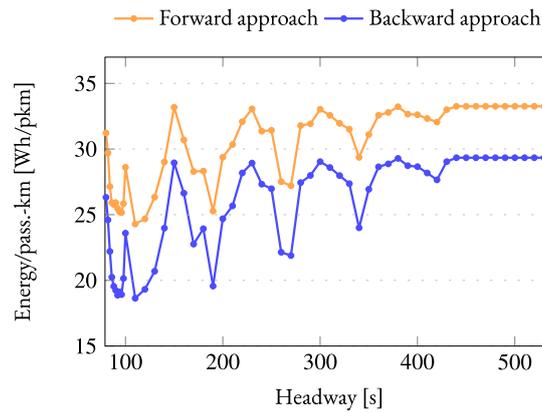
**Figure 3-12: Comparison of Backward and forward simulation (consumption per passenger-kilometer)**

I.3.b. <u>Carousel simulation on real line</u>

I.3.b.i. Headway analysis

In the operation of a real subway line, there is a systematic adjustment of the time intervals between consecutive vehicles based on fluctuating passenger demand. It is known that the interval varies in function of time slots of the day, and various operational points are assessed. Hence, the injection time is adjusted to respect the required headway.

For the real-line scenario, simulating a wide range of intervals, as done for the fictitious line, becomes impractical due to the computational cost required. This case requires multiple simulations with 10 TPSs and up to 34 vehicles running simultaneously. Therefore, in this specific case, a backward approach is employed with the aim of identifying consumption trends based on the operational headway. For this purpose, a vehicle velocity profile is recorded, in forward simulation, for both directions of the route (Figure 3-13a). Subsequently, the corresponding electrical power profile over time is obtained (Figure 3-13b).
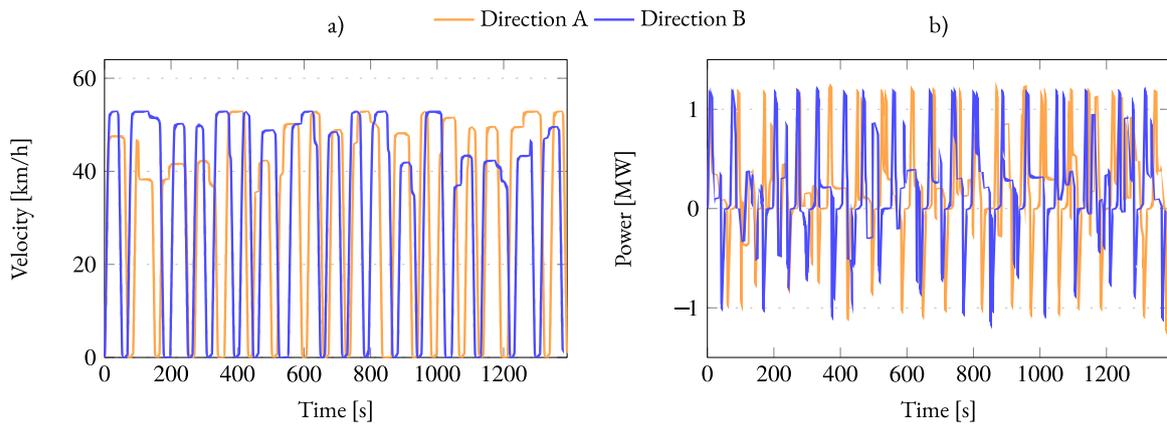
**Figure 3-13: Simulated velocity and power profile of real line.**

As observed, the power demand profile (Figure 3-13b) shows positive values, indicating traction phases, and negative values for regenerative braking phases. In the backward approach, the supply line is considered as a single ideal conductor. Therefore, to calculate the total power of the system, the power demand curves of each vehicle are simply added, respecting the headway under consideration. At this point, there is a loss in the precision of the simulation to identify local losses and energy flow between subsystems.

To estimate consumption, a specified number of injections is established, and the energy per passenger-kilometer is then calculated for a fixed headway. It can be inferred that positive power values indicate an energy demand from the TPS for vehicles. Conversely, negative power values suggest the presence of excess regenerative energy. Given that TPS power flows are unidirectional, the area of the curve where values are positive is considered for consumption calculation. An example with a headway of 135s is provided. In this case, throughout the simulation 50 vehicle are inserted on each terminal. The progression of power demand over time can be observed (Figure 3-14a), as well as a detailed view of the power demand in a steady state (Figure 3-14b).

It should be noted that the calculated consumption is based on the simplified backward approach. Although the consumption values are simplified, this methodology aids in identifying intervals where there is better synchronization between vehicles. This, in turn, facilitates the selection of operational intervals.
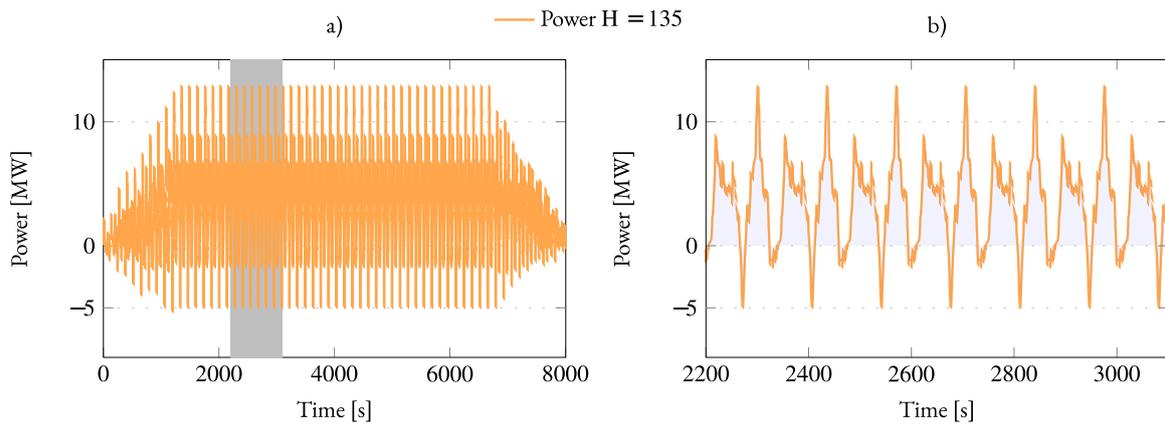
**Figure 3-14: Backward simulation of 50 injections considering a headway of 135 s.**

An estimated consumption per passenger-kilometer profile is obtained as a function of the headway from the backward approach (Figure 3-15). In function of the applied headway, local maximum and minimum points are identified. This profile suggests the presence of operational points that should be prioritized and others that should be avoided. A less oscillatory pattern is identified compared to the fictitious line. The real line exhibits asymmetry in terms of the distance between stations, stop time, and slopes. Overall, there is also a trend of improved consumption per passenger-kilometer at shorter intervals, that is, in intervals with a higher number of circulating vehicles.
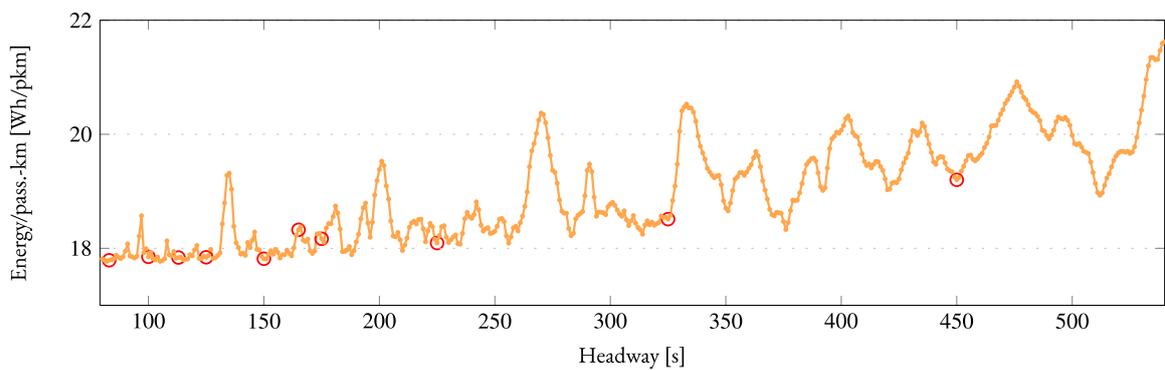


**Figure 3-15: Backward simulation - consumption per passenger-kilometer on real line.**

I.3.b.ii. Carousel real line regular operation

Once the consumption behavior of the system has been estimated, an analysis of a regular daily operation of the subway can be conducted. Now, the model in forward simulation is applied and detailed losses are analyzed. For this purpose, a realistic timetable is selected as the base reference. This chosen timetable corresponds to the operational conditions encountered on a

typical weekday on the studied line, considering the migration to new vehicle NMR. Different operating headways are designated for different time slots throughout the day (Figure 3-16).
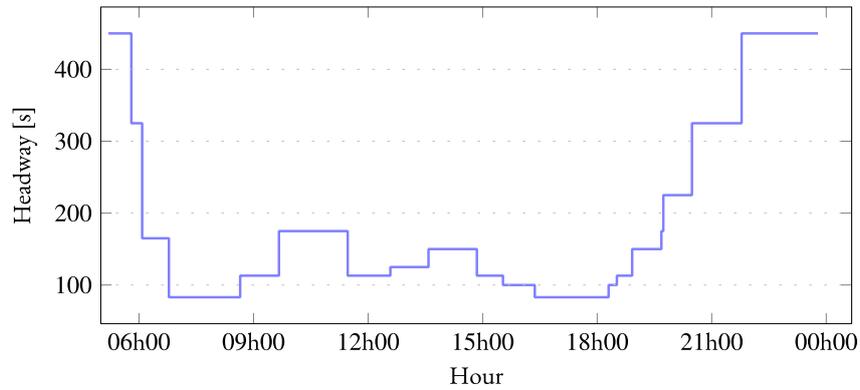


**Figure 3-16: Typical headway evolution during a working day.**

Different from a constant headway simulation, now there is a mechanism that recalibrates the injection time to ensure the application of predefined timetable. Whenever there is a change in headway, the system enters a transient period until the steady-state cycle is achieved for this new operation point. For visualization, the position of vehicles on first hours of simulation is presented (Figure 3-17). It is also noteworthy to mention the computational challenges faced, as the simultaneous simulation of multiple vehicles necessitates substantial computational resources. The full-day full-line simulation corresponds to 12.5 kilometers of line, 10 TPSs, 34 vehicles (on peak-hours) during 68700 seconds of simulation (about 19h).
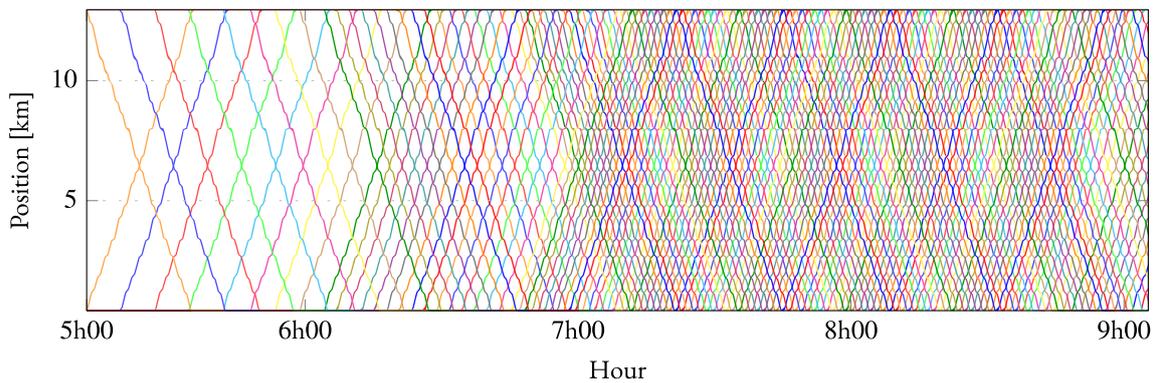


**Figure 3-17: Position evolution for fist hours of carousel operation on real line.**

The presented timetable is incorporated into the simulation. To assist in the visual interpretation, the operating values have been accentuated in red on Figure 3-15. From a comprehensive observation of the data, it is noted that most of the points are positioned under conditions that favorize the use of regenerative braking energy. Within this simulation framework,

94

two distinct scenarios are undertaken, one using the traditional TPS topology and the other employing a receptive line for comparison purposes.

Simulation results indicate a total energy consumption of 82.6 MWh for the base daily operational scenario. In contrast, a consumption of 80.8 MWh is observed for the same route when considering a receptive line (Figure 3-18). This suggests that a potential reduction of 2.2% is theoretically achievable for the selected operation day. The data also reveals that losses due to mechanical braking are minimal in comparison to other losses. This implies that the operational points are beneficial to the use of regenerative braking. Furthermore, in the simulation of a complete line, a larger number of vehicles operate simultaneously, increasing the possibility of energy exchange between vehicles. Results suggest that busy and larger lines tend to be more receptive. However, attention should be paid to voltage fluctuations on dc level with the increasing of circulation vehicles.
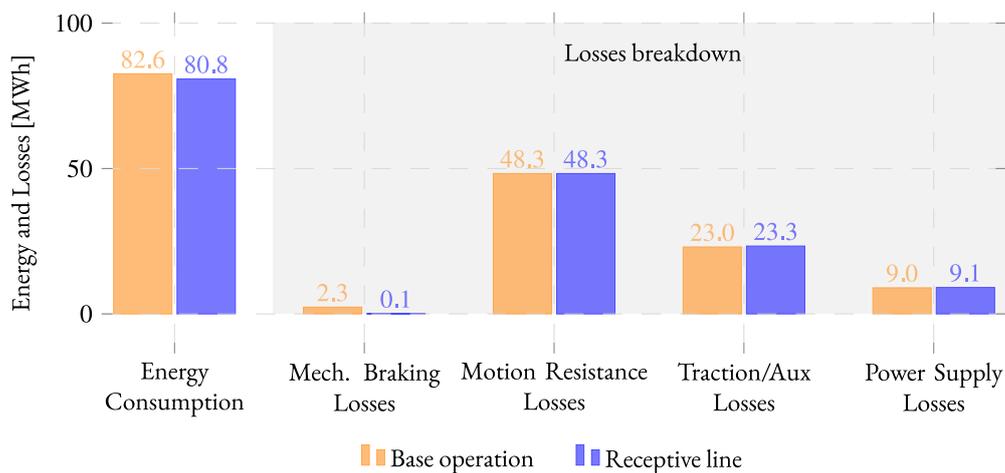


**Figure 3-18: Energy consumption for carousel operation on full day vs. receptive line.**

Motion resistance losses remain at same value since the same velocity profile and distances are covered in both simulations. Power supply and traction and auxiliary losses are slightly higher in the case of a receptive line, suggesting a larger proportion of regenerative braking in the system. The potential reduction in consumption due to enhanced utilization of regenerative braking might appear neglectable, however, it still accounts for an additional 2.2 MWh per day of operation. This amount is significant in terms of energy quantity. The energy, considered as wasted, offers potential for alternative use, promoting system efficiency. Beyond energy savings, reducing mechanical brakes activation brings about environmental benefits by decreasing microparticle emissions and reducing brake wear, leading to reduced maintenance and operational costs.

It can also be noted that other types of losses have a substantial impact on a line energy consumption. For instance, motion resistance losses in general account for over 50% of the line consumption. Measures aimed at an overall reduction in energy consumption need to take into account the reduction of losses at all levels.

In a carousel system, it can be concluded that the behavior of a short, less busy line is more subject to mechanical braking losses. Analysis of a line requires consideration of the entire system. A small section of the line cannot represent the entire system.

It is important to emphasize that the presented results are based on the assumption that there are no disturbances in the line. Blocked doors and mechanical incidents would alter the energy consumption results as delays would be imposed to the trajectory. The subsequent sections aim to explore ways to minimize energy consumption and their detailed impact on reducing energy losses.

## II. Improvements of subway operation parameters

This sub-section aims to assess measures to reduce overall consumption. Clearly, it remains imperative to ensure transportation availability for passengers while maintaining the safety and comfort of the operation. In this section, interventions related to velocity and acceleration parameters, line voltage, and adaptation of vehicle injection into the line are analyzed. The focus is given to real line operation.

### II.1. Reference velocity reduction

The modification of the reference velocity of the line aims to reduce the overall system losses, focusing on motion resistance and mechanical braking losses. The implemented methodology involves multiplying the line final reference value by a constant coefficient. This adaptation does not alter maximal acceleration available.

Analyses are conducted taking into account the real operation of the subway line under study. Cases are examined individually for conditions of a single vehicle and carousel operation. The values are compared with the outcomes from the previous session (base operation) to assess the true impact. For a more comprehensive analysis, values both below and above the nominal velocity are taken into account. Thus, it is possible to define the adaptation coefficient $k_{vel}$ based on the nominal final reference velocity $v_{ref-f}$ and the adapted velocity $v'_{ref-f}$,

$$v'_{ref-f} = k_{vel}\, v_{ref-f}.$$
(57)

The velocity profile is adapted and subsequently imposed on vehicles traveling on the line. For instance, Figure 3-19 illustrates the impact on a generic route. It can be seen that acceleration parameters remain constant, while the reference velocity is decreased. As a result, there is an observable increase in the travel time,. Thus, a detailed investigation is essential to understand the potential energy savings and the impact of imposing delays on the trajectory. Even if velocity is reduced the simulation control objective remain the arrival at final destination.
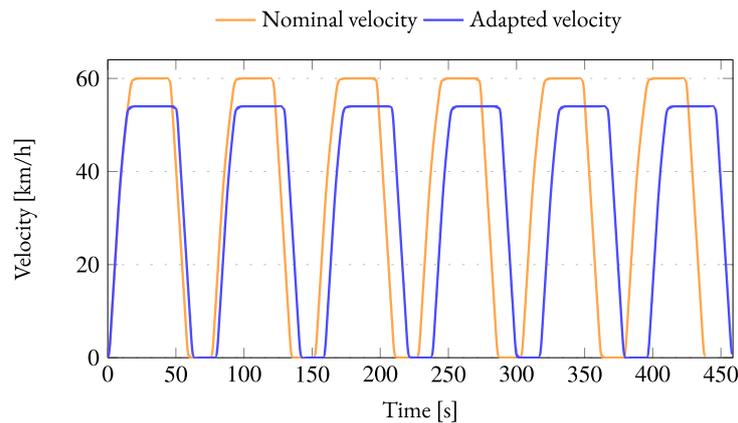


**Figure 3-19: Adaptation of reference velocity.**

II.1.a. <u>Single vehicle analysis</u>

The analysis of the velocity adaptation begins by the evaluation of simulation results for a single vehicle. In this context, a round trip is assessed. The impact of the velocity adaptation coefficient in the reduction in final consumption is presented (Figure 3-20a). A reduction of 15% on energy consumption is obtained with a 20% decrease in the reference velocity. However, the total journey time changes as well. A 14% increase in travel time is noted for the same 20% reduction in reference velocity. In practical terms, this represents an additional 3.3 minutes for a one-way trip that typically takes about 23 minutes.
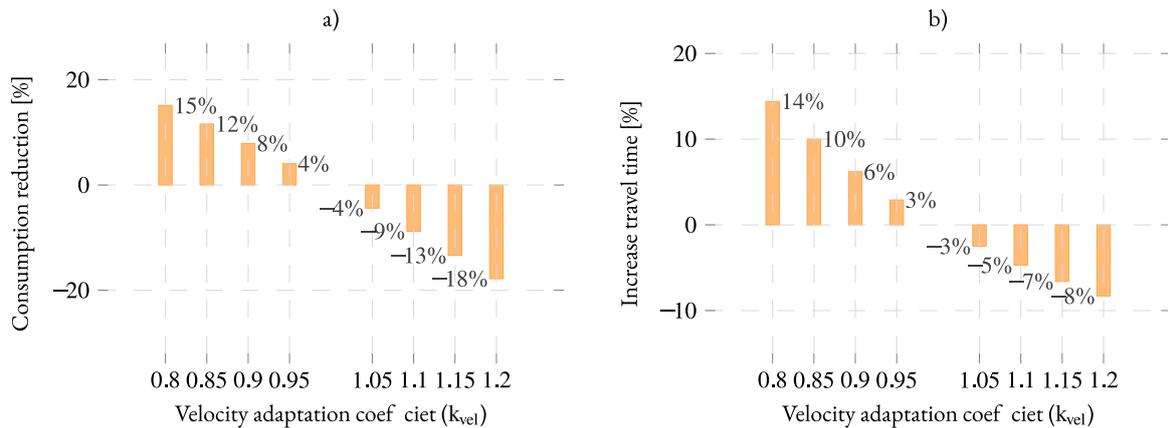
**Figure 3-20: Adaptation of reference velocity on real line with single vehicle operation.**

Still focusing on a single vehicle operation, a comprehensive examination compares the losses for the scenario where $k_{vel} = 0.9$. The finds observed for this scenario suggest a good trade-off between extended travel duration and potential energy savings. The operation of a single vehicle on the tracks reveals 8% of energy savings. Additionally, the one-way trip time is increased by only 1.4 minutes. Significant energy savings can be achieved without causing substantial delays in transit time.

Hence, detailed energy consumption and losses for the selected scenario is presented (Figure 3-21). Simulation results show reduction in losses in all evaluated categories. Among them, mechanical braking losses significantly influence consumption reduction. When the vehicle operates at reduced velocity, it possesses less kinetic energy at the braking moment, leading to reduced mechanical braking losses. Motion resistances losses are also reduced, following the direct reduction of resistance force magnitude (square of the velocity). Consequently, a reduction in traction system losses. Even though auxiliaries are activated for a longer period, it is not enough to increase losses in this category. The decrease in supply losses is justified by the reduction of current magnitude during cruise phases due to less motion resistance losses.
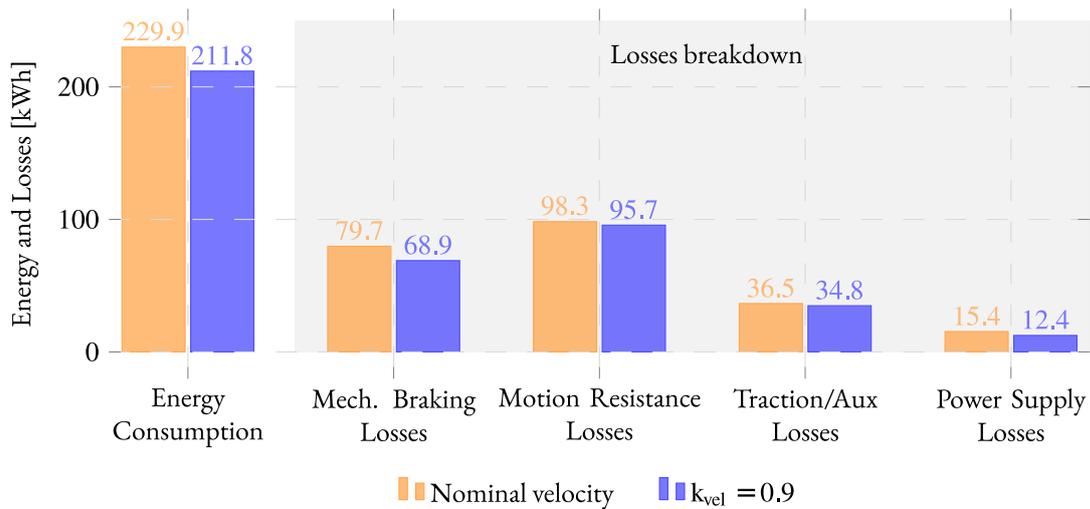
**Figure 3-21: Single vehicle energy consumption and losses detail for real line with velocity adaptation.**

II.1.b. <u>Operation points analysis</u>

The same adaptation coefficient is selected for analysis in the carousel mode. The reduced velocity profiles for both directions are recorded for the chosen coefficient. Subsequently, consumption per passenger-kilometer is analyzed in a backward approach for possible operational headways (Figure 3-22). It is observed that, in general, consumption is reduced for the presented operational points. Local maximum and minimum values are also noticed; however, these are not situated at the same points as in base operation. With the modification of the velocity profile, the braking and acceleration moments of vehicles change.

At certain operating headways, consumption per passenger-kilometer at reduced velocity surpasses that of regular operation. This suggests the existence of operation points where there is no advantage in reducing the line reference velocity. Thus, even with a lowered reference velocity, careful consideration is necessary when choosing the operating intervals for the line.
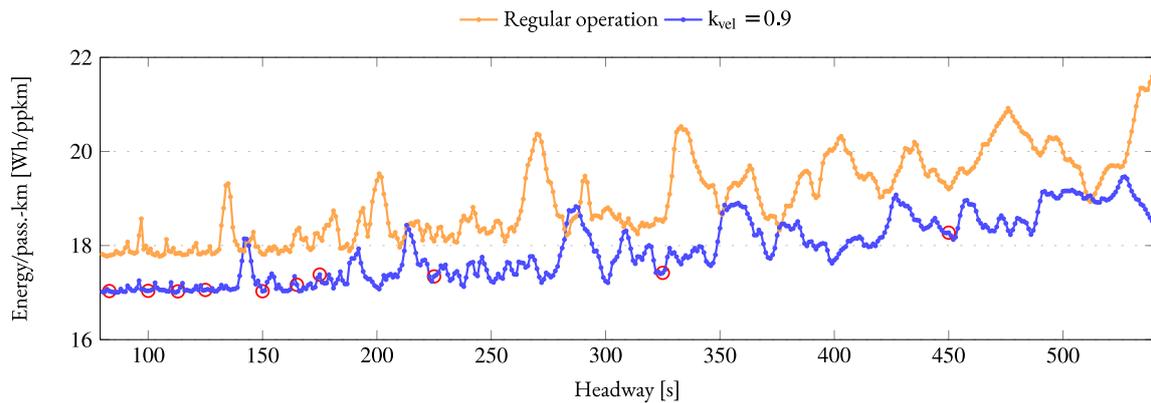
**Figure 3-22: Backward simulation - consumption per passenger-kilometer on real line with vel. factor.**

## II.1.c. Full day operation

A new simulation for a full day of operation has been conducted with the imposition of $k_{vel}$ equals to 0.9. The regular working day timetable is respected. Hence, energy consumption results and losses details are compared with the base operation (Figure 3-23). Energy consumption decreases from 82.6 MWh to 77.1 MWh, representing a 6.7% reduction. A decrease in all system losses is noted for same reason of single vehicle operation. Notably, there is a significant reduction in mechanical braking losses.
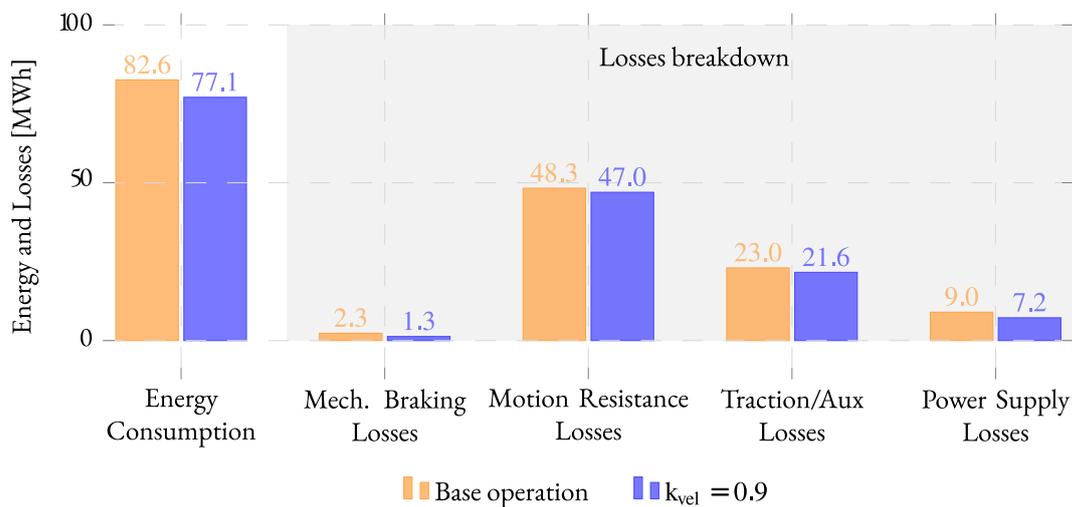


**Figure 3-23: Single vehicle energy consumption and losses detail for real line with velocity adaptation.**

The velocity adaptation implicates a need for a greater number of vehicles to be simultaneously in operation during peak-hours to maintain the imposed timetable. For this simulation, 36 vehicles are needed during peak-hours, an increase of 2 vehicles compared to

standard operation. Since the objective is to respect the timetable, the same number of passengers are transported in both scenarios. This outcome aligns with the trend of achieving better usage of regenerative braking energy in scenarios with a higher number of circulating vehicles. Additionally, this scenario also causes an additional 1min 24s on a one-way trajectory.

From an operational perspective, having an additional vehicle in circulation implies an anticipated increase in maintenance costs and the requirement to actually have an extra vehicle available. It is essential for the line operator to evaluate the energy advantages to find a balance between financial implications and operational priorities.

## II.2. Limiting Maximal Acceleration

Modifying the reference acceleration of the line also seeks to diminish the overall system losses. The applied methodology involves adjusting the maximal allowed acceleration value with a multiplicative factor. Even if acceleration is modified, it is ensured that the reference velocity remains consistent with regular operation.

Analyses are conducted considering the actual operation of the subway line under study. Again, cases are examined individually for conditions of a single vehicle and carousel operation. Results from these analyses are compared with data from standard base operation. To ensure a wide range of study, values both below and above the maximal allowed acceleration are considered. From this, the adaptation coefficient $k_{acc}$ can be deduced. It corresponds to the relation between the standard maximal reference acceleration $a_{max}$ with the adapted maximal acceleration $a'_{max}$. For the subway vehicle in study, the nominal maximal value is 1.3 m/s$^2$,

$$a'_{max} = k_{acc}\, a_{max}. \tag{58}$$

The acceleration parameter plays a significant role in shaping the velocity profile. When the acceleration factor is adjusted, as demonstrated with $k_{acc} = 0.9$ (Figure 3-24), there are observable effects on the profile. While the reference velocity remains at its nominal value, a decrease in the maximum acceleration also results in a noticeable delay on the applied trajectory. The implications of altering this parameter are further analyzed in the context of the real line operation.
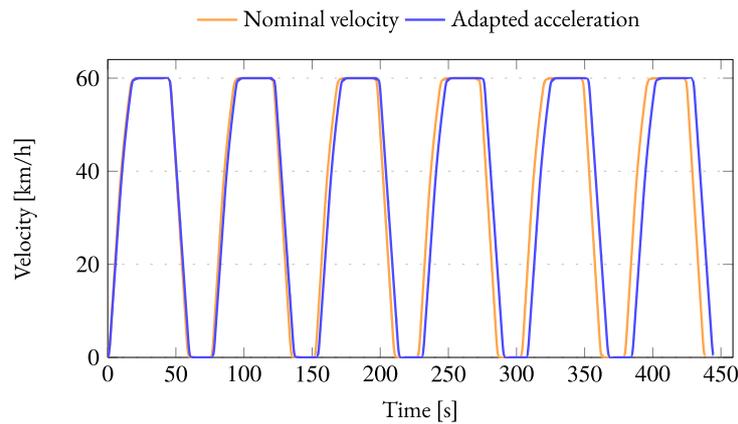
**Figure 3-24: Adaptation of maximal acceleration.**

II.2.a. <u>Single vehicle analysis</u>

The analysis of the operation also begins by examining the simulation results for a single vehicle. A round trip is also considered. It is possible to observe the influence acceleration factor on overall energy consumption. A reduction of only 1.8% is obtained with a 20% decrease in the reference acceleration (Figure 3-25a). Additionally, the total journey time is also impacted (Figure 3-25b). A 2.5% increase in travel time is noted for the same 20% reduction in maximal acceleration. In general form, single vehicle simulation results suggest that modifying maximal acceleration does not significantly impact energy consumption. This result has already been obtained in [Desreveaux 19] for an electric car in the CUMIN-EVE project: only the maximal velocity has a significant impact on energy consumption.
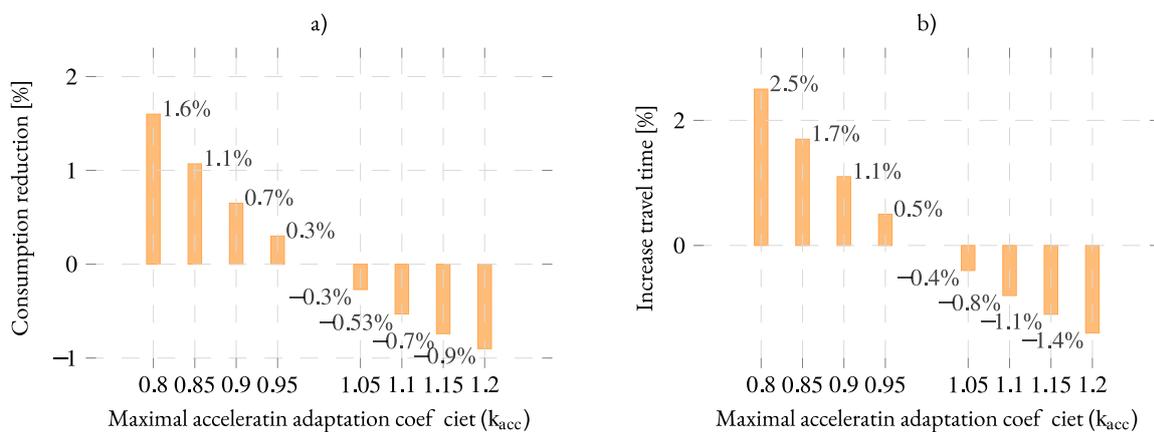


**Figure 3-25: Adaptation of maximal acceleration on real line with single vehicle operation.**

Since no significant gain is observed on single vehicle operation, the carrousel analysis is not performed.

102

## II.3. Adjusting nominal voltage

The influence of the nominal voltage values imposed by the TPS is examined. Even though this solution might require a more significant intervention in the TPS equipment, the energetic consequences are still of interest. Various voltage levels are examined for a single vehicle operation. Further a detailed study is conducted on a chosen voltage level for multiple vehicle operation. In this section, it is not possible to analyze the operation points using the backward approach. The voltage value does not affect calculated power profile. This fact highlights the importance of the forward approach in being capable of precising the impact of different variables on the assessment of energy consumption of a subway line.

As previously discussed, the dc bus voltage plays a critical role in the strategy of mechanical braking activation. In the given analysis, even if the line nominal voltage is modified, the mechanical braking activation rule remains unchanged. Thus, the vehicle operates with standard configuration. Complete mechanical braking is always ensured at a voltage of 950V, transitioning from 900V (refer to Chapter 2).

II.3.a. <u>Single vehicle analysis</u>

A single-vehicle simulation is conducted for a round-trip on a real line. For each simulation, the nominal voltage on TPS is varied and the final consumption is recorded (Figure 3-26). It is observed that within the 750 to 925 V range there is a tendency for a reduction in consumption with an increase in voltage. From 950 V onwards, the system shows no more significant gains. Notably, 950 V is the voltage at which mechanical braking is ensured.
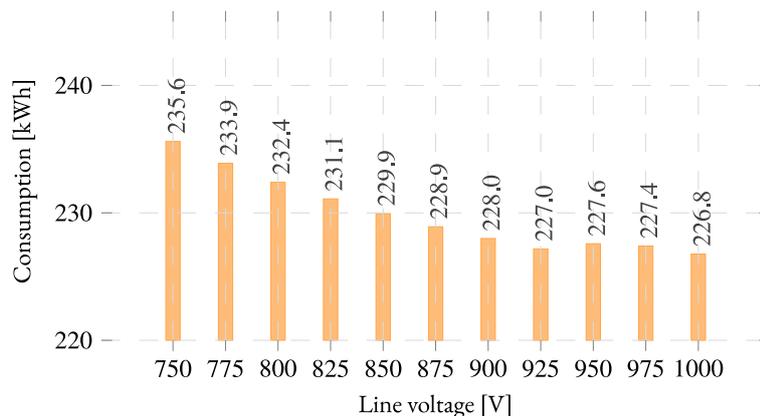


**Figure 3-26: Impact of voltage level on energy consumption for a real line with single vehicle operation.**

For a detailed analysis of consumption, a voltage point of 925V is selected. At this point, there is a slight reduction of 1.1% in energy consumption compared to base operation (Figure 3-27). It is noted that, in general, the only energy loss that is significantly affected is the power supply losses. Higher line voltage results in lower current levels in the power network. Consequently, reduced resistive losses are anticipated if same power demand is requested. Losses due to mechanical braking are relatively higher as the brake is activated earlier. Even if there is only one vehicle on the line, regenerative braking can supply the auxiliaries. Other factors such as motion resistance and traction and auxiliaries losses do not show changes.
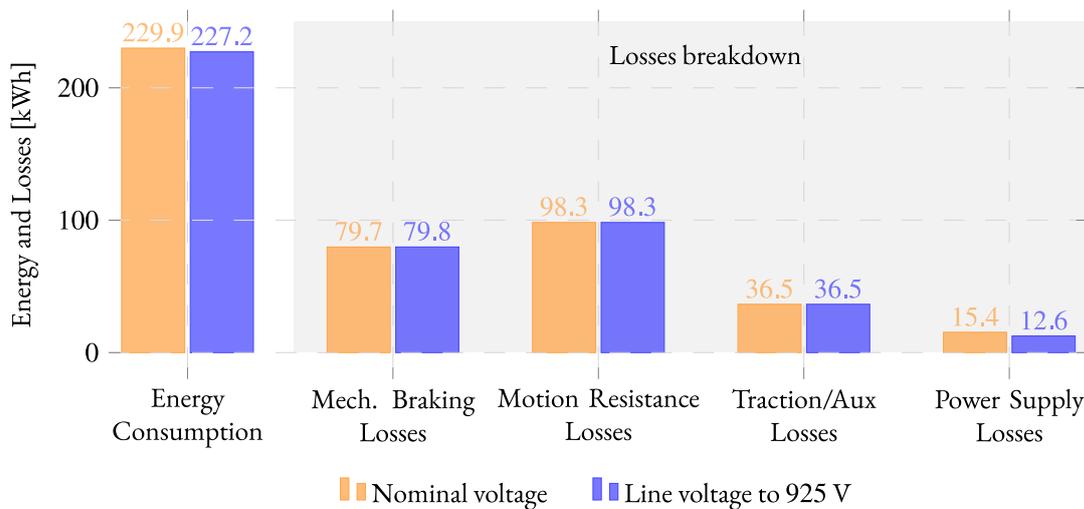


**Figure 3-27: Single vehicle energy consumption and losses detail for real line with voltage adaptation.**

II.3.b. Full day operation

A new simulation is carried out for a complete day, where the timetable corresponds to regular operations on a standard working day. In this simulation, a nominal voltage of 925V on TPS level is applied. Subsequently, the values obtained from the simulation are compared with the simulation results for operations with base operational parameters. The consumption and losses details are presented (Figure 3-28).

It can be observed that this case exhibits a behavior different from that seen for the single vehicle simulation. An energy consumption increases of 34.0% is recorded. The mechanical braking losses significantly rise, increasing from 1.6 MWh under regular conditions to 39.2.0 MWh when the voltage is raised to 925 V. Such an elevated nominal voltage brings the dc bus fluctuation above to the mechanical braking activation threshold. Therefore, while transmission losses might reduce, the adoption of regenerative braking becomes less advantageous.
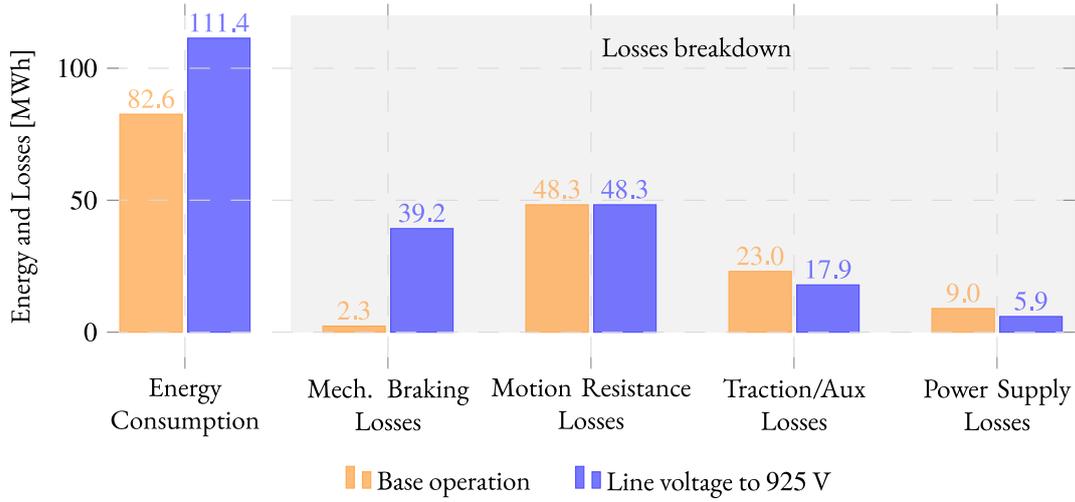
**Figure 3-28: Carousel energy consumption and losses detail for real line with voltage adaptation.**

This result, although anticipated, highlights the sensitivity of the system efficiency in relation to the power supply voltage levels. This emphasizes the interconnection between parameter modification and their impact on energy flow.

The results indicate that the analysis of single-vehicle operation differs from carousel operation. In single-vehicle mode, there is fundamentally no utilization of regenerative braking energy. Even as the line voltage approaches the mechanical braking activation point, the losses due to braking are not significantly affected. This is not the case with carousel mode, where there is a significant increase in mechanical braking losses, and the energy exchange between vehicles is impacted.

## II.4. Delay on injection time

During the operation of the line, vehicles are deployed at their specific injection time $t_I^k$. Conventionally, these vehicles enter both line terminals simultaneously. This section proposes desynchronization of these insertions to reduce energy consumption. This involves defining a delay, denoted as $D$, to modify the original injection time. At this first moment, only side B is delayed since the interest is to find a mismatch between both sides. As a result, the revised injection time for the B terminus can be determined,

$$t_{IB}^k = t_{IB}^{k-1} + H_k + D_{Bk}. \tag{59}$$

The goal is to find the best delay that can lead to minimized energy consumption. This process starts with collecting velocity data over time for every route. From this data, the required

power demand curve is extracted using backward simulation techniques. By aggregating the power contribution of each vehicle, a comprehensive power profile for the entire system emerges. The objective is to find the delay that reduces the area of negative values from power profile. It can be understood as a reduction of surplus of mechanical braking energy.

A range of acceptable delays has been defined. It is chosen a maximal value equal to half of the smallest observed headway. As a result, the maximal tolerated delay for the line is 42 seconds. Based on this limitation, an appropriate delay value is chosen for each operational headway. A power demand profile is taken as example (Figure 3-29a) and a focus highlighted (Figure 3-29b). The outcome of this strategy is provided (Figure 3-29c). A delay of 38 seconds is identified as the best choice to reduce the negative area of the specified power demand curve. The result corresponds to an operational headway of 125 seconds.
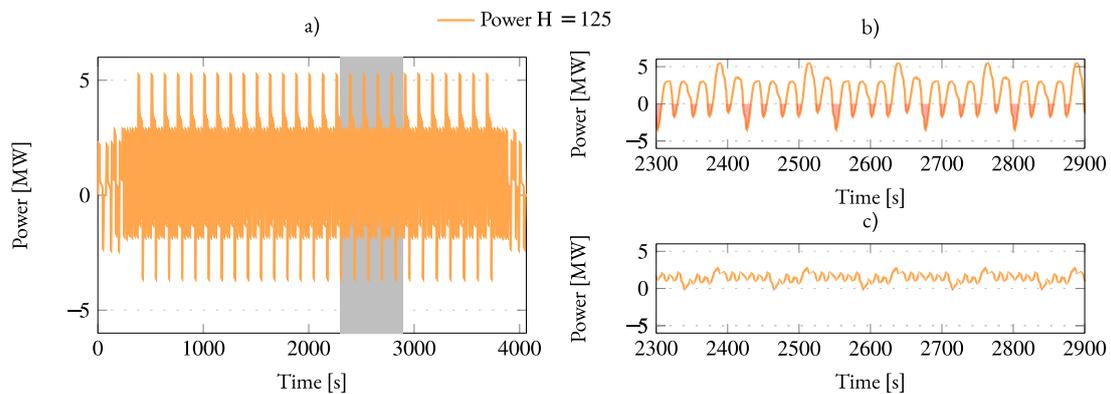


**Figure 3-29: Adaptation of maximal acceleration on real line with single vehicle operation.**

The strategy is first tested on a fictitious line, and the outcomes are assessed. Subsequently, the same strategy is implemented for the real line following the timetable under study.

II.4.a. <u>Application on fictitious line</u>

Based on the defined strategy, the fictitious line is simulated and the final consumption is assessed. For each headway, a corresponding delay is obtained and applied on simulation. Global consumption (Figure 3-30a) and value per passenger-kilometer (Figure 3-30b) at each operating point are compared with the outcome during nominal operation and receptive line. The implemented strategy is capable of reducing consumption for the operating points analyzed. The implemented delay can compensate for the points where acceleration and braking phases do not favor the use of regenerative braking.
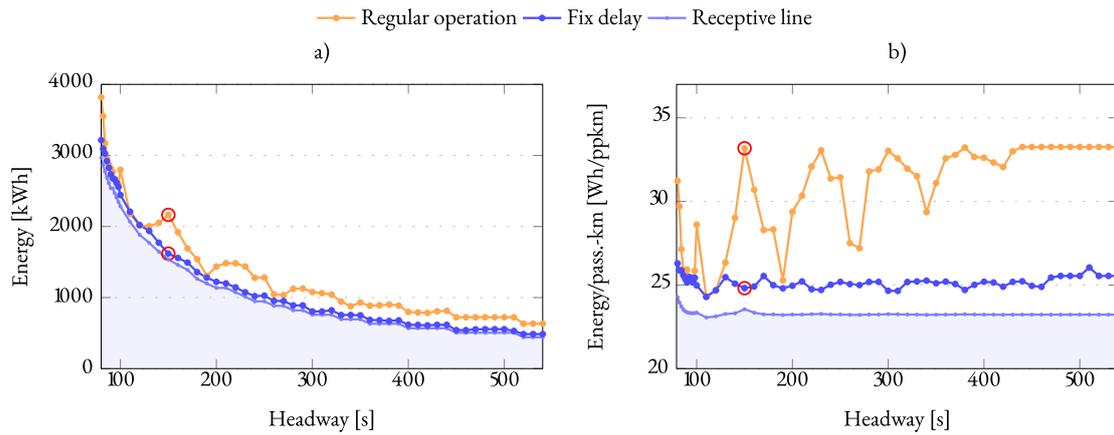
**Figure 3-30: Energy global and per passenger-kilometer for fictitious line.**

An operation point is selected for a detailed analysis of losses. This point is highlighted on the curve. Intentionally, a condition is chosen where a significant change in consumption is observed ($H = 150s$). The consumption details and losses are then examined (Figure 3-31). The strategy can significantly reduce mechanical braking losses, reducing from 782.4 kWh to 94kWh. A global energy reduction of 25.2% is observed. Consequently, increased traction and auxiliaries and power supply losses are recorded. The motion resistance losses remain constant, as the trajectory profile and number of vehicles injected are the same for both simulations.
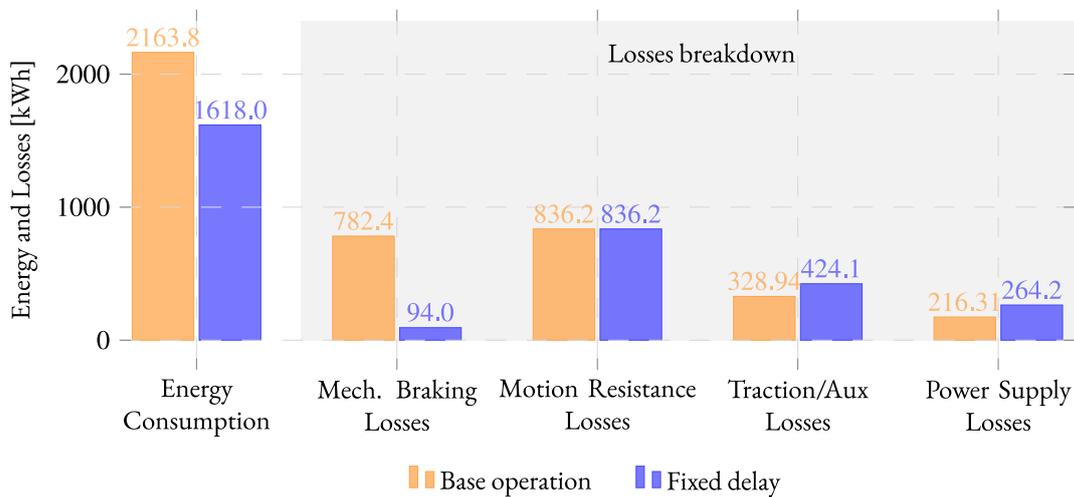


**Figure 3-31: Fix delay impact on fictitious line with headway of 150s.**

The simulation results show that it is possible to reduce energy consumption and keep the same transport offer. A proper synchronization of vehicle injection time is necessary.

II.4.b. Application on real line

The principle of injection delay is now applied for the real line topology. Initially, the effect on the consumption curve per passenger-kilometer in a backward simulation is observed. For each operating headway, the delay $D$ that minimizes the excess of regenerative braking power is applied. The result is presented (Figure 3-32). In general terms, the reduction in consumption at these points suggests that better synchronization between vehicles can be achieved with the aim of reducing consumption. Some operation points are better improved than others due to line asymmetry and limitations on the imposed delay.
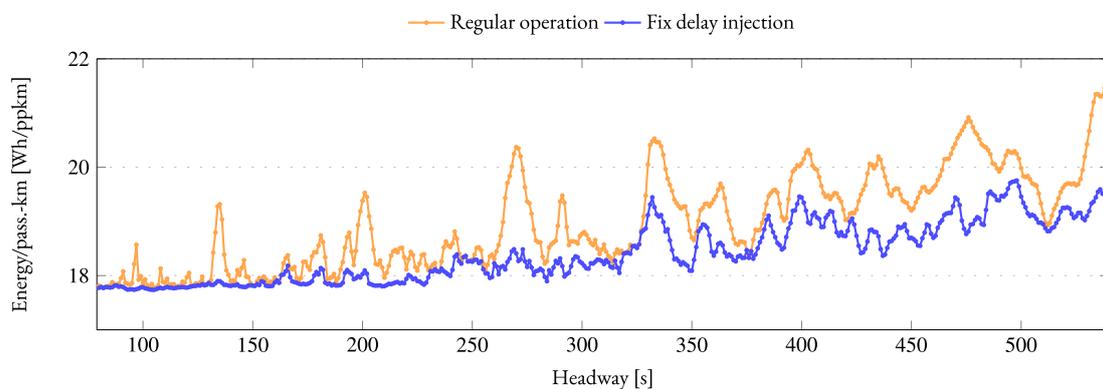


**Figure 3-32: Backward simulation - consumption per passenger-kilometer with fix delay injection.**

II.4.c. Full day operation

The complete line simulation with a timetable corresponding to daily operation has been conducted. The best delay found for each operation point is imposed to the simulation. When the headway changes, the delay is also modified. In this scenario, the imposed delay is adjusted based on the operational headway using a lookup table. The energy consumption and detailed losses are compared to the traditional baseline operation (Figure 3-33).

A reduction in mechanical braking losses can be achieved. However, this does not significantly impact the overall consumption. A reduction of only 0.2% is recorded.
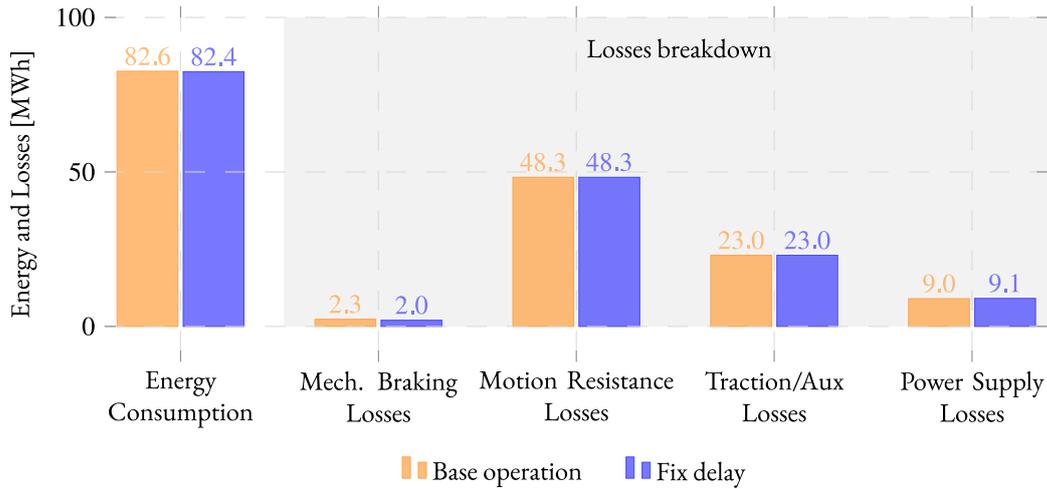
**Figure 3-33: Carousel energy consumption and losses detail with fix delay on real line.**

As the headway changes over time, during periods outside of steady-state operation, the imposed delay does not necessarily lead to a better synchronization of braking and accelerating phases. Moreover, if a vehicle experiences a delay for any reason, the desired synchronization between vehicles is lost. To address this issue, an adaptive strategy is suggested.

II.4.d. <u>Adaptive delay on injection time</u>

A modification can be made to the injection time by introducing the possibility of a delay at both terminals of the line. Therefore, the new injection time for side A is defined as

$$t_{IA}^k = t_{IA}^{k-1} + H_k + D_{Ak.} \tag{60}$$

In the previous section, a fixed delay is predetermined for each headway operation point. It is calculated based on knowledge of an expected velocity profile. Now, a delay for each terminus of the line is determined immediately before the insertion of a new vehicle onto the line. From the position information it is possible to deduce the power demand profile the vehicle should follow. Newly inserted vehicles on the line are delayed so that the resulting power demand minimizes excessive regenerative braking. In this context, before the insertion of a vehicle, the current condition of the line is checked using information on the position of each circulating vehicle. Furthermore, this strategy can adapt to transition moments between headways throughout the day. Put simply, a new vehicle is inserted at an opportune time to minimize energy losses.

The application of this new strategy enables a more significant reduction in mechanical braking losses. However, it only offers a modest 0.4% reduction in overall consumption. From the perspective of the subway carousel system studied, it is concluded that any attempt to reduce losses

through better synchronization of vehicles on the actual line does not significantly impact consumption reduction. However, results on the fictitious line show a substantial decrease in consumption. These findings suggest that on a line with heavy vehicle traffic, energy exchange between vehicles is already strongly favored.
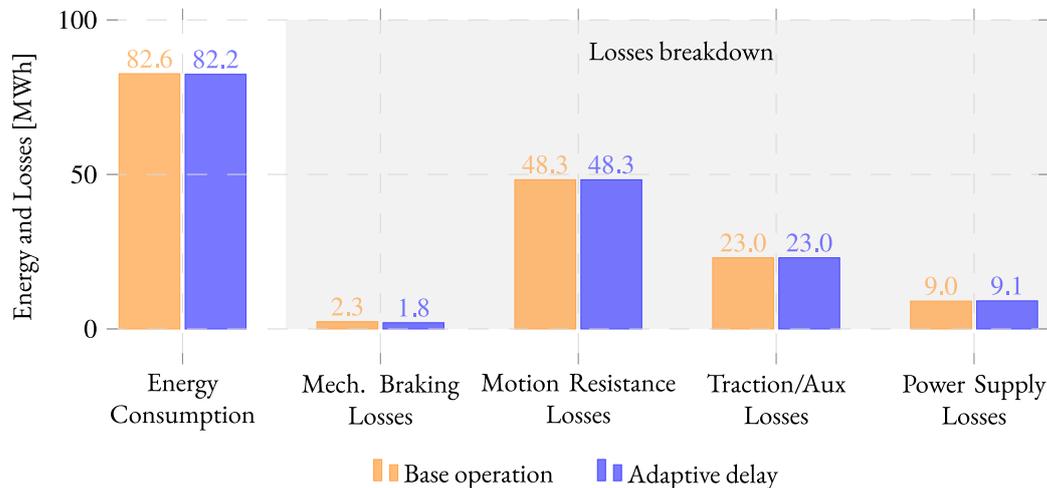


**Figure 3-34: Carousel energy consumption and losses detail with adaptative delay on real line.**

## III. Case study: supply charging stations for EVs

Actions aimed at reducing consumption depend on the synchronized operation of the vehicles and include side effects such as delays in journey times or the need for more vehicles. One way to enhance line receptivity involves utilizing the subway power system for a secondary purpose concurrently. This section analyzes the use of the system supply line to power electric vehicles. As seen previously, the subway carousel operation presents energy losses of 2.3MWh in a standard operational day due mechanical braking activation. Proportional to the subway consumption, it may appear relatively minor; nevertheless, it can be useful for other purposes.

The growing presence of electric vehicles or buses requires an increase in charging infrastructure, especially within urban centers. This highlights the necessity for retrofitting or adding facilities capable of meeting this rising electrical power demand. The close proximity of subway systems to urban areas, along with their significant power capacity, creates a mutually advantageous situation. Unused energy from the subway system can be redirected to charging facilities. Also, charging stations can take advantage of unused power capability of TPS, specially in off-peal hours.

This concept has been previously studied in the literature [Go 18] [Fernandez-Rodriguez 17]; however, the vehicle presents a simplified model. Furthermore, a full line operation with a detailed analysis of losses is not conducted. These studies are based on a backward approach.

## III.1. Braking energy recovery

III.1.a. Definition of recovery potential

In order to quantify the potential gain, a modification is carried out in the simulation. Initially, an analysis is conducted to assess the energy recovery potential at specific point in the line. For this purpose, an ideal energy-absorbing element is introduced. This element is based on the operation of the TPS but in reverse energy flow. During its ON operation, this element imposes a nominal voltage and enforces zero current in the blocked mode (OFF). Unlike the TPS, this element switches to the ON mode when the voltage at the connection point $u_{rec}$ exceeds the nominal voltage, and to the OFF mode when the current of the element $i_{rec}$ reaches null value (Figure 2-19). Thus, only negative current values are recorded. The recovered power can be calculated based on the exchanged voltage and current values with the system. Essentially, this element conducts when the TPSs are blocked.



| Actual state | Event | Next state |
|:---:|:---:|:---:|
| OFF | $i_{rec} \geq 0$ | OFF |
| ON | $u_{rec} > u_{nom}$ | ON |
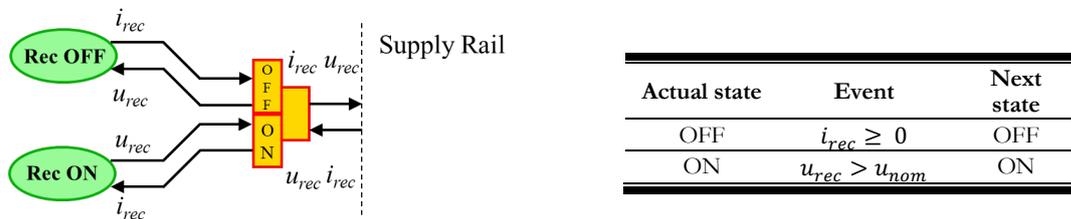
**Figure 3-35: The EMR of recovery energy element.**

This ideal element is implemented so that it is not necessary to define a maximum power for the system. Therefore, an overall idea of the power curve to be recovered can be analyzed. A practical implementation necessitates an energy recovery strategy based on the supply line voltage fluctuation and a maximal power capacity. First, a simulation is carried out considering the recovery element. Secondly, nominal power is defined and a recovery strategy established. An additional simulation is performed considering the recovery strategy.

In the framework of the CUMINI-REMUS project, the energy recovery element is situated in the surrounding area of 4 Cantons station. It is worth noting that the installation is within the campus "cité scitifique", of Université de Lille, with a nearby garage building. This strategic location

significantly reinforces the interest in the charging infrastructure for electric vehicles. Furthermore, the presence of a bus terminal in close proximity opens up opportunities for the charging of electric buses. This decision is strategically aligned with the unique realities of the metropolis.

Hence, a first simulation is carried out considering the ideal recovery element. It consists of a full day simulation of the studied timetable. It can be observed that the recovered power profile is significantly affected by the operating headway. Values in the order of 1.9 MW are registered, however, most of the operation is situated below 1 MW range. In this way, it is chosen a maximal power ($P_{rec-max}$) of 1 MW for the energy recovery strategy.
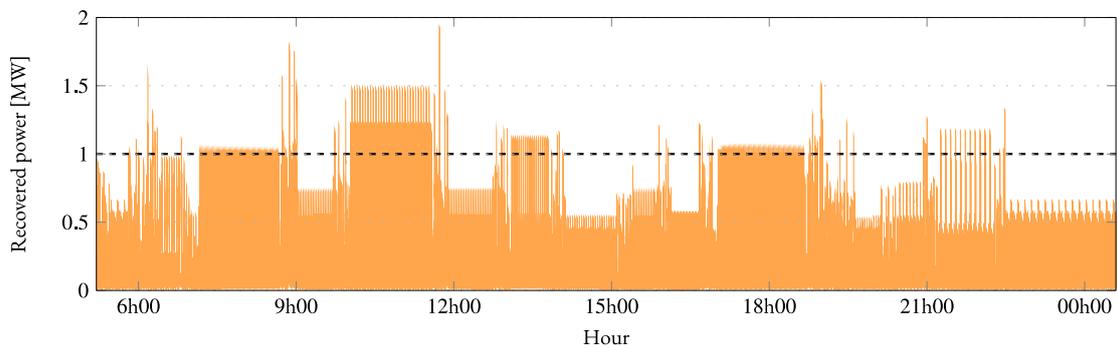


**Figure 3-36: Recovery power profile without power limitation.**

III.1.b. <u>Energy recovery strategy</u>

It is known that when the rail voltage rises, a lack of accelerating vehicles is observed. Thus, the recovery energy strategy is defined in function of the supply line voltage level. It is essential that the maximal recovery power is applied before the mechanical braking activation on vehicle initiates (900V for the studied vehicle). Furthermore, to facilitate the natural energy exchange between the vehicles, the device initiates energy recuperation at a voltage above the nominal voltage. First, a coefficient ($k_{rec}$) is employed to determine the reference power applied by on the energy recovery process as,

$$P_{rec-ref} = k_{rec}P_{max-rec}. \tag{61}$$

It is chosen $k_{rec}$, so that energy recovery is started at 870 V and maximal power is applied at 900V, with a smooth transition in between. The strategy depicted in Figure 3-37.
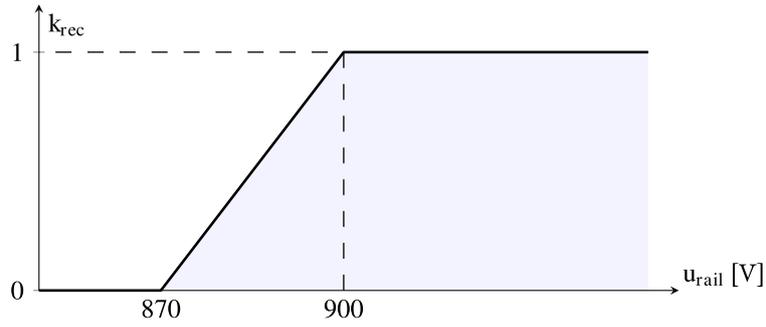
**Figure 3-37: Definition of $k_{rec}$ for energy recovery strategy.**

Finally, the reference current for the energy recovery can be defined by the reference power and the voltage measured at the connection point. An efficiency η is applied to take account of losses in the device.

$$i_{rec-ref} = \frac{P_{rec-ref}}{\eta \, u_{rl}} \tag{62}$$

The reference current is applied to the circuit solution respecting the assigned position. Now, the energy recovery system is represented as a source element that imposes the reference current to the system. A static model is considered and no delay between reference and applied value is seen. This element is coupled with other subsystems considering the MNA block (Figure 3-38).
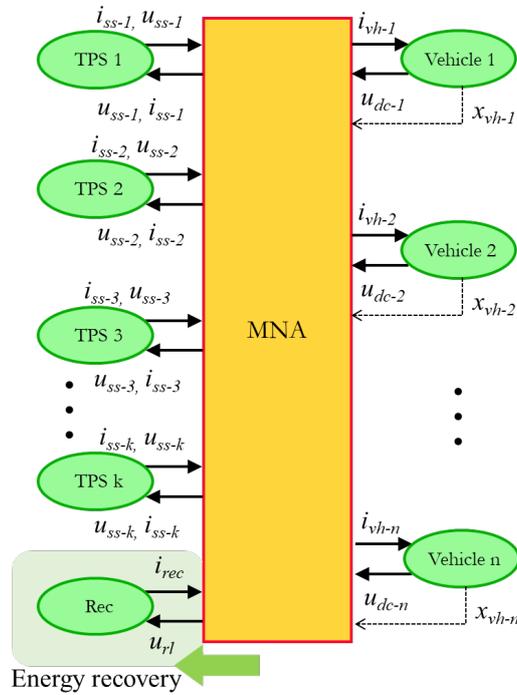


**Figure 3-38: System simulation topology with energy recovery element.**

## III.2. Case study simulation and analysis

Simulation results display consistent overall energy consumption following the introduction of the energy recovery strategy. A consumption of 82.6 MWh is recorded for a daily operation. However, a reduction in mechanical braking losses is noticeable, decreasing from 2.3 MWh to 2.0 MWh (Figure 3-39). Alongside, there is a noted rise in power supply losses. This is justified because the integration of the energy recovery device means that braking energy must be absorbed at a fixed location, reducing the energy utilization by adjacent vehicles. Both motion resistance and traction and auxiliaries losses remain relatively unchanged with or without the energy recovery device. The energy fed into the charging system equals 0.3 MWh.
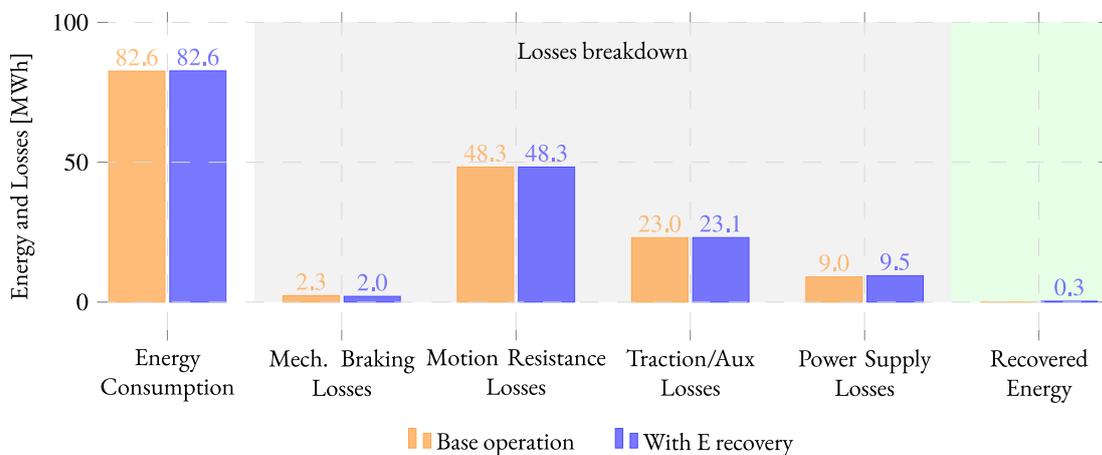


**Figure 3-39: Carousel energy consumption, losses and recovered energy for case study.**

The positioning of the energy recovery system cannot fully reduce the losses due to mechanical braking activation. However, this system emerges as an alternative to reduce energy consumption that does not affect the transport offer, allowing the subway system to operate under normal conditions.

While a 0.3 MWh recovery has a minimal impact on the subway system, it is still notable for electric vehicle applications. Considering the obtained results, the annual energy recovery would be around 80 MWh, if only weekdays are accounted. This can provide approximately 1600 full charges for electric vehicles with an average battery capacity of 50 kWh.

An analysis considering the placement of other braking energy recovery devices along the line can be conducted. A potential of 2MWh for daily operation remains available for utilization. Furthermore, this energy can be allocated for other purposes, such as track heating on cold days, or for use in passenger stations for lighting and escalators, for instance.

# IV. Conclusion

In this chapter, the energy flow and losses in a subway system has been analyzed. Simulations were conducted to investigate the energy consumption of a single vehicle on the track, as well as an entire carousel system. Both a fictitious and a real line have been studied. Details of the losses in the subway system are provided through the use of a forward approach.

In a single-vehicle simulation, the importance of regenerative braking energy management becomes evident for system efficiency improvements. A 30% reduction in energy consumption can be achieved with a receptive line. The analysis of a subway carousel system highlights the significance of headway selection in enhancing energy exchange between vehicles.

Interventions aimed at reducing consumption have been evaluated on a complete line with several vehicles. A decrease in the reference velocity yields significant results for energy consumption reduction. A balance between travel delay and consumption reduction should be considered. A simulation carried out considering a real line indicates a 6.7% decrease in energy consumption for a 10% reduction in reference velocity and a 6% supplementary travel time. Most of the consumption reduction originated from a decrease in mechanical braking losses. A negative effect noted is the need to incorporate a higher number of vehicles on the line. A change in maximal acceleration does not have significant impacts on the reduction of energy consumption.

Changing the nominal voltage of the system may result in improved energy reduction for single-vehicle operation. A decrease in supply line losses is observed. However, in carousel operation, energy consumption worsens. An increase in voltage causes the activation of mechanical braking to occur earlier. Future studies might explore the modifications in the vehicle braking strategy to align with the system voltage elevation.

A modification in the injection timing of a vehicle aims to reduce the system consumption by a better synchronization of acceleration and braking phases. The power demand curve of each circulating vehicle serves as the basis for this strategy. Better consumption reduction is observed in the case of the fictitious line, where synchronization can be more easily achieved. The case example registered 25.2% on energy consumption for a fixed headway operation. However, operating a real line with varied headways and line asymmetry results in a slight improvement of 0.2% in consumption.

Utilizing regenerative braking energy to power external loads, such as electric vehicles, serves as an alternative. In this case, modifications in the operation of the line are not required.

The case study indicates that it is possible to reduce losses from regenerative braking. However, incorporating additional devices along the line might provide a more significant reduction in regenerative braking losses. The impact of the position needs to be better evaluated.

The difference results are influenced by factors such as station distance, TPSs number, and number of circulating vehicles. For instance, in the case of Line 1 of Lille, it is primarily the maximal velocity that significantly impacts energy consumption. However, for other lines, the flexible simulation model must be used for a comprehensive analysis.

*Conclusions and perspectives*

# I. Conclusion

Transportation plays a fundamental role in addressing the challenges posed by urbanization, energy consumption, and greenhouse gas emissions. Subways, known for their high capacity and low emissions, are well-suited to meeting this growing demand.

Many interrelated factors have an impact on energy consumption for subways and the definition of relevant solutions is difficult. One of the most pressing issues is the handling of regenerative braking energy. When not managed effectively, the surplus energy generated during braking can lead to system inefficiencies. Addressing these challenges requires innovative solutions.

In this thesis, the presented methodology for subway carousel modeling provides an in-depth framework for the analysis of the system behavior. An accurate dynamical model has been developed for energetic studies of subway carousels. The inclusion of capacitor filter dynamics through a forward approach is pivotal for accurately determining the braking strategy, which in turn affects the system energy flow. The model validity has been confirmed through tests based on experimental results, ensuring a low margin of error in evaluating energy consumption (<3%). Moreover, a Hardware-In-the-Loop testing platform has been developed to carry out other cases for the model validation.

To face computational challenges of such complex simulations, simplified models have been proposed. These models can effectively reduce computational cost, up to 93% reduction on simulation time is noticed. A quasi-static model is chosen for its ability to simulate carousels without sacrificing much accuracy (2%). Such a trade-off is essential when multiple vehicles and subsystems need to be simulated concurrently.

To understand the energy usage, simulations have been executed for both individual vehicles on a track and the entire carousel system. When simulating a single vehicle, the central role of managing regenerative braking energy for enhancing system efficiency becomes clear. Energy consumption can be reduced by up to 30%.

Efforts to reduce energy consumption have been assessed on a full line with multiple vehicles. Lowering the reference velocity proves effective in reducing energy usage. It is essential to determine a balance between minimizing travel delays and reducing energy consumption. Simulations based on a real subway line showed a 6.7% drop in energy consumption when the reference velocity was reduced by 10%, resulting in an added 6% travel time (less than 2 min).

Other analysis such as altering the maximal acceleration, adjusting the system nominal voltage and modifying vehicle injection timing have been done. They aim to reduce system energy usage and promote better coordinating acceleration and deceleration phases. However, they do not present significant impact on the reduction of energy consumption.

Using regenerative braking energy for external utilities, like electric vehicles, emerges as a viable alternative. This does not necessitate any operational changes to the subway line. Case studies suggest potential in minimizing regenerative braking losses. Yet, integrating more devices along the line could lead to even greater reductions. The placement of these devices deserves further evaluation.

Various factors, including the distance between stations, the number of TPSs, and the count of vehicles in circulation, influence the energy flow on the system. Hence, impacting on energy consumption. For instance, for Line 1 in Lille, the dominant factor affecting energy consumption is the maximal velocity. For other lines, further investigation should be done.

## II. Perspective

By the analysis of subway systems and their energy management, it becomes evident that the research still has room for expansion. The future of subway transportation and its energy efficiency lies in a combined approach that not only addresses the technical aspects but also the economic and environmental implications.

**Short-term perspective**

For the simulation model, from a short-term perspective, future work could focus on incorporating the dynamics of passenger flow, a feature not considered in this study. This task necessitates preliminary research to establish a methodology for quantifying the number of passengers on each segment of the route based on the operating schedule. This task also requires ongoing collaboration with MEL.

Furthermore, for the full-line simulation, results have been analyzed based on overall consumption. A deeper understanding could be achieved by analyzing the impact in relation to the operation interval. This would involve detailing the energy losses also in terms of the headway.

**Definition of variable global energy management**

It is essential to highlight the potential for future studies to explore the variation of maximal velocity in different scenarios. These studies can focus on how altering the maximal velocity impacts energy consumption and efficiency in various timetable scenarios. This can prioritize either energy consumption or travel time reduction.

Future research could delve into the impact of adjusting maximal velocity in response to fluctuating passenger demands, on peak and off-peak hours This exploration can extend to understanding how these adjustments affect the overall energy management of a subway system, particularly in balancing the trade-offs between energy savings and meeting timely travel requirements. Additionally, investigations might consider the integration of adaptive control systems that dynamically modify velocity in real-time, prioritizing energy efficiency or velocity based on immediate operational goals.

**Development of a charging station using energy recovery**

Future work may involve the utilization of tools and methodologies to determine the most strategic locations for charging stations implementation. This decision-making process should consider various factors such as the frequency of stops, the intensity of regenerative braking opportunities. Additionally, it may consider proximity to areas with high charging demands. By analyzing these elements, transit authorities can identify locations where energy recovery and subsequent redistribution would be most effective. This ensures that the recovered energy is utilized optimally and contributes significantly to the overall energy efficiency of the transit system.

Another aspect revolves around designing the energy storage system and defining an optimal energy management strategy. The design of the energy storage system should focus on maximizing the capture and reuse of regenerative braking energy, which is typically lost in traditional systems. This involves selecting the right type of energy storage technology that aligns with the specific energy and power characteristics of the transit system. Furthermore, developing an optimal energy management strategy is crucial. This strategy can also consider the integration of renewable energy sources.

**Inclusion of fine particle emission model during braking phases**

Environmental sustainability goes beyond just energy consumption. The emission of fine particles during braking is an environmental concern that has not been addressed in the current

study. Incorporating this aspect would provide a more comprehensive view of the environmental impact of subway systems. A new project on CUMIN framework is planned to consider mechanical braking emissions (CUMIN-TIM). This would entail:

- Developing a model to quantify the emission of fine particles during the braking process.
- Understanding the health implications for commuters and subway workers exposed to these particles.
- Exploring solutions to minimize these emissions, such as alternative braking materials or technologies.
- Evaluating the environmental trade-offs between energy savings from regenerative braking and potential decrease in fine particle emissions.

**Technical-economic analysis**

While the technical aspects of energy management in subway systems have been extensively studied, there is a pressing need to integrate these findings with an economic perspective. A technical-economic analysis would provide a complete view of the costs and benefits associated with implementing the proposed solutions. This would involve:

- Evaluating the financial implications of adopting new energy management strategies.
- Assessing the return on investment (ROI) for proposed solution.
- Understanding the economic impact on commuters, especially in terms of fare adjustments due to energy savings.
- Analyzing the cost-effectiveness of integrating external utilities, such as electric vehicles, into the subway energy ecosystem.

In conclusion, while the current study provides a robust foundation for understanding energy management in subway systems, the perspective section highlights the need for a more integrated approach. Addressing the technical, economic, and environmental aspects concurrently will pave the way for sustainable subway transportation in the future.

# *References*

[Allègre 10a]        A. -L. Allègre, A. Bouscayrol, P. Delarue, P. Barrade, E. Chattot and S. El-Fassi, "Energy Storage System with Supercapacitor for an Innovative Subway," IEEE Transactions on Industrial Electronics, vol. 57, no. 12, pp. 4001-4012, Dec. 2010.

[Allègre 10b]        A. L. Allègre, "Méthodologies de modélisation et de gestion de l'énergie de systèmes de stockage mixtes pour véhicules électriques et hybrides", Thèse de doctorat l'Université Lille1, Septembre 2010.

[Allègre 10c]        A. -L. Allègre, A. Bouscayrol, J. -N. Verhille, P. Delarue, E. Chattot and S. El-Fassi, "Reduced-Scale-Power Hardware-in-the-Loop Simulation of an Innovative Subway," IEEE Transactions on Industrial Electronics, vol. 57, no. 4, pp. 1175-1185, April 2010.

[Allen 21]          L. Allen and S. Chien, "Application of Regenerative Braking with Optimized Speed Profiles for Sustainable Train Operation," Journal of Advanced Transportation, vol. 2021, p. 8555372, Sep. 2021.

[APTA 23]           APTA American Public Transportation Association, Public Transportation Ridership Update, 2023. Online: https://www.apta.com/wp-content/uploads/APTA-POLICY-BRIEF-Transit-Ridership-03.06.2023.pdf, consulted in June 2023.

[Arboleya 18]       P. Arboleya, B. Mohamed and I. El-Sayed, "DC Railway Simulation Including Controllable Power Electronic and Energy Storage Devices," IEEE Transactions on Power Systems, vol. 33, no. 5, pp. 5319-5329, Sept. 2018.

[Arboleya 22]       P. Arboleya, C. Mayet, A. Bouscayrol, B. Mohamed, P. Delarue and I. El-Sayed, "Electrical railway dynamical versus static models for infrastructure planning and operation," IEEE Transactions on Intelligent Transportation Systems, vol. 23, no. 6, pp. 5514–5525, 2022.

[Barrena 14]        E. Barrena, D. Canca, L. C. Coelho and G. Laporte, 'Single-line rail rapid transit timetabling under dynamic passenger demand', Transportation Research Part B: Methodological, vol. 70, pp. 134–150, 2014.

[Barrero 08]        R. Barrero, J. V. Mierlo and X. Tackoen, "Energy savings in public transport," IEEE Vehicular Technology Magazine, vol. 3, no. 3, pp. 26-36, Sept. 2008, doi: 10.1109/MVT.2008.927485.

[Barrero 12]        R. Barrero, "Energy recovery technologies in public transport", Ph.D Thesis, Vrije University of Brussels, Belgium, November 2012.

[Bouscayrol 00]     A. Bouscayrol, B. Davat, B. de Fornel, B. François, J. P. Hautier, F. Meibody-Tabar, M. Pietrzak-David, "Multimachine Multiconverter

System: application for electromechanical drives," European Physics Journal - Applied Physics, vol. 10, no. 2, pp. 131-147, May 2000.

[Bouscayrol 02]     A. Bouscayrol, P. Delarue, E. Semail, J. P. Hautier, J. N. Verhille, "Application de la macro-modélisation à la représentation énergétique d'un système de traction multimachine", Revue Internationale de Génie Electrique, vol. 5, n° 3-4/2002, pp. 431-453, octobre 2002 (article commun L2EP Lille, Matra Transport International).

[Bouscayrol 13]     A. Bouscayrol, J.-P. Hautier and B. Lemaire-Semail, Graphic Formalisms for the Control of Multi-Physical Energetic Systems: COG and EMR. John Wiley & Sons, Ltd, 2013, chapter 3, pp. 89–124.

[Bouscayrol 15]     A. Bouscayrol, P. Delarue, W. Lhomme and B. Lemaire-Semail, "Teaching drive control using Energetic Macroscopic Representation — From maximal to practical control schemes," 2015 17th European Conference on Power Electronics and Applications (EPE'15 ECCE-Europe), Geneva, Switzerland, 2015, pp. 1-10,

[Bouscayrol 17]     A. Bouscayrol et al., "Campus of University with Mobility Based on Innovation and Carbon Neutral," 2017 IEEE Vehicle Power and Propulsion Conference (VPPC), Belfort, France, 2017, pp. 1-5, doi: 10.1109/VPPC.2017.8331039.

[Bouscayrol 23]     A. Bouscayrol, B. Lemaire-Semail, "Energetic Macroscopic Representation and Inversion-Based Control ", Encyclopedia of electrical and electronic power engineering, Vol. 3, pp 365-375, Elesevier, DOI : 10.1016/B978-0-12-821204-2.00117-3, ISBN : 978-0-12-823211-8, 2023.

[Caimi 17]     G. Caimi, L. Kroon and C. Liebchen, 'Models for railway timetable optimization: Applicability and applications in practice', Journal of Rail Transport Planning & Management, vol. 6, no. 4, pp. 285–312, 2017.

[Cascetta 21]     F. Cascetta, G. Cipolletta, A. Delle Femine, J. Quintana Fernández, D. Gallo, D. Giordano, D. Signorino, 'Impact of a reversible substation on energy recovery experienced on-board a train', Measurement, vol. 183, p. 109793, 2021.

[Ceder 21]     A. Ceder, 'Urban mobility and public transport: future perspectives and review', International Journal of Urban Sciences, vol. 25, no. 4, pp. 455–479, 2021.

[Chen 19]     X. Chen, W. Ma, G. Xie, X. Hei, F. Wang and S. Tan, "A Survey of Control Algorithm for Automatic Train Operation," 2019 14th IEEE Conference on Industrial Electronics and Applications (ICIEA), Xi'an, China, 2019, pp. 2405-2410, doi: 10.1109/ICIEA.2019.8833794.

[Chen 23]     M. Chen, Q. Wang, P. Sun and X. Feng, "Train Control and Schedule Integrated Optimization with Reversible Substations," IEEE Transactions on Vehicular Technology, vol. 72, no. 2, pp. 1586-1600, Feb. 2023.

| [Chen 23a] | X. Chen, X. Guo, J. Meng, R. Xu, S. Li and D. Li, "Research on ATO Control Method for Urban Rail Based on Deep Reinforcement Learning," IEEE Access, vol. 11, pp. 5919-5928, 2023. |
|---|---|
| [Cheng 18a] | L. Cheng, W. Wang, S. Wei, H. Lin and Z. Jia, 'An Improved Energy Management Strategy for Hybrid Energy Storage System in Light Rail Vehicles', Energies, vol. 11, no. 2, 2018. |
| [Cheng 18b] | L. Cheng, P. Acuna, S. Wei, J. Fletcher, W. Wang and J. Jiang, "Fast-Swap Charging: An Improved Operation Mode for Catenary-Free Light Rail Networks," IEEE Transactions on Vehicular Technology, vol. 67, no. 4, pp. 2912-2920, April 2018. |
| [Chiniforoosh 16] | S. Chiniforoosh, H. Atighechi and J. Jatskevich, "A Generalized Methodology for Dynamic Average Modeling of High-Pulse-Count Rectifiers in Transient Simulation Programs," IEEE Transactions on Energy Conversion, vol. 31, no. 1, pp. 228-239, March 2016. |
| [CUMIN 23] | CUMIN Program, "CUMIN: Campus of University with Mobility based on Innovation and carbon Neutrality," Online: https://cumin.univ-lille.fr/, consulted in June 2023. |
| [Desreveaux 19] | A. Desreveaux, A. Bouscayrol, R. Trigui, E. Castex and J. Klein, "Impact of the Velocity Profile on Energy Consumption of Electric Vehicles," in IEEE Transactions on Vehicular Technology, vol. 68, no. 12, pp. 11420-11426, Dec. 2019. |
| [Dominguez 12] | M. Dominguez, A. Fernández-Cardador, A. P. Cucala and R. R. Pecharroman, "Energy Savings in Metropolitan Railway Substations Through Regenerative Energy Recovery and Optimal Design of ATO Speed Profiles," IEEE Transactions on Automation Science and Engineering, vol. 9, no. 3, pp. 496-504, July 2012. |
| [Drabek 11] | Drabek, Streit and Blahnik, 'Practical Application of Electrical Energy Storage System in Industry', Energy Storage in the Emerging Era of Smart Grids, InTech, Sep. 22, 2011. doi: 10.5772/22115. |
| [Dutta 20] | O. Dutta, M. Saleh, M. Khodaparastan and A. Mohamed, 'A Dual-Stage Modeling and Optimization Framework for Wayside Energy Storage in Electric Rail Transit Systems', Energies, vol. 13, no. 7, 2020. |
| [Fernandez-Rodriguez 17] | A. Fernandez-Rodriguez, A. Fernandez-Cardador, A. De Santiago-Laporte, C. Rodriguez-Sanchez, A. Cucala, A. Lopez-Lopez and R. Pecharroman, "Charging Electric Vehicles Using Regenerated Energy from Urban Railways," 2017 IEEE Vehicle Power and Propulsion Conference (VPPC), Belfort, France, 2017, pp. 1-6. |
| [Figueroa 14] | M. Figueroa, O. Lah, L. M. Fulton, A. McKinnon, G. Tiwari, Energy for Transport, Annual Review of Environment and Resources 2014 39:1, 295-325 |

[Givoni 13]      M. Givoni, and D. Banister (Eds.). (2013). Moving towards low carbon mobility. Cheltenham, UK: Edward Elgar Publishing. Retrieved Aug 20, 2023, from https://doi.org/10.4337/9781781007235.

[Go 18]      H.-S. Go, I.-H. Cho, G.-D. Kim, and C.-H. Kim, "Reduction of Electricity Prices Using the Train to Grid (T2G) System in Urban Railway," Energies, vol. 11, no. 3, p. 501, Feb. 2018,

[González-Gil 14]      A. González-Gil, R. Palacin, P. Batty and J. P. Powell, "A systems approach to reduce urban rail energy consumption", Energy Conversion and Management, vol. 80, pp. 509–524, 2014.

[Graber 22]      G. Graber, V. Calderaro, V. Galdi, L. Ippolito and G. Massa, "Impact Assessment of Energy Storage Systems Supporting DC Railways on AC Power Grids," IEEE Access, vol. 10, pp. 10783-10798, 2022.

[Grbovic 11]      P. J. Grbovic, P. Delarue, P. Le Moigne and P. Bartholomeus, "Modeling and Control of the Ultracapacitor-Based Regenerative Controlled Electric Drives," IEEE Transactions on Industrial Electronics, vol. 58, no. 8, pp. 3471-3484, Aug. 2011.

[Hao 20]      F. Hao, G. Zhang, J. Chen, Z. Liu, D. Xu and Y. Wang, "Optimal Voltage Regulation and Power Sharing in Traction Power Systems with Reversible Converters," IEEE Transactions on Power Systems, vol. 35, no. 4, pp. 2726-2735, July 2020.

[Hao 21]      F. Hao, G. Zhang, J. Chen and Z. Liu, "Distributed Reactive Power Compensation Method in DC Traction Power Systems with Reversible Substations," IEEE Transactions on Vehicular Technology, vol. 70, no. 10, pp. 9935-9944, Oct. 2021.

[Hassannayebi 16]      E. Hassannayebi, S. H. Zegordi and M. Yaghini, 'Train timetabling for an urban rail transit line using a Lagrangian relaxation approach', Applied Mathematical Modelling, vol. 40, no. 23, pp. 9892–9913, 2016.

[Hautier 96]      J. P. Hautier, J. Faucher, "Le graphe informationnel causal" (Text in French), Bulletin de l'Union des Physiciens, vol. 90, pp. 167–189, 1996

[Ho 75]      C.-W. Ho, A. Ruehli, and P. Brennan, "The modified nodal approach to network analysis," IEEE Transactions on Circuits and Systems, vol. 22, no. 6, pp. 504–509, 1975.

[Horrein 15]      L. Horrein, "Gestion d'énergie décomposée d'un véhicule hybride intégrant les aspects thermiques via la Représentation Energétique Macroscopique", Thèse de doctorat, Université Lille1, France, Septembre 2015.

[Huang 16]      Y. Huang, L. Yang, T. Tang, F. Cao and Z. Gao, "Saving Energy and Improving Service Quality: Bicriteria Train Scheduling in Urban Rail Transit Systems," IEEE Transactions on Intelligent Transportation Systems, vol. 17, no. 12, pp. 3364-3379, Dec. 2016.

| | |
|---|---|
| [IEA 18] | IEA, Energy intensity of passenger transport modes, 2018, IEA, Paris https://www.iea.org/data-and-statistics/charts/energy-intensity-of-passenger-transport-modes-2018, IEA. Licence: CC BY 4.0 |
| [IEA 21] | IEA "Global Energy Review: CO2 Emissions in 2021". Online: https://www.iea.org/reports/global-energy-review-co2-emissions-in-2021-2, consulted in June 2023. |
| [IEA 22a] | Global CO2 emissions from transport by sub-sector in the Net Zero Scenario, 2000-2030", IEA, Paris https://www.iea.org/data-and-statistics/charts/global-co2-emissions-from-transport-by-sub-sector-in-the-net-zero-scenario-2000-2030, IEA. Licence: CC BY 4.0 |
| [IEA 22b] | IEA, Rail, Paris https://www.iea.org/reports/rail, License: CC BY 4.0 |
| [IEA 22c] | Renewables Data Explorer, IEA, Paris https://www.iea.org/data-and-statistics/data-tools/renewables-data-explorer. |
| [INSEE 18] | Institut National de la Statistique e des Études Économiques. Population Census 2018. |
| [Iwasaki 94] | I. Iwasaki, H.A. Simon, "Causality and model abstraction", Artificial Intelligence, Elsevier, Vol. 67, pp. 143-194, 1994 |
| [Khodaparastan 19a] | M. Khodaparastan, A. A. Mohamed and W. Brandauer, "Recuperation of Regenerative Braking Energy in Electric Rail Transit Systems," IEEE Transactions on Intelligent Transportation Systems, vol. 20, no. 8, pp. 2831-2847, Aug. 2019, doi: 10.1109/TITS.2018.2886809. |
| [Khodaparastan 19b] | M. Khodaparastan and A. Mohamed, 'Flywheel vs. Supercapacitor as Wayside Energy Storage for Electric Rail Transit Systems,' Inventions, vol. 4, no. 4, p. 62, Oct. 2019, doi: 10.3390/inventions4040062. |
| [Killada 18] | M. Killada, R. Mohana and G. V. R. Raju, "World's Top Economies and their Metro Systems' Ridership and Financial Performance," International Journal of Traffic and Transportation Engineering, pp. 91-97, 2018. |
| [Kleftakis 19] | V. A. Kleftakis and N. D. Hatziargyriou, "Optimal Control of Reversible Substations and Wayside Storage Devices for Voltage Stabilization and Energy Savings in Metro Railway Networks," IEEE Transactions on Transportation Electrification, vol. 5, no. 2, pp. 515-523, June 2019. |
| [Liu 17] | J. Liu, H. Guo and Y. Yu, "Research on the Cooperative Train Control Strategy to Reduce Energy Consumption," IEEE Transactions on Intelligent Transportation Systems, vol. 18, no. 5, pp. 1134-1142, May 2017, doi: 10.1109/TITS.2016.2598425. |
| [Liu 19] | H. Liu, M. Zhou, X. Guo, Z. Zhang, B. Ning and T. Tang, "Timetable Optimization for Regenerative Energy Utilization in Subway Systems," IEEE Transactions on Intelligent Transportation Systems, vol. 20, no. 9, pp. 3247-3257, Sept. 2019. |

| | |
|---|---|
| [Liu 20] | P. Liu, M. Schmidt, Q. Kong, J. C. Wagenaar, L. Yang, Z. Gao and H. Zhou, 'A robust and energy-efficient train timetable for the subway system,' Transportation Research Part C: Emerging Technologies, vol. 121, p. 102822, 2020. |
| [Mao 21] | R. Mao, Y. Bao, H. Duan and G. Liu, "Global urban subway development, construction material stocks, and embodied carbon emissions," Humanit Soc Sci Commun 8, 83, Mar. 2021. |
| [Mayet 14] | C. Mayet; L. Horrein, A. Bouscayrol, P. Delarue, J. -N. Verhille, E. Chattot and B. Lemaire-Semail, "Comparison of Different Models and Simulation Approaches for the Energetic Study of a Subway," IEEE Transactions on Vehicular Technology, vol. 63, no. 2, pp. 556-565, Feb. 2014. |
| [Mayet 16a] | C. Mayet, "Modélisation énergétique d'un carrousel de métros automatique au travers de la Représentation Energétique Macroscopique ", Thèse de doctorat l'Université Lille1, mars 2016. |
| [Mayet 16b] | C. Mayet, P. Delarue, A. Bouscayrol, E. Chattot and J. -N. Verhille, "Comparison of Different EMR-Based Models of Traction Power Substations for Energetic Studies of Subway Lines," IEEE Transactions on Vehicular Technology, vol. 65, no. 3, pp. 1021-1029, March 2016. |
| [Mayet 17] | C. Mayet, P. Delarue, A. Bouscayrol and E. Chatot, "Hardware-In-the-Loop Simulation of Traction Power Supply for Power Flows Analysis of Multi-Train Subway Lines", IEEE transactions on Vehicular Technology, vol. 66, no. 7, July 2017, pp. 5564-5571, DOI: 10.1109/TVT.2016.2622245 |
| [Mayet 18] | C. Mayet, A. Bouscayrol, P. Delarue, E. Chattot, and J. N. Verhille, "Electrokinematical simulation for flexible energetic studies of railway systems," IEEE Transactions on Industrial Electronics, vol. 65, no. 4, pp. 3592–3600, 2018. |
| [MEL 19] | 19C0060 (2019), « Partenariat entre la MEL et l'Université de Lille - Optimisation énergétique sur le métro avec le laboratoire d'électrotechnique et d'électronique de puissance et évaluation de la navette autonome - Convention - Autorisation de signature » délibération du Conseil métropolitain n° 19 C 0060 en date du 05 avril 2019 |
| [Meng 22] | G. Meng, C. Wu, B. Zhang, F. Xue, and S. Lu, 'Net Hydrogen Consumption Minimization of Fuel Cell Hybrid Trains Using a Time-Based Co-Optimization Model', Energies, vol. 15, no. 8, 2022. |
| [Mo 20] | P. Mo, L. Yang, A. D'Ariano, J. Yin, Y. Yao and Z. Gao, "Energy-Efficient Train Scheduling and Rolling Stock Circulation Planning in a Metro Line: A Linear Programming Approach," IEEE Transactions on Intelligent Transportation Systems, vol. 21, no. 9, pp. 3621-3633, Sept. 2020. |

| | |
|---|---|
| [Mohamed 17] | B. Mohamed, P. Arboleya and C. González-Morán, "Modified Current Injection Method for Power Flow Analysis in Heavy-Meshed DC Railway Networks with Nonreversible Substations," IEEE Transactions on Vehicular Technology, vol. 66, no. 9, pp. 7688-7696, Sept. 2017. |
| [O. Berriel 20] | R. O. Berriel, A. Bouscayrol, P. Delarue and C. Brocart, "Mechanical Braking Strategy Impact on Energy Consumption of a Subway," 2020 IEEE Vehicle Power and Propulsion Conference (VPPC), Gijon, Spain, 2020, pp. 1-5. |
| [O. Berriel 22] | R. O. Berriel, D. Ramsey, L. Ferreira, A. Bouscayrol, P. Delarue and C. Brocart, "Analysis of Power Flows in a DC Railway System with Hardware-in-the-Loop Simulation," 2022 IEEE Vehicle Power and Propulsion Conference (VPPC), Merced, CA, USA, 2022, pp. 1-6. |
| [OMNIL 22] | OMNIL - Observatoire de la mobilité en Île-de-France. "Caractéristiques du réseau, accessibilité et intermodalité", 2022. Online https://www.omnil.fr/spip.php?article117, consulted in June 2023. |
| [Pam 21] | A. Pam, "Méthodologie d'émulation pour le test de chaîne de puissance de véhicules électrifiés", Thèse de doctorat l'Université Lille, Oct. 2020. |
| [Ramsey 21] | D. Ramsey, T. Letrouve, A. Bouscayrol and P. Delarue, "Comparison of Energy Recovery Solutions on a Suburban DC Railway System," IEEE Transactions on Transportation Electrification, vol. 7, no. 3, pp. 1849-1857, Sept. 2021. |
| [Shang 23] | M. Shang, Y. Zhou, Y. Mei, J. Zhao and H. Fujita, "Energy-Saving Train Operation Synergy Based on Multi-Agent Deep Reinforcement Learning on Spark Cloud," IEEE Transactions on Vehicular Technology, vol. 72, no. 1, pp. 214-226, Jan. 2023, doi: 10.1109/TVT.2022.3205379. |
| [Shixiong 22] | Shixiong Jiang and Canhuang Cai. "Unraveling the dynamic impacts of COVID-19 on metro ridership: An empirical analysis of Beijing and Shanghai, China", Transport Policy, vol. 127, pp. 158-170, 2022. |
| [UITP 22] | International Association of Public Transport (UITP). "World Metro Figures 2021", 2022. |
| [UITP 23] | International Association of Public Transport (UITP). The road to sustainability. Transition to renewable energy in public transport. 2023. |
| [UN 2018] | United Nations (2018). World Urbanization Prospects 2018. Retrieved from https://population.un.org/wup/Publications/Files/WUP2018-Report.pdf |
| [Verhille 07] | J. N. Verhille, "Représentation Énergétique Macroscopique du métro VAL 206 et structures de commande déduites par inversion", Thèse de doctorat l'ENSAM, juillet 2007. |

| | |
|---|---|
| [Verhille 10] | J. N. Verhille, R. Béarée and A. Bouscayrol, "Causal-based generation of velocity reference for automatic subways," 2010 IEEE Vehicle Power and Propulsion Conference, Lille, France, 2010, pp. 1-6. |
| [Wei 17] | L. Wei and Z. Yuan, "A Robust Timetabling Model for a Metro Line with Passenger Activity Information," Information, vol. 8, no. 3, p. 102, Aug. 2017, doi: 10.3390/info8030102. |
| [Xun 20] | J. Xun, T. Liu, B. Ning and Y. Liu, "Using Approximate Dynamic Programming to Maximize Regenerative Energy Utilization for Metro," IEEE Transactions on Intelligent Transportation Systems, vol. 21, no. 9, pp. 3650-3662, Sept. 2020. |
| [Yang 17] | Z. Yang, Z. Yang, H. Xia, F. Lin, and F. Zhu, 'Supercapacitor State Based Control and Optimization for Multiple Energy Storage Devices Considering Current Balance in Urban Rail Transit', Energies, vol. 10, no. 4, 2017. |
| [Yin 21] | J. Yin, A. D'Ariano, Y. Wang, L. Yang and T. Tang, 'Timetable coordination in a rail transit network with time-dependent passenger demand', European Journal of Operational Research, vol. 295, no. 1, pp. 183–202, 2021. |
| [Yuan 22] | J. Yuan, Y. Gao, S. Li, P. Liu and L. Yang, 'Integrated optimization of train timetable, rolling stock assignment and short-turning strategy for a metro line', European Journal of Operational Research, vol. 301, no. 3, pp. 855–874, 2022. |
| [Zelaya 21] | E. B. Zelaya, "Metro systems in Latin America, comparison of planning and development models versus other regions in the world," R-Evolucionando el transporte Jul. 2021, doi: 10.36443/10259/7051. |
| [Zhu 21] | C. Zhu, G. Du, X. Jiang, W. Huang, D. Zhang, M. Fan and Z. Zhu, "Dual-Objective Optimization of Maximum Rail Potential and Total Energy Consumption in Multitrain Subway Systems," IEEE Transactions on Transportation Electrification, vol. 7, no. 4, pp. 3149-3162, Dec. 2021. |

# Appendix A – Elements of EMR

| | | | |
|---|---|---|---|
| Action reaction variables | $s$ $\longrightarrow$ $\longleftarrow$ $e$ | Distribution or coupling | $e_1$ $s_3$ / $s_1$ $e_3$ / $s_2$ / $e_2$ |
| Signal variable | $\longleftarrow$ | | $e_1$ $s_3$ / $s_1$ $e_3$ / $s_2$ / $e_2$ |
| | $\longleftarrow\text{-----}$ | Accumulation inversion | $e_{2\,meas}$ $s_{meas}$ / $e_{1\,ref}$ $s_{ref}$ |
| Measurement | $\mathbb{0}$ | Conversion inversion | $e_{3\,ref}$ / $e_{1\,meas}$ $s_{1\,ref}$ |
| Source | Label $s$ $\longrightarrow$ $\longleftarrow$ $e$ | | $e_{3\,meas}$ / $e_{1\,ref}$ $s_{1\,ref}$ |
| Accumulation | $e_1$ $s$ / $s$ $e_2$ | Distribution or coupling inversion | $e_{1\,ref}$ / $e_{2\,ref}$ $s_{3\,ref}$ / $k_d$ |
| Mono-domain conversion | $e_1$ $s_2$ / $s_1$ $e_2$ / $e_3$ | Estimation or model | $e_1$ $s_2$ / $s_1$ $e_2$ |
| Multi-domain conversion | $e_1$ $s_2$ / $s_1$ $e_2$ / $e_3$ | Strategy | $k_d$ strategy |
| Power adaptation | $e_1$ $s_2$ / $s_1$ $e_2$ | Adaptation element | $e_1$ $s_2$ / $s_1$ $e_2$ |
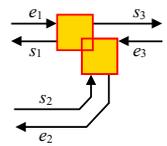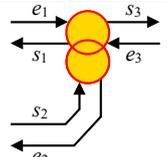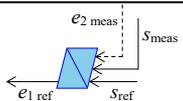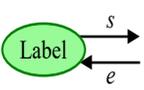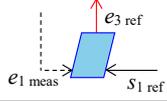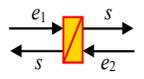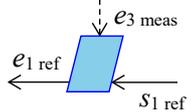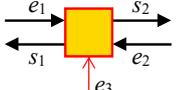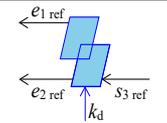
131
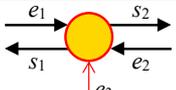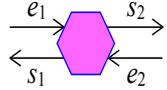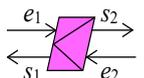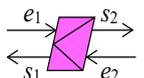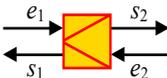
# Appendix B – Data from Line 1 of Lille - France

Table 6.    Passenger station position and stop time.

| No | Station | Position [m] | Stop Time [s] |
|----|---------|--------------|---------------|
| 1 | 4 Cantons | 417 | 16 |
| 2 | Cité scientifique | 1193 | 14 |
| 3 | Triolo | 1820 | 12 |
| 4 | Villeneuve d'Ascq Hôtel de Ville | 2703 | 16 |
| 5 | Pont de Bois | 3395 | 18 |
| 6 | Lezennes | 4266 | 12 |
| 7 | Hellemmes | 4817 | 14 |
| 8 | Marberie | 5683 | 12 |
| 9 | Fives | 6245 | 14 |
| 10 | Caulier | 6794 | 12 |
| 11 | Gare de Lille Flandres | 8000 | 26 |
| 12 | Rihour | 8697 | 14 |
| 13 | République Beaux-Arts | 9137 | 14 |
| 14 | Gambetta | 9927 | 14 |
| 15 | Wasemmes | 10367 | 12 |
| 16 | Porte des Postes | 10953 | 18 |
| 17 | CHR Oscar Lambret | 12368 | 14 |
| 18 | CHR B-Calmette | 12959 | 13 |

Table 7.    TPS position and nominal power before and after retrofit.

| TPS code | Previous nominal power [kVA] | New nominal power [kVA] | Position [m] |
|----------|------------------------------|--------------------------|--------------|
| GA4C | 2200 | 3500 | 0 |
| 4C | 2200 | 3500 | 289 |
| TRI | 2200 | 3500 | 1819 |
| PDB | Non-existent | 2500 | 3394 |
| HEL | 2200 | 2500 | 4817 |
| CAU | 2200 | 2500 | 6805 |
| GLF | Non-existent | 2500 | 8001 |
| GAM | 2200 | 2500 | 9927 |
| LAM | 2200 | 3500 | 12368 |
| CAL | Non-existent | 2500 | 12959 |
| Total | 15400 | 29000 | |